

Project title: East Texas Mussel Surveys and Tolerances

Date: January 15, 2025

Personnel:

Principal Investigator
Timothy H. Bonner, PhD
Department of Biology
Texas State University
601 University Drive
San Marcos, Texas 78666
TBonner@txstate.edu

Co-Principal Investigator
Bradley M. Littrell
BIO-WEST, Inc.
1405 United Drive, Suite 111
San Marcos, Texas 78666
blittrell@bio-west.com

Co-Principal Investigator
Charles Randklev, PhD
Texas A&M Natural Resources Institute
Texas A&M AgriLife Research and Extension Center at Dallas
17360 Coit Road
Dallas, Texas 75252
crandklev@ag.tamu.edu

Co-Principal Investigator
Jim Stoeckel, PhD
Auburn University
School of Fisheries, Aquaculture and Aquatic Sciences
121B Swingle Hall
Auburn, Alabama 36849
jimstoeckel@auburn.edu

Task 1: A literature review on freshwater mussel sampling and monitoring methods

Task 2: Life history and reproductive patterns of the Louisiana Pigtoe

Task 3: Part I. Evaluating lethal thermal tolerances and vulnerability of three east Texas freshwater mussels.

Task 3: Part II. Laboratory bioassays to evaluate thermal, ammonia, and hypoxia tolerances and limits for the Louisiana Pigtoe.

Task 4: Species distribution models for Louisiana Pigtoe and Texas Heelsplitter.

Task 5: Establishing long-term monitoring protocols for Louisiana Pigtoe and Texas Heelsplitter via a series of standardized survey methods at varying spatial scales

Task 1: A literature review on freshwater mussel sampling and monitoring methods

The objective of this task was to summarize literature on sampling guidelines and methodologies for freshwater mussels (Family: Unionidae) to inform future efforts targeting *Pleurobema riddellii* (Louisiana Pigtoe) and *Potamilus amphichaenus* (Texas Heelsplitter).

Effective conservation and management of rare and endangered mussels require a detailed understanding of species distribution, abundance and population dynamics over time. Monitoring programs incorporating occupancy surveys and mark-recapture sampling play a key role in gathering this type of information. For these programs to succeed, sampling designs must clearly define objectives, use standardized methods, and account for incomplete detection (Yoccoz et al., 2001). A monitoring program should address three critical questions: 1) Why conduct the survey? 2) What should be surveyed? and 3) How should the survey be conducted? Following this, factors affecting species detection must be considered to refine the survey design.

Detectability, the probability of finding a species if present (Martin et al., 2006), is influenced by observer skill, species traits, and environmental conditions (Yoccoz et al., 2001; Martin et al., 2006). Observer expertise in species identification and familiarity with habitat use for target species is critical for successful surveys. Generally, mussel identification relies on morphological traits such as shell size, color and texture, which can vary greatly between species and among individuals. Additionally, mussel species exhibit varying levels of habitat specialization and seasonal behavioral changes, such as burrowing, which influence detectability. These behaviors are also affected by environmental factors like water temperature, quality, and availability. Consequently, untrained surveyors or those unfamiliar with the local species pool are more likely to misidentify species or fail to detect those with specific habitat preferences in the field.

Standardizing sampling methods and ensuring surveyors are well-trained in species identification and survey techniques can help reduce variability in detectability and allow for comparisons across studies. Sampling programs must clearly state their goals, define key variables of interest (e.g., species richness), and adopt methods to mitigate detection errors. Without these elements, survey results risk being biased, potentially leading to ineffective or misguided management decisions.

Qualitative Sampling for Mussels

Qualitative sampling is used to determine mussel presence/absence and to provide assemblage structure data (such as a species list) at a given site (Miller and Payne 1993; Strayer et al. 1995; Vaughn et al. 1997; Dunn and Strayer 2010). Dunn and Strayer (2010) identify three main methods: **reconnaissance**, **timed-searches**, and **semi-quantitative transects**. Generally, qualitative methods are cost-effective and suitable for detecting species presence and estimating abundance, with standardized efforts improving detectability (Metcalf-Smith et al. 2000; Smith et al. 2006). The following is summary of the three types of qualitative surveys:

- **Reconnaissance Sampling:**
Involves haphazard surveys to document mussel presence and distribution with minimal effort. This method is useful for large areas but lacks standardized search areas or times, leading to potential bias (Smith 2006; Clayton et al. 2015).
- **Timed-Search Sampling:**
Conducted in predefined areas for specific time intervals to gather data on presence, abundance, and assemblage structure. Search time is often determined by species accumulation curves (Garner et al. 2009). While cost-effective, results depend on surveyor skill and may be biased toward detecting larger or more exposed mussels.
- **Semi-Quantitative Transects:**
Uses transects at fixed intervals to map mussel distribution and habitat associations. While this method offers robust data, it is limited by surveyor experience and may miss aggregated mussels if spacing is too wide.

Quantitative Sampling for Mussels

Quantitative sampling assesses population size and structure using methods such as simple random sampling, systematic sampling with random starts, and stratified random sampling (Strayer and Smith 2003). The following is summary of the three types of quantitative surveys:

- **Simple Random Sampling:**
Random quadrat placement (typically 0.25 m²) ensures unbiased estimates but is costly and density estimates can be imprecise if abundances are low or mussels are aggregated into clusters, which may leave many quadrats without mussels.
- **Systematic Sampling:**
Improves spatial coverage with evenly spaced quadrats, providing precise density estimates, but spacing between points must be small enough to detect mussel aggregations.
- **Stratified Random Sampling:**
Focuses effort on high-density areas based on prior knowledge. While effective for targeted efforts, it is resource-intensive and less suitable for rare species.

Mark-recapture Sampling for Mussels

Mark-recapture is a quantitative method used to estimate population size, survival rates, and movement patterns of mussels. It involves capturing individuals, marking them, releasing them back into their habitat (150 to 300 m², but adjustable depending on mussel densities), and then recapturing individuals during subsequent surveys. Subsequent surveys consist of two types: primary surveys and secondary surveys. Primary surveys are conducted periodically (e.g., twice

a year, once a year, once every two years) or opportunistically (e.g., following an extended period of low flows or following a high flow event; Sotola et al. 2020) and enable assessments of mussel abundances, survival, and site fidelity through time or following an opportunistic event (e.g., low flows, flood, chemical spill). Secondary surveys immediately follow (e.g., hours) the initial sampling event or each primary survey and consist of two repeated sampling surveys, where individuals are captured, marked or noted if already marked, and released back into their habitat each time. The secondary surveys enable calculation of detection probabilities, which then can be applied to primary survey estimates of mussel abundances, survival, and site fidelity using a Bayesian robust design model (Pollock 1982, Nichols and Pollock 1990, Rieke et al. 2018).

For marking, laminated vinyl shellfish tags (e.g., Floy®) are attached to both sides of each mussel with cyanoacrylic glue (Loctite Gel Control Super Glue®). In some instances, a Passive Integrated Transponder (PIT) tag (e.g., Biomark®) can also be attached to the mussel, which facilitates detection in areas with complex habitat (e.g., gravels and cobbles deposited into crevices of bedrock) or in areas with low mussel abundances.

Literature Cited

- Clayton, J. L., Douglas, B., and Morrison, P. 2015. West Virginia mussel survey protocols. Available from: <http://www.wvdnr.gov/Mussels/Main.shtm>.
- Dunn, H. L., & Strayer D. L. 2010. Overview of sampling techniques for freshwater mussels. FMCS 2010 workshop: Regional Fauna Identification and Sampling.
- Garner, J. T., McGregor, S. W., Tarpley, T. A., & Buntin, M. L. 2009. Freshwater mussels (Unionidae) in the headwaters of Chipola River, Houston County, Alabama. *Southeastern Naturalist* 8: 687–694.
- Martin, J., Kitchens, W. M., & Hines J. E. 2006. Importance of well-designed monitoring programs for the conservation of endangered species: case study of the snail kite. *Conservation Biology* 21: 472–481.
- Metcalf-Smith, J. L., Maio, J. D., Staton, S. K., & Mackie, G. L. 2000. Effect of sampling effort on the efficiency of the timed search method for sampling freshwater mussel communities Effect of sampling effort on the efficiency of the timed search. *Journal of the North American Benthological Society* 19: 725–732.
- Miller, A. C., & Payne, B. S. 1993. Qualitative versus quantitative sampling to evaluate population and community characteristics at a large-river mussel bed. *American Midland Naturalist* 130: 133–145.
- Nichols, J. D., & Pollock, K. H. 1990. Estimation of recruitment from immigration versus in situ reproduction using Pollock's robust design. *Ecology* 71:21–26.

- Pollock, K. H. 1982. A capture-recapture design robust to unequal probability of capture. *The Journal of Wildlife Management* 46:752–757.
- Riecke, T. V., Leach, A. G., Gibson, D., & Sedinger, J. S. 2018. Parameterizing the robust design in the BUGS language: Lifetime carry-over effects of environmental conditions during growth on a long-lived bird. *Methods in Ecology and Evolution* 2018:1–12.
- Smith, D. R. 2006. Survey design for detecting rare freshwater mussels. *Journal of the North American Benthological Society* 25: 701–711.
- Sotola, V. A, K. T. Sullivan, B. M. Littrell, N. H. Martin, D. S. Stich, and T. H. Bonner. 2021. Short-term responses of freshwater mussels to floods in a southwestern U.S.A. river estimated using mark-recapture sampling. *Freshwater Biology* 66:349-361.
- Strayer, D. L., Claypool, S., & Sprague, S. J. 1995. Assessing unionid populations with quadrats and timed searches. *Conservation and Management of Freshwater Mussels II: Initiatives for the Future*, 163–169.
- Strayer, D. L., & Smith, D. R. 2003. *A Guide to Sampling Freshwater Mussel Populations*. American Fisheries Society Monograph 8.
- Vaughn, C. C., Taylor C. M., & Eberhard, K. J. 1997. A comparison of the effectiveness of timed searches vs. quadrat sampling in mussel surveys . Pages 157-162, in Cummings, K.S., A.C. Buchanan, C.A. Mayer and T.J. Naimo (eds)., *Conservation and Management of Freshwater Mussels II: Initiatives for the Future*. Proceedings of a UMRCC symposium, 16-18 October 1995, St. Louis, Missouri. Upper Mississippi River Conservation Committee, Rock Island, Illinois.
- Yoccoz, N. G., Nichols, J. D., Boulinier, T. 2001. Monitoring of biological diversity in space and time. *Trends in Ecology & Evolution* 16: 446–453.

Task 2: Life history and reproductive patterns of the Louisiana Pigtoe

Contributing authors: Alex Zalmat, Kyle Sullivan, Brad Littrell, and Timothy H. Bonner

Study objectives

Goal of this study was to use nonlethal field techniques to quantify and characterize the periodicity of major reproductive life history events in the Louisiana Pigtoe *Pleurobema riddellii*. This involved two major objectives: 1) to quantify and characterize gametogenesis over two years in order to assess temporal variation in spermatogenesis and oogenesis, and 2) to quantify and characterize the timing of brooding in females over the course of a full year.

Methods

Field Collections

From February 2022 to December 2023, three sites in the Lower Neches Valley Authority (LNVA) canal system in Beaumont, TX were visited monthly and sampled for *Pleurobema riddellii* (Figure 1). Mussels were collected using tactile hand searches while wading and snorkeling. Once mussels were positively identified as *P. riddellii*, at least 10 individuals were measured for length and sampled for gonadal fluid using a non-lethal syringe technique (Tsakiris et al., 2016). Gonadal-fluid samples were stored in 1.5ml of 10% formalin and placed on ice to be transported back to the laboratory for microscopy. Starting in October, 2022, each mussel was also sampled for gill contents (brood) using a non-lethal gill scraping technique (Beaver et al., 2019). The gill contents were stored separately from gonadal fluid samples in 10% formalin and then placed on ice to be transported to the laboratory for further analysis. Water quality data including temperature, pH, conductivity, dissolved oxygen, and current velocity was measured at each site during each visit. Day length and monthly climatological data (daily precipitation, daily humidity, average daily temperature, etc.) for the Beaumont, TX area was downloaded from the visual crossing website and database (<https://www.visualcrossing.com/weather/weather-data-services#>).

Quantification of gametogenesis

Gonadal-fluid samples were each examined to determine sex by identifying the presence of either spermatocytes or oocytes (or their cellular precursors). If a sample contained spermatocytes or identifiable precursors, it was labeled a male and a sperm-count was conducted using a hemocytometer to obtain a sperm concentration (mature spermatocytes/ml). If a sample contained oocytes or identifiable precursors, a 10 μ l aliquot of the sample was placed on a slide, and the diameters of up to 100 oocytes were measured using a Nikon DS-F1 camera and screen micrometer system.

Brood Characterization

A 10 μ l aliquot of each gill-scrape sample was placed on a slide and examined under a microscope at 40X magnification. Samples were characterized by the presence of the following qualities: no brood (0), the presence of oocytes (OO), the presence of immature glochidia (IMG), and the presence of developed glochidia (DG). Each sample was scored for each of these

categories, and this was quantified for each month as the proportion of females sampled with a particular stage of brood (0, OO, IMG, and DG). These methods are an adaptation of Beaver et al. (2019).

Statistical Analysis

Generalized additive models (GAMs) were implemented in R to assess environmental predictors of reproductive activity. Each of three response variables: monthly sperm count, oocyte diameter, and percent females with glochidia in the gills were used to generate several models, each consisting of combinations of the many predictor variables. An AIC model selection approach was then used to find the best fitting models and their predictor variables in each case.

Results

Reproductive cycle

Spermatogenesis appears to ramp up over the winter months and into the spring, peaking in late spring/early summer and then ramping down into the late summer (Figure 2). This largely coincides with oocyte diameter which also ramps up over the fall and winter months, peaking in mid-summer, and then ramps back down into the late summer/early fall seasons (Figure 3). Brooding activity follows closely behind gametogenesis, although there appears to be two peaks throughout the year: one occurring in the mid to late summer months, and another occurring in the winter. It should be noted that the summer brooding period were observed to contain larger numbers of females with developed glochidia (DG) than in the winter months, suggesting that perhaps in the summer months the brood size is larger (thus making it easier to find developed glochidia) and the brooding period more pronounced than in the winter months.

Environmental Predictors

Generalized additive models (GAMs) were employed to identify environmental factors associated with reproductive processes. The model with the lowest Akaike Information Criterion (AIC) for spermatogenesis included average day length, average daily precipitation, and average daily humidity as predictors (AIC = 355.35; Table 1). However, only average day length was found to be a statistically significant predictor ($F = 14.085$, $p = 0.00559$; Table 2). For oocyte diameter, the best-fitting model also incorporated average day length, precipitation, and humidity (AIC = -68.87, Table 1), with average day length being the sole significant predictor ($F = 7.315$, $p = 0.0304$; Table 2). The model for brooding activity, which measures the percentage of females containing glochidia in their gills, included only average day length (AIC = 105.574; Table 1), although it did not achieve statistical significance ($F = 3.826$, $p = 0.0545$; Table 2).

Synthesis

This study characterizes the reproductive cycle of *Pleurobema riddellii* and explores the environmental factors that influence its gametogenesis and brooding activity. The results reveal distinct seasonal patterns for both spermatogenesis and oocyte development in *P. riddellii*. Spermatogenesis begins to increase during the winter months and continues through the spring, peaking in late spring or early summer, before tapering off into the late summer. Similarly, oocyte diameter follows a comparable seasonal trajectory, increasing in the fall and winter, reaching its peak in mid-summer, and declining in late summer/early fall. Brooding activity,

which tracks closely with gametogenesis, shows two distinct peaks throughout the year: one in mid to late summer and another in winter. The summer brooding period is marked by a higher number of females with developed glochidia, suggesting that the summer brooding period may involve larger brood sizes, facilitating the identification of developed glochidia and a more pronounced brooding activity compared to the winter months.

To identify environmental drivers of these reproductive processes, GAMs were applied. The findings indicate that average day length is the most consistent and significant environmental predictor of both spermatogenesis and oocyte diameter, with statistical significance observed in both models. While average precipitation and humidity were also considered in the models, neither was found to be a significant predictor. For brooding activity, average day length was included in the best-fitting model, though it did not reach statistical significance. These results underscore the importance of photoperiod as a primary environmental cue regulating reproductive timing in *P. riddellii*, suggesting that seasonal changes in day length may play a pivotal role in driving the timing of gametogenesis and brooding activity, particularly during the summer months.

Overall, this study furthers our understanding of the reproductive cycle of *P. riddellii* and highlights the significant role of environmental factors, particularly day length, in shaping its reproductive life history. These findings provide valuable insights into the species' reproductive ecology, with implications for conservation efforts, as understanding the timing and triggers of reproduction can inform strategies for protecting critical habitats and managing populations of *P. riddellii*. In addition to the data provided above, we are currently processing a similar dataset for another species collected from the LNVA canal system: *Cyclonaias pustulosa*. This will allow for valuable comparisons to previously published data from the *Cyclonaias* genus in natural riverine systems (Dudding et al., 2020). We plan to publish these data by the end of 2025.

Literature Cited

- Beaver, C. E., S. R. Geda, and N. A. Johnson. 2019. Standardizing a non-lethal method for characterizing the reproductive status and larval development of freshwater mussels (Bivalvia: Unionida). *Journal of Visualized Experiments*, 159, e60244
- Dudding, J. F., Hart, M., Khan, J. M., Robertson, C. R., Lopez, R., & Randklev, C. R. 2020. Reproductive life history of 2 imperiled and 1 widely-distributed freshwater mussel species from the southwestern United States. *Freshwater Science*, 39(1), 156-168.
- Tsakiris, E. T., C. R. Randklev, and K. W. Conway. 2016. Effectiveness of a nonlethal method to quantify gamete production in freshwater mussels. *Freshwater Science* 35: 958–973.

Table 1: The top 3 GAM models for each of the three response variables and their AIC scores. DL = average monthly day length (hrs.), P = average monthly precipitation/day (mm), H = average monthly humidity/day (%).

Model	AIC
<i>Spermatogenesis:</i>	
Sperm count ~ DL + P + H	355.356
Sperm count ~ DL + H	355.701
Sperm count ~ DL + P	359.136
<i>Oocyte diameter:</i>	
Oocyte diameter ~ DL + P + H	-68.876
Oocyte diameter ~ DL + H	-66.132
Oocyte diameter ~ P + H	-65.715
<i>Brooding activity:</i>	
% Females with glochidia ~ DL	105.574
% Females with glochidia ~ H	106.580
% Females with glochidia ~ DL + H	106.742

Table 2: The best fitting models from each of the response variables and their predictors, F statistics, and p-values. DL = average monthly day length (hrs.), P = average monthly precipitation/day (mm), H = average monthly humidity/day (%).

Model	F	p-value
Sperm count ~ DL + P + H		
DL	14.085	0.00559 **
P	1.727	0.22525
H	4.959	0.05675
Adjusted R square =	0.694	
Oocyte diameter ~ DL + P + H		
DL	7.315	0.0304 *
P	1.379	0.265
H	0.052	0.9535
Adjusted R square =	0.615	
% Females with glochidia ~ DL		
DL	3.283	0.0545
Adjusted R square =	0.694	

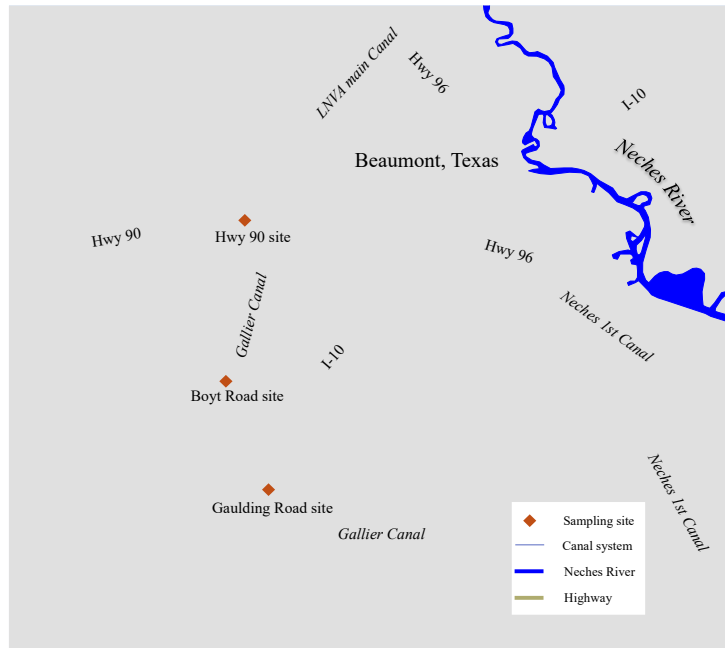


Figure 1. Map of the Lower Neches Valley Authority Canal system near the city of Beaumont, Texas showing the location of the three sites sampled. These sites were chosen based on LNVA records of high numbers of *P. riddellii* individuals.

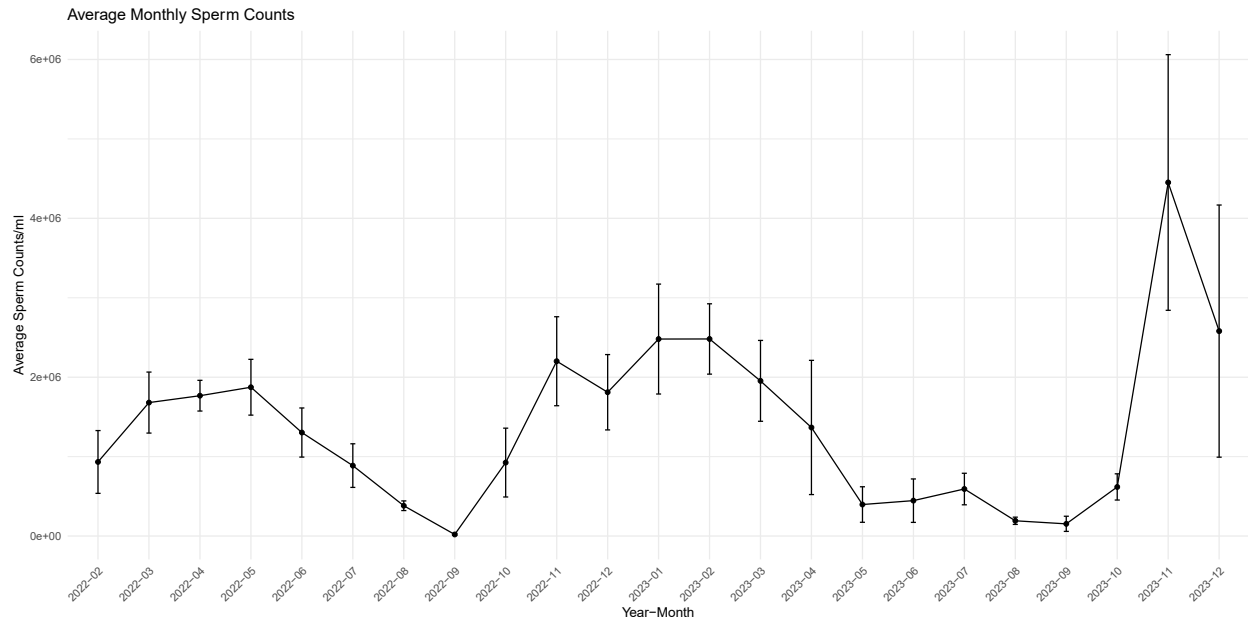


Figure 2. Monthly average sperm counts/ml plotted over the course of the study period with standard error bars. Spermatogenesis appears to ramp up over the winter months and into the spring, peaking in late spring/early summer and then ramping down into the late summer.

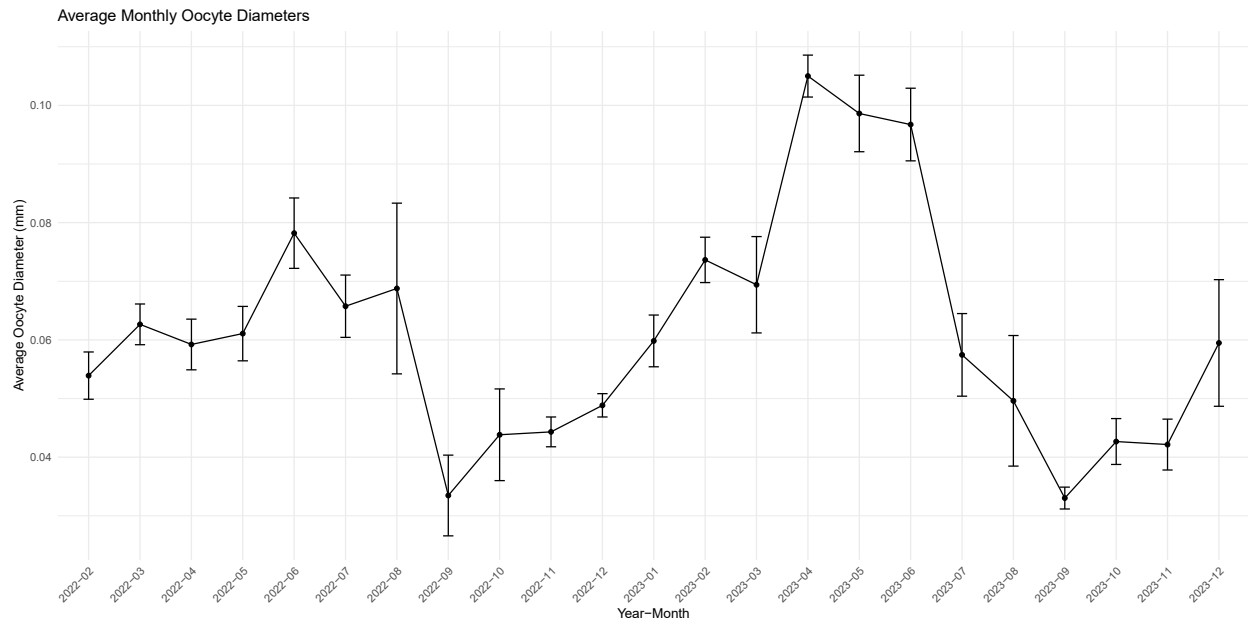


Figure 3. Monthly average oocyte diameters (mm) plotted over the course of the study period with standard error bars. Oogenesis appears to ramp up over the fall and winter months peaking in mid-summer, and then ramping down into the late summer/early fall months.

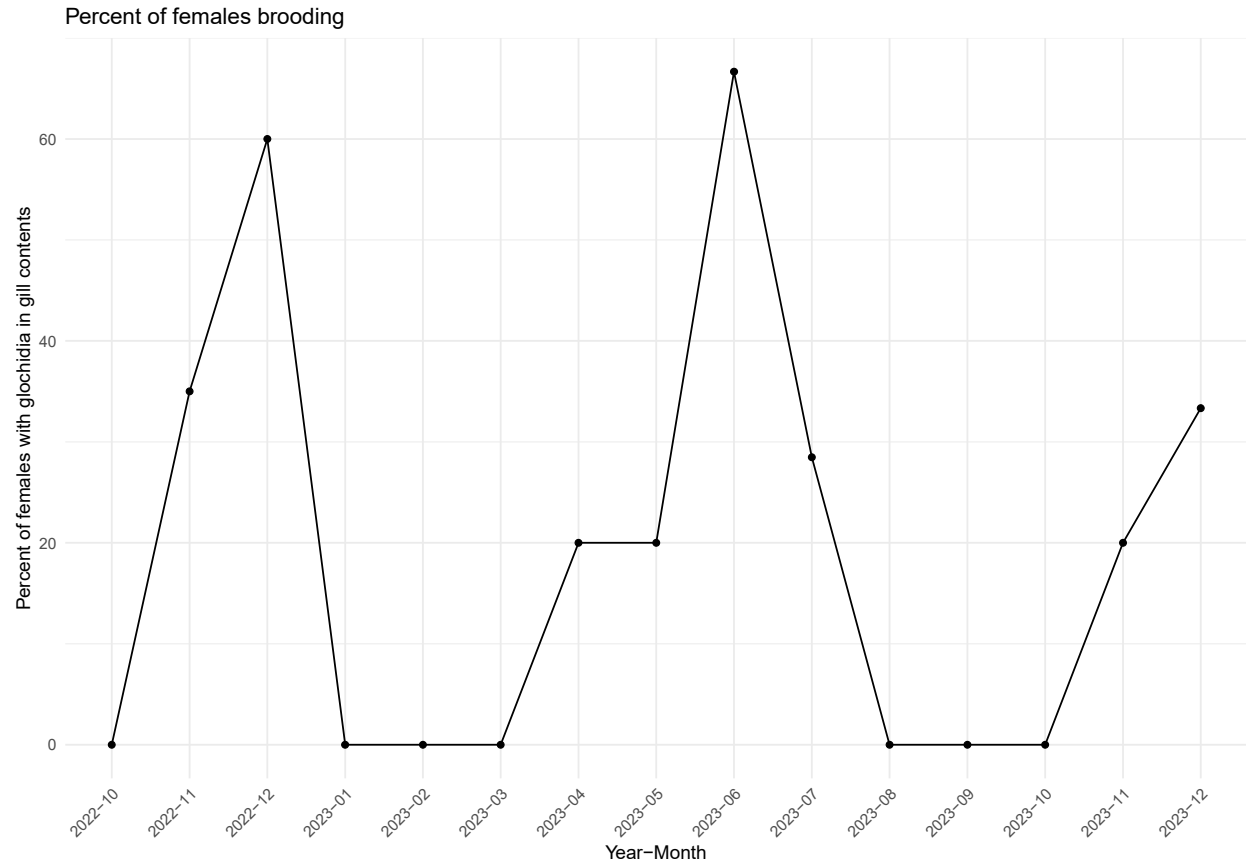


Figure 4. Monthly brooding activity represented by the percentage of females sampled that contained any developing glochidia or mature glochidia in the gill contents. Percentages are plotted over the course of a year (starting in October, 2022). Brooding activity appears to occur in two periods: a pronounced period in the summer months, and again, to a slightly lesser degree in the winter months.

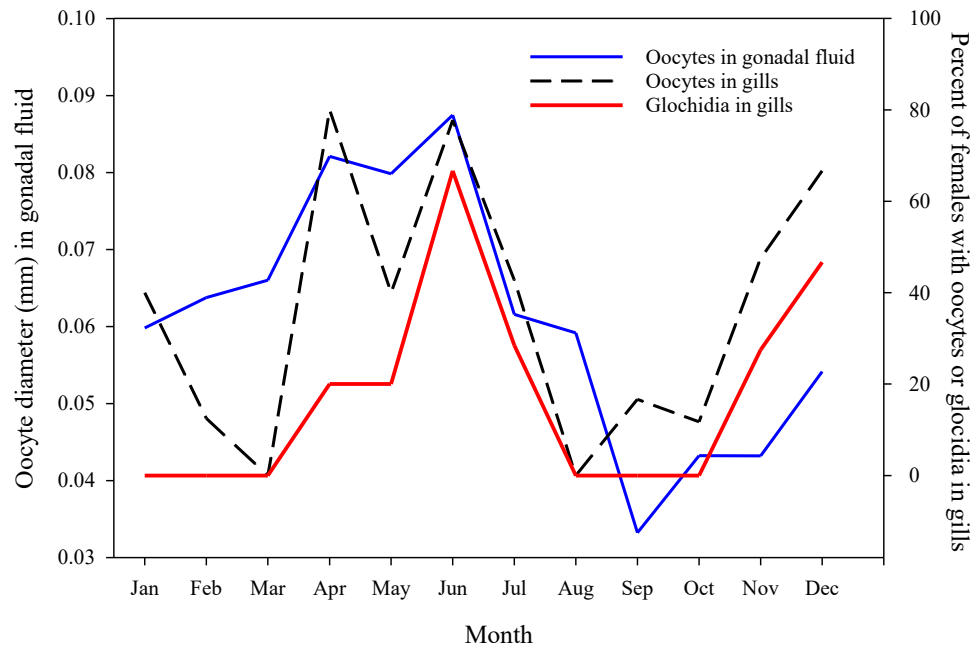


Figure 3. The yearly reproductive cycle in *P. riddellii*. Data were averaged over the two years (when applicable) for oocyte diameter, percentage of females with oocytes in the gills, and percentage of females with any stage of glochidia in the gills.

Task 3: Laboratory bioassays to evaluate thermal, ammonia, and hypoxia tolerances and limits for the Louisiana Pigtoe.

Part I. Evaluating lethal thermal tolerances and vulnerability of three east Texas freshwater mussels.

Contributing authors: Charles R. Randklev and Dorothea P. Mildenerberger

Study objectives

Unionid mussels are globally imperiled, and many species are living near or at their upper thermal limit, which means future increases in water temperature will likely have negative impacts to their long-term persistence. Despite this threat, there remains a knowledge gap on sublethal and lethal temperature thresholds for most mussel species. To better understand how rising water temperatures will affect the survival of freshwater mussel populations, we tested the upper thermal limits (i.e., lethal tolerance estimates resulting in 5% and 50% mortality) of 3 mussel species for which thermal tolerance information is lacking: *Cyclonaias pustulosa* (Lea, 1831), *Fusconaia askewi* (Marsh, 1896), and *Pleurobema riddellii* (Lea, 1862).

Methods

To address our research questions, we evaluated the upper thermal limits of 3 species of adult freshwater mussels from the Sabine and Neches River basins in east Texas, USA: the Pimpleback *Cyclonaias pustulosa* (Lea, 1831), which is presently considered common and is widely distributed, the Texas Pigtoe, *Fusconaia askewi* (Marsh, 1896), which is endemic to east Texas and is of conservation concern, and the Louisiana Pigtoe, *Pleurobema riddellii* (Lea, 1862), which has a larger regional range and has been proposed for listing under the United States Endangered Species Act (ESA). The upper thermal limits resulting in 5% and 50% mortality (LT05 and LT50, respectively) of adult mussels were determined in 240-h laboratory experiments then fitting the survival data to dose response regression curves. After identifying the thermal tolerances of the mussel species, exceedance events were identified within in situ water temperature data collected from water loggers and, when possible, hindcasted/forecasted with a random forest model. To further evaluate the impact and frequency of exceedance events and its relationship to streamflow and discharge, a uniform continuous above-threshold (UCAT) analysis was completed.

This study was conducted in the Neches and Sabine River basins of east Texas (Figure 1). The Sabine River originates in northeast Texas, flowing 893 km before emptying into the Gulf of Mexico and draining an area of 25,268 km² (19,233 km² in Texas and 6035 km² in Louisiana). The Sabine River has a small drainage basin relative to other major river basins in the state, but it has the 2nd-highest flow volume because of high precipitation, which on average is 1067 to 1422 mm/y (Griffith et al. 2007). Climate in the basin is humid subtropical with air temperatures averaging 32.5°C during the summer and 18.2°C during the winter (Larkin and Bomar 1983). The study site on the upper Sabine River was located at the Highway 14 crossing near Hawkins, Texas. Daily discharge at the site ranged from lows of 1.6 m³/s in September to highs of 439

m³/s in May (United States Geological Survey [USGS] gauging station #08019200, 2022). Adjacent land use comprises agriculture and commercial uses, dominated by grazing land and timber production, and undeveloped areas consist of woody wetland and mixed-forest land cover (Dewitz and USGS 2021, Texas A&M Natural Resources Institute 2020).

The study site on the Neches River was located in the Lower Neches Valley Authority (LNVA) Canal near Beaumont, Texas, which is part of a 644-km canal system sourced from the lower Neches River and Pine Island Bayou to supply freshwater for commercial and agricultural purposes (Harrel and Hall 1991). Climate for this region is also humid subtropical, with summer temperatures averaging 32.8°C and winter temperatures averaging 13.3°C. LNVA Canal water temperature, recorded at the USGS gauging station at Beaumont, Texas (#08041770, 2010-2022), ranges from 6 to 33°C. Mean annual precipitation averages 940 to 1473 mm/y (Griffith et al. 2007). Adjacent land use comprises industrial development, crops, and grazing with herbaceous land cover (Dewitz and USGS 2021).

Study species

We estimated thermal tolerances of adult *C. pustulosa*, *F. askewi*, and *P. riddellii*. *Cyclonaias pustulosa* is widely distributed throughout Texas, ranging from the Nueces River basin east to the Sabine River and north to the Red River drainage, but it also occurs outside of the state and is considered stable within its range (Randklev et al. 2023). Previous studies on *C. pustulosa* have suggested it is thermally sensitive, based on short-term exposure to 35°C water causing increased catabolism rates (Spooner and Vaughn 2008). *Fusconaia askewi* is endemic to rivers in east Texas, occurring in the Neches and Sabine drainages (Randklev et al. 2023), and is considered state threatened by Texas Parks and Wildlife (Randklev et al. 2023). *Pleurobema riddellii* ranges outside of Texas (Randklev et al. 2023), but within the state it ranges from the San Jacinto drainage east to the Sabine River and potentially north to the Red River drainage (Randklev et al. 2023). This species is currently listed as state threatened in Texas and has been proposed as threatened under the ESA (Randklev et al. 2023). *Fusconaia askewi* and *P. riddellii* have yet to be evaluated for their upper thermal tolerances.

We collected *C. pustulosa* ($n = 60$) and *F. askewi* ($n = 60$) from the upper Sabine River in November 2022 and *P. riddellii* ($n = 60$) from the LVNA Canal in February 2023. Following collection, we wrapped the mussels in damp paper towels and transported them in an insulated cooler to the Texas A&M AgriLife Extension Center in Dallas, Texas. Upon arrival at the laboratory, we held the mussels in quarantine for ~3 wk at ~20°C in a recirculating mesocosm system with reconstituted water. Moderately hard reconstituted water was made with a four-salt recipe following Smith et al. (1997). During the quarantine period, we fed the mussels daily with 20 mL of a 50/50 mix Shellfish/Nano3600 diet (LPB™ Frozen Shellfish Diet® and Nanno3600™, Reed Mariculture, Campbell, California). We monitored water quality parameters (NH₃, NO₂⁻, and NO₃⁻) daily and kept them within standard ranges (ASTM 2006). Prior to the experiment, we weighed the mussels, measured their length, and tagged them with a vinyl ID number. The mean length (\pm SE) of *C. pustulosa* was 37.53 ± 0.45 mm and the mean mass was 22.54 ± 0.80 g. For *F. askewi*, mean length was 39.84 ± 0.44 mm, and the mean mass was 14.93 ± 0.50 g. Individuals of *P. riddellii* were slightly larger, with mean length of 50.83 ± 0.68 mm and mean mass of 60.37 ± 2.40 g.

Thermal tolerance experiment

Laboratory experiment

Upper thermal tolerances were determined following the methods described by Khan et al (2020). Prior to the experiment, we acclimated the non-control mussels to 27°C. Acclimation was completed in a recirculating system (62 L) within a refrigerated incubator (Heratherm™ Refrigerated Incubator IMP400, Thermo Fisher Scientific, Waltham, Massachusetts). We raised the water temperature from the holding temperature (20°C), at a rate of 2.5°C/d until it reached 27°C. We then held the temperature at 27°C for 96 h. During acclimation, mussels were fed 20 mL/d of the 50/50 mix Shellfish/Nano3600 diet. We monitored water quality daily throughout acclimation and performed a 50% water renewal at 72 h in the acclimation and control tanks.

After acclimation, we tested mussels for 10 d (240 h) at 4 experimental temperatures (30, 33, 36, 39°C) alongside a nonacclimated control that remained at 20°C for the duration of the experiment (Figure 2). We placed mussels into water baths, which consisted of 190-L fiberglass tanks, and each tank was assigned an experimental temperature or control. Tanks were partitioned into 3 chambers by watertight acrylic sheets sealed with silicone. Each chamber was equipped with its own heater, temperature controller, and air stone and was filled with 46 L of moderate hard water, making each chamber an independent replicate. We placed mussels in 1.2-L plastic containers modified with plastic 10-mm-mesh bottoms. There were 3 replicates of each temperature–species combination ($n = 3$), including the 20°C control, with 4 mussels in each replicate, testing a total of 60 mussels of each species across all temperatures. After acclimation, an individual of *C. pustulosa* and *F. askewi* was found not alive and was excluded from the experimental sample, leaving the final sample size of the species tested, *C. pustulosa* ($n = 59$), *F. askewi* ($n = 60$), and *P. riddellii* ($n = 59$). We fed each replicate 20 mL/d of 50/50 shellfish/Nano3600 diet, and we visually assessed mussel survival every 24 h. We completed 50% water renewals at the 96-h and 168-h marks during the 10-d experiment. We confirmed consistent and accurate water temperatures in each replicate throughout the trials with a HOBO® pendant water temperature data logger (HOBO UA-002-64 Pendant Temperature/Light 64K Data Logger, Onset Computer Corp., Bourne, Massachusetts). We checked water quality daily for NH_3 , NO_2^- , NO_3^- and DO (monitored with test strips and YSI probe; Yellow Springs Instruments, Yellow Springs, Ohio). Water quality parameters were kept within standard ranges (ASTM 2006) and were comparable across all trials and replicates.

Thermal tolerance estimates

We calculated the lethal temperature estimates resulting in 5% and 50% mortality (LT05 and LT50, respectively), and their 95% CIs, based on observed mortality at 24, 48, 96, 120, and 240 h (10 d). We determined the estimates by using the *drc* package (version 3.0-1; Ritz et al. 2015) in R (version 4.3.1 R Project for Statistical Computing, Vienna, Austria) to fit several types of regression curves (models included two-parameter log-logistic, three-parameter log-logistic, four-parameter log-logistic, four-parameter Weibull type 1, four-parameter Weibull type 2, three-parameter Weibull type 1, and three-parameter Weibull type 2) to survival data separately for each species and at each timepoint. We carried out model selection by comparing

the Akaike information criterion corrected for small sample size (AICc) for each model to choose the best-fitting and most parsimonious model. We made statistical comparisons of the LT thresholds with the CI ratio test, according to the methods of Wheeler et al. (2006), also with the *drc* package in R. The null hypothesis states that if the LTs are the same, the ratio should be equal to 1. We constructed a 95% CI using the variance of each LT estimate, and we rejected the null hypothesis if the interval did not contain 1 (Wheeler et al. 2006). We also performed the Wald test with a Bonferroni correction for multiple comparisons using the *comped* function in the *drc* package to corroborate the CI ratio test. The Wald test examines the fitted coefficients of a logistic regression over their standard errors to test whether the fitted coefficients are equal.

Lethal temperature threshold exceedances

Water temperature and depth measurements

To create a biological overlay and compare our upper thermal limits within situ water temperature conditions, we deployed a HOBO water level logger (HOBO U20L-0x Water Level Data Logger, Onset Computer Corp.) at each site. Water level loggers were housed in a perforated PVC casing and were anchored to the stream bed with rebar. Loggers on the upper Sabine River were deployed from September to October 2022. Loggers on the LNVA Canal were deployed from February to October 2023. Water depth and temperature data were recorded at 15-min intervals.

Random forest hindcasting

We used a random forest (RF) model to hindcast and forecast Sabine River water temperature from logger data. The model used the water temperature data we collected with HOBO loggers (September – October 2022), hourly stream discharge data from the USGS station (#08019200, January 2010 – December 2023) on the Sabine River near Hawkins, Texas, and hourly weather data from the Surface Weather Observation Station at Tyler Pounds Regional Airport in Smith, Texas. Weather data obtained from the Tyler Pounds Regional Airport included air temperature, relative humidity, dewpoint, and precipitation (January 2010 – December 2023). Additionally, we calculated the previous hour's air temperature and air temperature change. We chose these variables because they are strongly correlated with water temperature (Gu and Li 2002, Toffolon and Piccolroaz 2015). Using the *randomForest* package (version 4.7-1.1; Liaw and Wiener 2002) in R, we created a 500-tree RF model using 80% of the data to train the model and the remaining 20% to test it. We used mean square error and R^2 to determine model accuracy. Once the model was trained and tested, we used it to expand our data range of upper-Sabine-River water temperature to span from January 2010 to December 2023.

Observed threshold exceedances

To add biological context to in situ water temperatures, we analyzed threshold exceedances, with exceedances based on the observed maximum daily water temperature. If the observed maximum daily water temperature was higher than any one of the LT thresholds, no matter the corresponding timepoint duration, we counted the entire day as an exceedance. Cumulative exceedances occurred when the threshold was exceeded by maximum daily water temperatures at least once on a date and during the following sequential day(s). We calculated exceedance frequencies for the entire period of record and for the spring/summer bioperiod from March to August. The bioperiod focuses on the biologically active time period when mussel

reproduction and the highest thermal stress occur (Rangaswami et al. 2023b). Exceedance frequencies, similar to thermal vulnerability indices, are a less data-intensive way of estimating thermal sensitivity and vulnerability (Clusella-Trullas et al. 2021). We evaluated exceedances for each species according to the water temperatures of the site from which the species was collected.

UCAT analysis

As a 2nd measure of temperature threshold exceedances, we conducted a uniform continuous above-threshold (UCAT) analysis following the methods of Castelli et al. (2012). This method uses cumulative temperature-duration-frequency curves to evaluate events where the water temperature exceeds the given LT05 or LT50 threshold. Using the hindcasted temperatures and corresponding times, we produced a continuous time series for the upper Sabine River. We calculated the frequency of events by tallying continuous temperature events above either the LT05 or the LT50, summing them, then dividing by the total duration of the period of interest (Castelli et al. 2012, Khan et al. 2020, Goldsmith et al. 2021, Rangaswami et al. 2023b). Using the *segmented* package (version 2.0-2; Muggeo 2017) in R, we fit a 3-segment, piecewise linear regression to plotted UCAT values, identifying 2 inflection points. We used these 2 breakpoints to define durations as typical, persistent, or catastrophic (Castelli et al. 2012). Typical events occur multiple times a year for short durations and should have negligible consequences on biological processes. Persistent events occur every 2 to 3 y, only affecting a single generation. Catastrophic events should be rare in nature, having consequences that affect multiple generations (Castelli et al. 2012). We performed the UCAT method only on *C. pustulosa* 96-h LT05 exceedances. Neither *F. askewi* nor *P. riddellii* had enough records of thermal exceedance events that spanned continuous days to perform the UCAT analysis on any of their estimated thresholds.

Results/Synthesis

Mussels had generally higher mortality as temperature increased, but there were some differences among species in their sensitivity to higher temperatures. Mussel survivorship for controls across all trials and timepoints was 100%. During the 240-h experiment, *F. askewi* and *P. riddellii* both experienced 100% mortality in the 36°C and 39°C treatments and no mortality in the 30°C and 33°C temperature treatments. In contrast, *C. pustulosa* experienced 100% mortality at the 39°C treatment, 92% mortality at the 36°C treatment and 33% mortality in the 30°C and 33°C treatments. Across all timepoints, LT05 estimates of *C. pustulosa* ranged from 31.69 to 37.22°C with a mean \pm 95% CI of $34.50 \pm 1.87^\circ\text{C}$, and LT50 estimates ranged from 34.75 to 38.43°C with a mean \pm 95% CI of $36.06 \pm 1.36^\circ\text{C}$ (Table 1). For *F. askewi*, the LT05 estimates ranged from 34.17 to 36.83°C, with a mean \pm 95% CI of $34.99 \pm 0.97^\circ\text{C}$, and the LT50 estimates ranged from 34.29 to 37.47°C with a mean \pm 95% CI of $35.81 \pm 1.06^\circ\text{C}$. For *P. riddellii*, the LT05 estimates ranged from 34.17 to 36.83°C, with a mean \pm 95% CI of $35.08 \pm 1.05^\circ\text{C}$, and the LT50 estimates ranged from 34.29 to 37.47°C with a mean \pm 95% CI of $35.96 \pm 1.09^\circ\text{C}$.

CI ratio test comparisons of thermal tolerance estimates across species demonstrated no substantial differences between *C. pustulosa*, *F. askewi*, and *P. riddellii* for LT05 and LT50 estimates at 48, 96, or 120 h or for the LT05 at 240 h (Figure 3). There was strong evidence that *C. pustulosa* had a higher LT05 at 24 h and LT50 at 24 h and 240 h than *F. askewi* and *P. riddellii*.

by 1°C (Figure 3). Comparing the difference between LT05 and LT50 within species showed that *C. pustulosa* had the largest mean difference of 1.56°C. In contrast, for *F. askewi* and *P. riddellii*, the LT05 and LT50 estimates were more similar, with mean differences of 0.82°C and 0.89°C, respectively. Generally, LT05 and LT50 estimates declined with time for all species.

RF hindcasting

The RF model accurately predicted water temperature in the upper Sabine River, with 99.6% variance explained and a low mean square error (MSE = 0.04). Comparing logged water temperature data with the predicted random forest values showed high congruence except in winter months (December, January, and February). Specifically, differences between observed and predicted water temperature during all months except the winter months ranged from 0 to 2.69°C with a mean difference of 0.16°C (± 0.20 SD). During winter months, the difference ranged from 0 to 4.91°C with a mean difference of 0.17°C (± 0.26 SD), with the observed temperatures being higher than the predicted temperatures.

Thermal exceedances

Biological overlay

From January 2010 to December 2023, the hindcast/forecast daily maximum water temperatures of the upper Sabine River ranged from 0.46 to 34.25°C. The warmest temperature occurred in July of 2022 and the lowest occurred in February of 2021. Comparing LT05 thresholds for *C. pustulosa* with water temperature during this period showed exceedances for the 96-h and 120-h time periods (Table 2). During the spring/summer bioperiod, exceedance frequencies of the 96-h LT05 threshold (31.69°C) reached 17.8% (Table 2, Figure 4). For the total hindcasted period, the LT05 threshold had an exceedance frequency of 8% (Table 2, Figure 4). The 120-h LT05 threshold (33.16°C) was exceeded 1 d in 2014, 2 d in 2013, and 19 d in 2022, all during the months of June and July, with mean daily discharges of 1.43, 1.24, and 1.79 m³/s, respectively. For *F. askewi*, exceedances were observed for the 96-h and 240-h LT05 thresholds in the upper Sabine River. Specifically, the 240-h LT05 threshold (34.17°C) was exceeded on 2 d in July of 2022, and the 96-h LT05 threshold (34.22°C) was only exceeded once during the same month. During those exceedances, the mean daily discharge was 1.37 m³/s. No LT50 thresholds for any species in the upper Sabine River were exceeded within the hindcasted data. In the Sabine River, all threshold exceedances occurred within the bioperiod range

From February to October 2023, the daily maximum water temperatures of the LNVA Canal site ranged from 13.85 to 34.79°C. Water temperatures in the LNVA Canal exceeded *P. riddellii*'s 96-h, 120-h, and 240-h LT05 thresholds and the 240-h LT50 threshold (Table 2). The 120-h (34.22°C) and 240-h (34.17°C) LT05 thresholds (Table 1) were exceeded 10 d in 2023 over the months of June, July, and August. The mean daily maximum water temperature and mean water level during these exceedances was 34.39°C and 1.4 m, respectively. Of the 10 d, there was only 1 event where the thresholds were exceeded on 2 continuous days, 14 and 15 August 2023, which had a mean daily maximum water temperature of 34.53°C and a mean water level of 1.3 m. The 96-h LT05 threshold (34.35°C) and the 240-h LT50 threshold (34.29°C; Table 1) were exceeded on 1 d in July and 5 d in August. The 240-h LT05 threshold was exceeded 5.4% of the bioperiod, and the 240-h LT50 was exceeded ~½ that amount (3.3%; Table 2). In the LNVA Canal, all threshold exceedances occurred within the bioperiod range.

UCAT

From 2010 to 2023, the *C. pustulosa* 96-h LT05 estimate (31.69°C; Table 1) was exceeded on 425 d in 70 separate events and was able to be analyzed with the UCAT method. The piecewise linear regression identified 2 breakpoints defining catastrophic, persistent, and typical categories for the exceedances that occurred in our data period. Catastrophic events were identified as lasting 25 d or more, persistent events lasted 15 to 25 d, and typical events lasted <15 d (Table 3). The duration of exceedance events ranged from 1 to 31 continuous days. In this study, 2 catastrophic events were identified from the past 13 y. The longest event, which spanned 31 d, occurred from 10 July through 8 August 2018 and had mean daily temperatures of 32.38°C and mean daily discharge of 1.48 m³/s. The 2nd longest event lasted 30 d, from 7 July to 8 August 2016, with mean daily temperatures of 32.45°C and mean daily discharge of 2.55 m³/s. The mean maximum daily temperature and daily discharge during catastrophic events were 32.42°C and 2.01 m³/s, respectively (Table 3). Persistent events had a mean maximum daily temperature of 32.58°C and mean daily discharge of 1.94 m³/s (Table 3). Of the event classifications, typical events displayed the lowest mean maximum daily temperature (32.11°C) and highest mean daily discharge (2.29 m³/s) (Table 3).

Table 1. Upper lethal tolerance estimates (°C) at 5% mortality (LT05) and 50% mortality (LT50), and their associated 95% CIs, at each experimental timepoint for the species *Cyclonaias pustulosa*, *Fusconaia askewi*, and *Pleurobema riddellii* collected from the Sabine and Neches River basins in east Texas, USA.

Species	LT05					LT50				
	24 h	48 h	96 h	120 h	240 h	24 h	48 h	96 h	120 h	240 h
<i>C.</i>	37.22	35.31	31.69	33.16	35.11	38.43	36.73	34.75	34.76	35.62
<i>pustulosa</i>	(36.93– 37.51)	(35.30– 35.30)	(28.66– 34.71)	(31.02– 35.31)	(32.64– 37.58)	(37.98– 38.87)	(36.73– 36.73)	(33.72– 35.77)	(33.75– 35.76)	(34.47– 36.77)
<i>F. askewi</i>	36.83	35.21	34.22	34.52	34.17	37.47	36.48	35.51	35.32	34.29
	(36.73– 36.94)	(34.40– 36.00)	(33.98– 34.47)	(33.68– 35.35)	(33.90– 34.43)	(37.37– 37.57)	(35.99– 36.97)	(34.99– 36.02)	(35.25– 35.41)	(33.99– 34.59)
<i>P. riddellii</i>	36.83	35.81	34.35	34.22	34.17	37.47	36.86	35.68	35.51	34.29
	(36.73– 36.94)	(35.05– 36.57)	(33.98– 34.72)	(33.98– 34.47)	(33.90– 34.43)	(37.37– 37.57)	(36.19– 37.28)	(34.94– 36.42)	(34.99– 36.01)	(33.99– 34.59)

Table 2. Thermal exceedance frequencies over the total and spring/summer bioperiod periods of record for *Cyclonaias pustulosa* and *Fusconaia askewi* in the upper Sabine River and *Pleurobema riddellii* in the Lower Neches Valley Authority Canal in Texas, USA. The spring/summer bioperiod spans from March to August, during the biologically active time period when mussel reproduction and the highest thermal stress occurs. Only lethal tolerance (LT) thresholds that were exceeded in water temperatures are included in the table. LT05 = lethal tolerance at 5% mortality, LT50 = lethal tolerance at 50% mortality. For the Sabine River, thermal exceedances were calculated with hindcasted water temperature data derived from a random forest model. For the Lower Neches Valley Authority Canal, thermal exceedances were calculated with water temperature data measured by a logger.

Species	LT estimate		Total	Bioperiod	Period of record
	LT threshold	(°C)	exceedance	exceedance	
			frequency (%)	frequency (%)	
<i>C. pustulosa</i>	96-h LT05	31.69	8.38	17.77	January 2010–December 2023 (hindcast)
	120-h LT05	33.16	0.43	0.92	
<i>F. askewi</i>	96-h LT05	34.22	0.02	0.04	February 2023–October 2023 (logger)
	240-h LT05	34.17	0.04	0.08	
<i>P. riddellii</i>	96-h LT05	34.35	2.63	3.26	
	120-h LT05	34.22	4.39	5.43	
	240-h LT05	34.17	4.39	5.43	
	240-h LT50	34.29	2.63	3.26	

Table 3. Water temperature and discharge data for catastrophic, persistent, and typical exceedance events for 96-h lethal tolerance at 5% mortality (LT05) thermal tolerance threshold of *Cyclonaias pustulosa* in the Sabine River, Texas, USA, from 2010 to 2023. Values are mean (min–max).

Event type	Duration (d)	Mean maximum daily temperature (°C)	Mean daily discharge (m ³ /s)
Catastrophic	>25	32.42 (32.38–32.45)	2.01 (1.47–2.55)
Persistent	15–25	32.58 (32.03–33.08)	1.94 (1.52–2.63)
Typical	<15	32.11 (31.69–32.98)	2.29 (0.89–4.25)

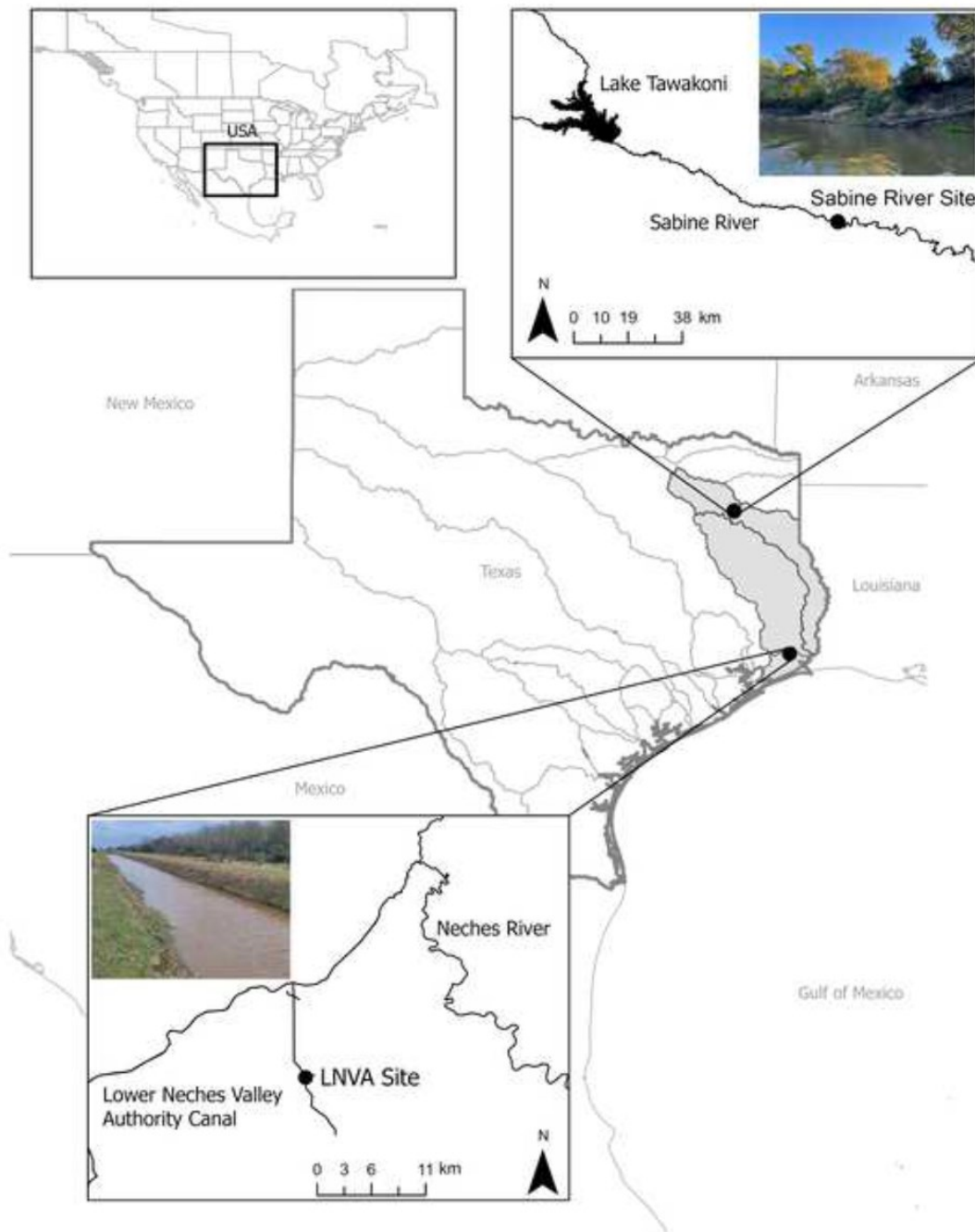


Figure 1. Map of study area showing locations of collection sites on the Sabine River (Sabine River site; upper righthand inset) and Lower Neches Valley Authority Canal (LNVA site; lower lefthand inset) in Texas, USA. The inset in the upper lefthand corner shows the location of Texas within the United States.

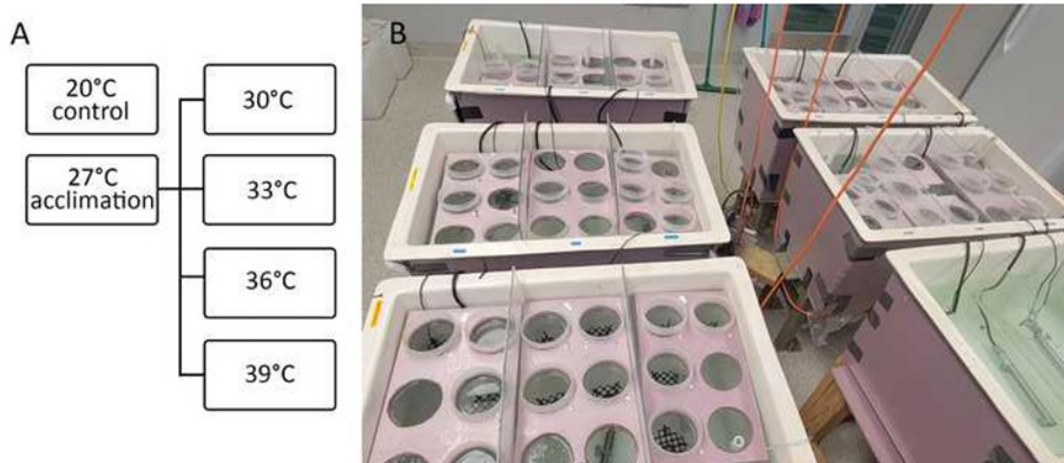


Figure 2. Experimental design following Khan et al. (2020) showing the control, acclimation, and experimental temperatures (A) and the experimental setup (B). The experimental setup included 5 fiberglass tanks, each assigned an experimental or control temperature and partitioned into 3 replicates by watertight acrylic sheets sealed with silicone. Individual mussels were placed in plastic containers modified with 10-mm-mesh bottoms

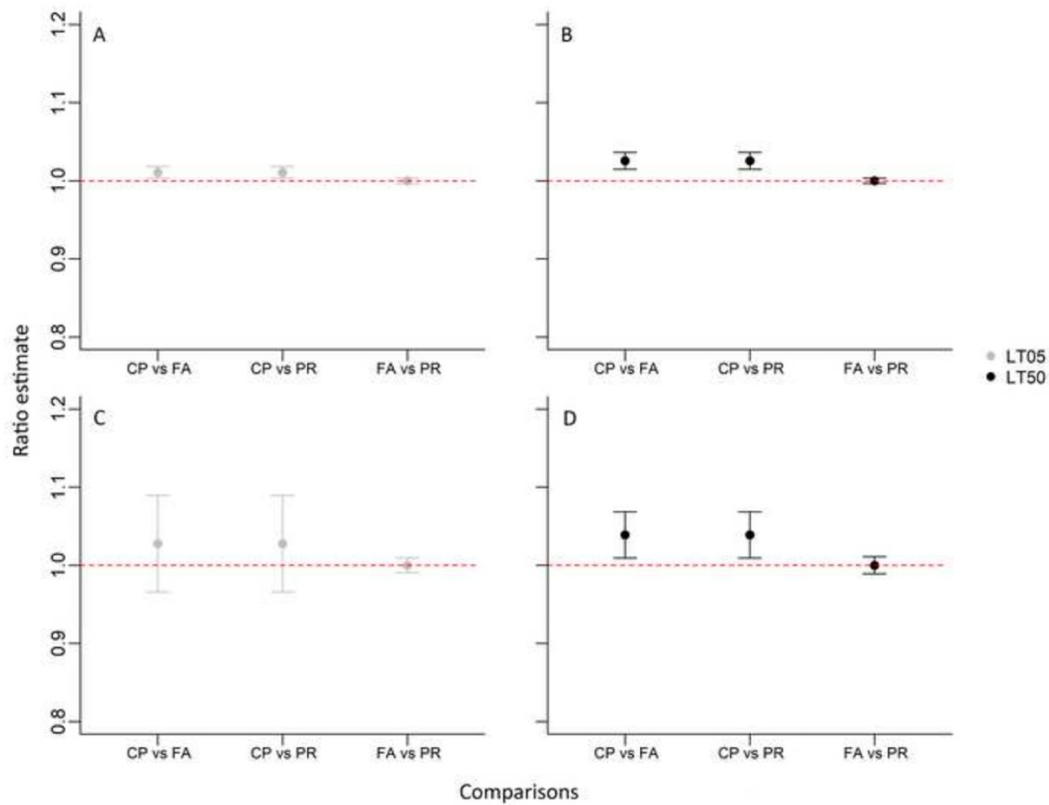


Figure 3. CI ratio estimates for comparisons between *Cyclonaias pustulosa* (CP), *Fusconaia askewi* (FA), and *Pleurobema riddellii* (PR) for the following treatments: 24-h lethal tolerance at 5% mortality (LT05) (A), 24-h lethal tolerance at 50% mortality (LT50) (B), 240-h LT05 (C), and 240-h LT50 (D). Error bars represent the 95% CI of the ratio. CI ratios that do not contain the value of 1, represented by a red dashed line, denote differences between the LT05 or LT50 estimates, whereas CIs that contain 1 denote similar LT05 or LT50 estimates.

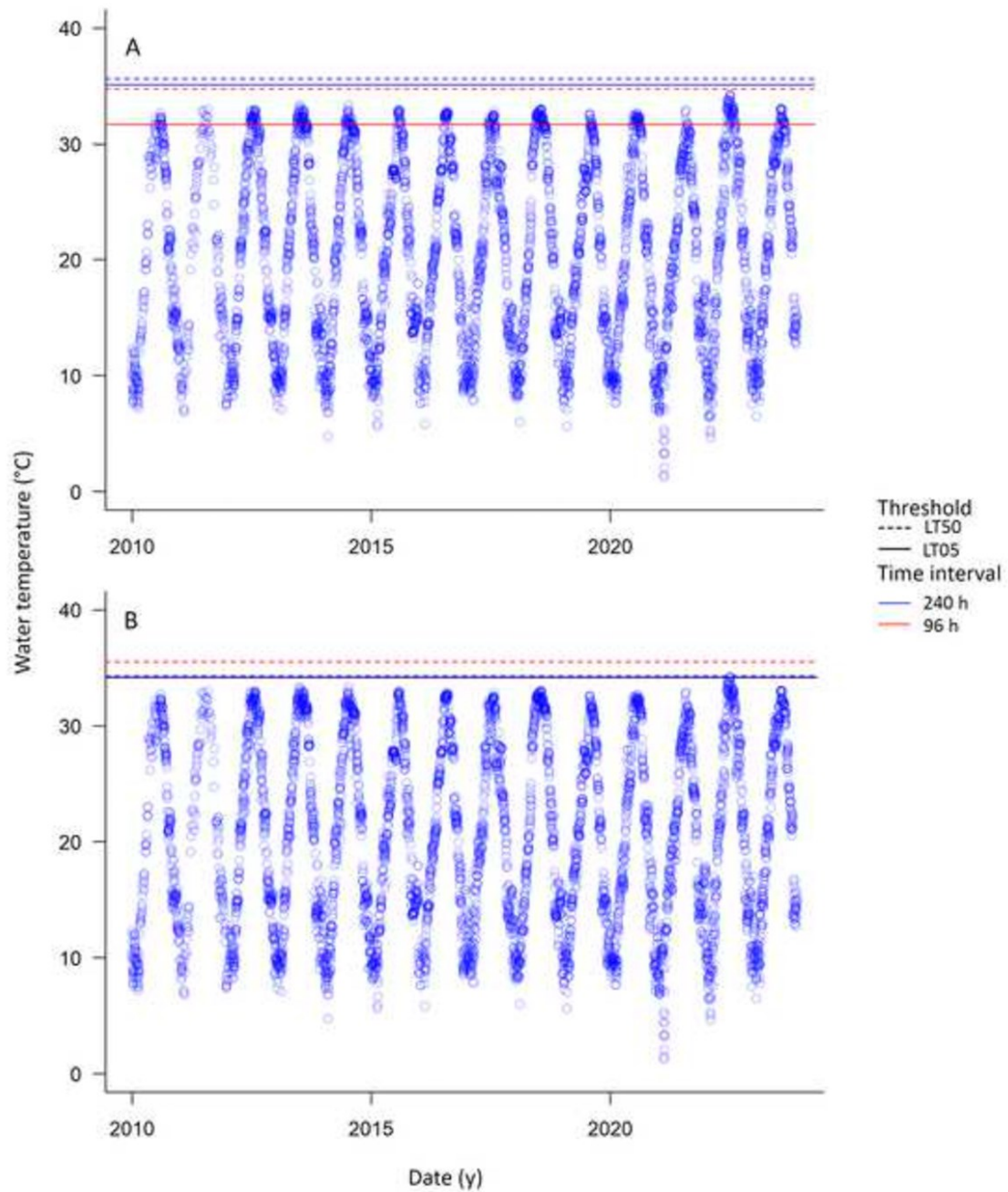


Figure 4. Maximum daily water temperature from January 2010 to December 2023 in the Sabine River overlain with thermal tolerance data at the 96-h and 240-h timepoints for *Cyclonaias pustulosa* (A) and *Fusconaia askewi* (B). Blue circles indicate maximum water temperature (°C). Red and blue lines represent the 96-h and 240-h estimates, respectively. Solid and dashed lines represent lethal tolerances at 5% mortality (LT05) and 50% mortality (LT50), respectively.

Literature Cited

- ASTM International. 2006. Standard guide for conducting laboratory toxicity tests with freshwater mussels. E2455-06. *In* Annual book of ASTM standards (volume 11.06). ASTM International, West Conshohocken, Pennsylvania.
- Castelli, E., P. Parasiewicz, and J. N. Rogers. 2012. Use of frequency and duration analysis for the determination of thermal habitat thresholds: Application for the conservation of *Alasmidonta heterodon* in the Delaware River. *Journal of Environmental Engineering* 138:886–892.
- Clusella-Trullas, S., R. A. Garcia, J. S. Terblanche, and A. A. Hoffmann. 2021. How useful are thermal vulnerability indices? *Trends in Ecology & Evolution* 36:1000–1010.
- Dewitz, J. 2021. National Land Cover Database (NLCD) 2019 Products. Version 2.0. Data Release. Earth Resources Observation and Science (EROS) Center, United States Geological Survey, Sioux Falls, South Dakota. (Available from: <https://www.usgs.gov/data/national-land-cover-database-nlcd-2019-products-ver-30-february-2024#publications>)
- Goldsmith, A., J. M. Khan, C. R. Roberston, R. Lopez, and C. R. Randklev. 2021. Using upper thermal limits of *Lampsilis bracteata* (Texas Fatmucket) from the North Llano and San Saba rivers, Texas to inform water management practices in the Edwards Plateau. *Aquatic Conservation: Marine and Freshwater Ecosystems* 32:85-97.
- Griffith, G., S. Bryce, J. Omernik, and A. Rogers. 2007. Ecoregions of Texas. Texas Commission on Environmental Quality, Austin, Texas. (Available from: https://gaftp.epa.gov/epadatacommons/ORD/Ecoregions/tx/TXeco_Jan08_v8_Cmprsd.pdf)
- Gu, R. R., and Y. Li. 2002. River temperature sensitivity to hydraulic and meteorological parameters. *Journal of Environmental Management* 66:43–56.
- Harrel, R. C., and M. A. Hall III. 1991. Macrobenthic community structure before and after pollution abatement in the Neches River estuary (Texas). *Hydrobiologia* 211:241–252.
- Johnson, N. A., C. E. Beaver, A. H. Kiser, M. A. Duplessis, M. D. Wagner, R. J. Ellwanger, C. R. Robertson, S. D. Kinney, B. B. Gregory, S. Wolverton, C. R. Randklev, P. D. Hartfield, J. D. Khan, J. M., J. Dudding, M. Hart, C. R. Robertson, R. Lopez, and C. R. Randklev. 2020. Linking flow and upper thermal limits of freshwater mussels to inform environmental flow benchmarks. *Freshwater Biology* 65:2037–2052.
- Larkin, T., and G. W. Bomar. 1983. Climatic Atlas of Texas. Texas Department of Water Resources, Austin, Texas.

- Liaw, A., and M. Wiener. 2002. Classification and Regression by randomForest. *R News* 2:18-22.
- Muggeo, V. M. R. 2017. Interval estimation for the breakpoint in segmented regression: A smoothed score-based approach. *Australian & New Zealand Journal of Statistics* 59:311–322.
- Randklev, C. R., C. R. Robertson, C. H. Smith, A. H. Kiser, N. B. Ford, M. Hart, J. M. Khan, M. Fisher, and R. R. Lopez. 2023. Mussels of Texas Project Database. Version 2.0.
- Rangaswami, X. L., A. H. Kiser, M. Ramey, J. A. Stoeckel, D. J. Berg, R. R. Lopez, and C. R. Randklev. 2023b. Thermal tolerance exceedances of an endangered unionid mussel in the Rio Grande Basin, with implications for river management. *Aquatic Conservation: Marine and Freshwater Ecosystems* 33:1431–1444.
- Smith, M. E., L. E. Herrin, W. T. Thoeny, J. M. Lazorchak, and S. Brewer-Swartz. 1997. A reformulated, reconstituted water for testing the freshwater amphipod, *Hyalella azteca*. *Environmental Toxicology and Chemistry* 16.
- Texas A&M Natural Resources Institute. 2020. Texas land trends: A database of compiled and analyzed values for working lands in Texas. Texas A&M Natural Resources Institute, College Station, Texas. (Available from: <https://txlandtrends.org/>)
- Toffolon, M., and S. Piccolroaz. 2015. A hybrid model for river water temperature as a function of air temperature and discharge. *Environmental Research Letters* 10:114011.
- Wheeler, M. W., R. M. Park, and A. J. Bailer. 2006. Comparing median lethal concentration values using confidence interval overlap or ratio tests. *Environmental Toxicology and Chemistry* 25:1441–1444.

Part II. Laboratory bioassays to evaluate thermal, ammonia, and hypoxia tolerances and limits for the Louisiana Pigtoe.

Contributing authors: Stoeckel JA, H Adkins, and E. Blackwell

Study objectives

Study objectives were to estimate acute thermal tolerance of adult *P. riddellii* using sublethal and lethal endpoints, to estimate sublethal sensitivity of adult *P. riddellii* to hypoxia, and determine whether sensitivity changes with warming temperature, and to estimate sublethal sensitivity of adult *P. riddellii* to ammonia.

Methods

Adult *P. riddellii* (Louisiana Pigtoe) were collected from the canal in the lower Neches River drainage on Sept. 19, 2020 when canal temperatures were ~28.5 C. Mussels were placed in a cooler sandwiched between moist paper towels with a few small ice packs and shipped overnight to Auburn University. Shipping was delayed by a day and arrived at Auburn on Sept. 21st. Cooler temperature was 25 °C. Upon receipt of the mussels at Auburn University, it was determined that two individuals experienced mortality during the shipping process. Mussels were transferred to upwellers containing artificial freshwater at 18°C for > 2 weeks prior to experiments.

For reference, various endpoints of *P. riddellii* are currently being compared to those of *Lampsilis straminea*, collected from a captive population in earthen ponds at Auburn University in 2024, *Cyclonaias pustulosa* collected from the same site as *P. riddellii*, and six *Fusconaia iheringi* collected from the San Gabriel River in 2024 as part of a separate ongoing project. The initial batch of *C. pustulosa* was collected and shipped to Auburn on August 25, 2023. This shipment was delayed in transit for several days, arriving on the 28th. The cooler was noticeably warm and four *C. pustulosa* were confirmed dead on arrival. Initial survivors exhibited high mortality over the following 3 weeks. A second shipment of *C. pustulosa* was sent on November 6th, 2023 and arrived the next day. All mussels survived the second shipment. Analysis of thermal and hypoxia tolerance assays is in progress and being used to compare results of a common allopatric (*L. straminea*), a common sympatric species (*C. pustulosa*), and a rare Texas endemic (*F. iheringi*) to those of *P. riddellii*. Some preliminary comparisons have been completed and are included in this report. We also took advantage of the shipment problems with *C. pustulosa* to test for effects of stressful shipping conditions on measured endpoints.

Objective 1: Acute Thermal Stress: Following collection, experimental animals were acclimated to a baseline temperature of 25°C for two weeks. After two weeks, individuals were placed in respiration chambers and allowed to acclimate to each chamber overnight. The following day, temperature was increased at a rate of 2°C/hr and respiration rate measured every 30 minutes. An additional subset of mussels were placed in open cups and exposed to the same increasing thermal regime as in the respirometry experiment. These were observed for multiple behavioral signs of thermal stress (i.e. foot extension, gaping, loss of response to probing) and critical

thermal maxima (CTMax) defined as the temperature at which mussels are gaping and do not respond to probing (modified from Galbraith et al. 2012).

Objective 2: Sublethal Hypoxia Stress: Sublethal hypoxia stress in adults was assessed using similar methodology as in Haney et al. (2020). Mussels were acclimated to lab conditions at 25°C or 32°C for ≥ 2 weeks. Following this period, mussels were fasted for 24 h and acclimated to respirometry chambers overnight. The next morning, respirometry chambers were closed and respiration rates measured as DO declined in the chambers. Respiration under normoxic conditions was calculated as the mean respiration rate of unfed mussels while dissolved oxygen levels were at $>80\%$ saturation. Regulation index and DO_{crit} were calculated following the methods of Mueller and Seymour (2011). In general, a higher DO_{crit} and a lower RI are considered indicative of reduced hypoxia tolerance. A higher respiration rate is indicative of increased energy demand.

Pleurobema riddellii appeared to be much more sensitive to disturbance than the two common species as well as previous mussel species we have worked with. They frequently closed for extended periods of time, making analysis of respiration data for DO_{crit} and RI difficult or impossible for most individuals. We therefore switched from running *P. riddellii* trials during the daytime to running trials on weekends during the nighttime hours. By minimizing disturbances and running trials primarily at night and/or on the weekends we were able to obtain useable results for 4-6 *P. riddellii* at each temperature.

Objective 3: Sublethal Effects of Ammonia: The proposed experimental design called for a screening study in which we gradually increased ammonia concentrations while measuring respiration at two temperatures. In this way we would be able to establish the ammonia threshold beyond which respiration is affected, as well as to test effects of temperature on this threshold. However, due to the frequent closing behavior of *P. riddellii* we were not able to follow this protocol. Mussels would close frequently in both the control and exposure treatments. This prevented us from determining the threshold beyond which the respiration rate of an individual changed because when mussels were closed, they avoided exposure to ammonia. Also, because they also closed frequently in the control, we could not use closure behavior as a surrogate endpoint to respiration when assessing effects of a relatively short ammonia ramp. We therefore switched to a “ramp and hold” design wherein we would ramp the ammonia concentration to a predetermined concentration and then hold it steady for ~ 24 hours during which we could measure respiration when the mussels did open.

Results

Objective 1: Acute Thermal Stress: A spline was fitted through a plot of respiration versus temperature for *P. riddellii* and *C. pustulosa*. Respiration increased relatively slowly with increasing temperature for both species until $\sim 34^\circ\text{C}$ for *P. riddellii* and 36°C for *C. pustulosa*, after which it increased rapidly. Interestingly, six of ten *P. riddellii* extended their foot (mean = 39.3°C) just before gaping (mean = 39.9°C) whereas *C. pustulosa* never exhibited foot extension prior to six of ten gaping (mean = 40.5°C). In *P. riddellii*, respiration rate continued to increase

until mussels reached CTMax, whereas for *C. pustulosa*, respiration rates declined prior to reaching CTMax. (Fig. 1A, B). CTMax was significantly higher for *C. pustulosa* compared to either the normal or the stressed shipment compared to *P. riddellii* (Dunn's post-hoc comparison; $p = 0.010$ and 0.022 respectively). CTMax did not significantly differ in *C. pustulosa* between the normal and stressed shipment (Dunn's post-hoc comparison; $p = 1.000$) (Fig. 2).

Objective 2: Sublethal Hypoxia Stress: Mean respiration at normoxia (dissolved oxygen concentrations $>80\%$ saturation) increased from $0.00821 \text{ mg/gWW/hr} \pm 0.0009 \text{ SE}$ at 25°C to 0.00977 ± 0.00174 at 32°C . However the difference was not significant (T-test; $p = 0.41$), likely due to a combination of small sample size and variation amongst individuals at each temperature (Fig. 3).

The critical dissolved oxygen concentration (DO_{crit} : DO threshold below which organisms switch from predominantly aerobic to anaerobic respiration) for *P. riddellii* showed no significant change with increasing temperature ($t = 1.532$, $p = 0.164$). Thus, there was no evidence that sensitivity to hypoxia increased as temperatures increased from 25 to 32°C . The mean DO_{crit} remained between 1 and $1.5 \text{ mg O}_2/\text{L}$ at both temperatures (Fig. 4A). Unlike *P. riddellii*, the DO_{crit} of *L. straminea* was significantly lower at 32°C than 25°C ($t = 92.5$, $p = 0.048$). However, because of the direction of the change (i.e. DO_{crit} decreased rather than increased with temperature), *L. straminea* was similar to *P. riddellii* in that that sensitivity to hypoxia did not increase with temperature. Also similar to *P. riddellii*, mean DO_{crit} was between 1.0 and $1.5 \text{ mg O}_2/\text{L}$ at both temperatures. Mean DO_{crit} of *C. pustulosa* did not differ between temperatures ($t = 1.384$, $p = 0.194$) and remained between 1.2 and $0.8 \text{ mg O}_2 / \text{L}$ at both temperatures.

The regulation index (RI: the ability to maintain a constant respiration rate as dissolved oxygen declined) of *P. riddellii* did not differ significantly between the two temperatures ($t = -0.449$, $p = 0.666$), providing additional evidence that sensitivity to hypoxia did not increase as temperature increased from 25 to 32°C . At each temperature, mean RI remained between 0.50 and 0.55 (Fig. 5A). Similarly, RI of *L. straminea* did not change significantly with temperature ($t = -2.002$, $p = 0.064$), nor did that of *P. pustulosa* ($t = 1.839$, $p = 0.0931$) (Fig. 5B).

When comparing DO_{crit} and RI among three species at 25°C , we found no difference in DO_{crit} among the species (ANOVA, $F = 1.325$, $p = 0.292$). However, the mean RI of *C. pustulosa* was significantly higher than that of *P. riddellii* or *F. iheringi*. This provides some evidence for increased sensitivity of the two rare species (*P. riddellii* and *F. iheringi*) to hypoxia compared to that of a more common sympatric species (*C. pustulosa*) (Fig. 6).

Objective 3: Sublethal Effects of Ammonia: During the first trial we ramped and then held the total ammonia nitrogen (TAN) concentration to $2.67 \text{ mg TAN} / \text{L} \pm 0.34$. However, because mussels exhibit an elevated respiration rate (MO_2) after reopening – which then decreases and stabilizes at a lower rate – results of this trial were highly variable in the control and exposure treatment (Fig. 7 A). We therefore modified our water sampling protocol experiment in an attempt to reduce disturbance events and subsequent closures during a trial. In the second trial, we ramped and held TAN to $3.91 \text{ mg TAN} / \text{L} \pm 0.05$ and followed the modified sampling

protocol. This decreased the variability of our data as shown by the decreased coefficient of variation in both the control and exposure treatment of trial 2 (Fig. 7B) compared to that of trial 1 (Fig. 7A). Results of both trials showed a lower mean respiration rate in exposed mussels compared to the controls (Fig. 7A,B). However, there was not a significant difference in mean MO_2 (mg O_2 /kg/hr) between the treatment (N=9) and control (N=8) groups ($t=-0.784$, $df=16$, $p=0.445$) in the first trial (Fig. 7A). There was also not a significant difference in mean MO_2 (mg O_2 /kg/hr) between the treatment (N=6) and control (N=6) groups ($t=-1.287$, $df=11$, $p=0.227$). There was a trend of increased valve closures by mussels exposed to ammonia compared to control mussels at both concentrations (Fig. 8A,B). We are continuing to work with the dataset to account for closure effects and will include updated results in the manuscript versions of these studies.

Synthesis

When exposed to acute thermal stress, *P. riddellii* reached its CTMax (i.e. functional death) at a significantly lower temperature than a common sympatric species (*C. pustulosa*). The behavioral and physiological responses of *P. riddellii* to acute thermal stress differed from that of *C. pustulosa* in that sublethal behavioral stress endpoints (foot extension and gaping) of *P. riddellii* occurred while respiration rates were still increasing whereas *C. pustulosa* gaped when respiration rates had peaked, and did not extend their foot. Respiration rates were still increasing when *P. riddellii* reached CTMax whereas respiration rates were decreasing as *C. pustulosa* reached CTMax. Whether or not these differences in response are robust predictors of differences in acute thermal tolerance will require comparisons among additional species. However, metabolic depression (reduced respiration rate) has previously been identified as a compensatory response of bivalves to thermal stress (Anestis et al., 2007), and the reduction in respiration rate prior to reaching CTMax by *C. pustulosa* may help explain its higher tolerance of acute thermal stress relative to *P. riddellii*.

Similar to a common sympatric (*C. pustulosa*) and a common allopatric (*L. straminea*) species, we found no evidence that sensitivity of *P. riddellii* to hypoxia increased with temperature. Increased sensitivity would have been indicated by an increase in DOcrit and a decrease in RI. However neither metric declined between 25 and 32°C for *P. riddellii* or *C. pustulosa*. DOcrit did change in *L. straminea*, but declined, rather than increased, suggesting a decrease in hypoxia sensitivity with increasing temperature for that species. Although hypoxia sensitivity did not change with temperature for *P. riddellii*, the RI estimates for *P. riddellii* and for a rare Texas endemic (*F. iheringi*) were significantly lower at 25°C compared to the RI of *C. pustulosa*. This provides some evidence that *P. riddellii* is generally more sensitive to hypoxia than the more common *C. pustulosa*.

There was evidence that TAN caused sublethal stress to *P. riddellii*. We observed a trend of decreased respiration rates and increased number of valve closure events for *P. riddellii* at TAN concentrations of 2.7 and 3.9 mg/L compared to control conditions. However, the greater tendency of *P. riddellii* to close under laboratory conditions compared to other bivalve species we have worked with made it difficult to determine the severity of these effects. We are currently working with the dataset to further improve our ability to assess sublethal effects of TAN on physiological (respiration) and behavioral (valve closure) endpoints.

On a final note, there is always concern that despite following proven protocols, stress during shipping may affect response of mussels to subsequent behavioral and physiological assays in the laboratory. We took advantage of an unexpected, stressful, shipping event to test this concern but found no difference in CT_{max} estimates from *C. pustulosa* that experienced high post-shipment mortality due to a shipping delay during the heat of August and those from a subsequent shipment in November that exhibited 100% survival. Thus, we found no evidence that major stress associated with a problematic shipment from Texas to Alabama had an impact on assay results. Even so, we recommend minimizing stress as much as possible during shipping and subsequent holding in the laboratory.

Literature Cited

- Anestis, A., Lazou, A., Pörtner, H. O., & Michaelidis, B. (2007). Behavioral, metabolic, and molecular stress responses of marine bivalve *Mytilus galloprovincialis* during long-term acclimation at increasing ambient temperature. *American Journal of Physiology. Regulatory, Integrative and Comparative Physiology*, 293(2), R911-921.
<https://doi.org/10.1152/ajpregu.00124.2007>
- Galbraith, H. S., Blakeslee, C. J., & Lellis, W. A. (2012). Recent thermal history influences thermal tolerance in freshwater mussel species (Bivalvia:Unionoida). *Freshwater Science*, 31(1), 83–92. <https://doi.org/10.1899/11-025.1>
- Haney, A., Abdelrahman, H., & Stoeckel, J.A. (2020). Effects of thermal and hypoxic stress on respiratory patterns of three unionid species: implications for management and conservation. *Hydrobiologia*, 847, 787-802.
- Mueller, C.A., & Seymour, R.S. 2011. The Regulation Index: A new method for assessing the relationship between oxygen consumption and environmental oxygen. *Physiological and Biochemical Zoology*, 84(5), 522-532.

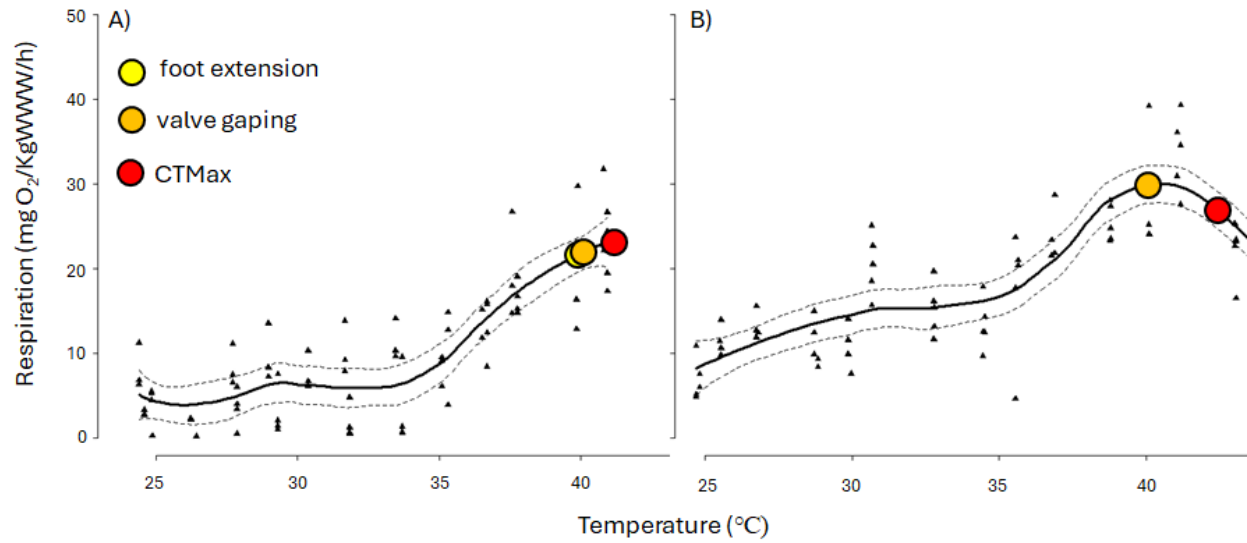


Figure 1. Spline showing changes in respiration rate with increasing temperature for A) *P. riddellii* and B) *C. pustulosa* (normal shipment). Dotted lines represent upper and lower 95% CI for each spline. Triangles represent data for each individual mussel. Circles represent behavioral endpoints. Temperature was increased at a rate of 2°C/hr.

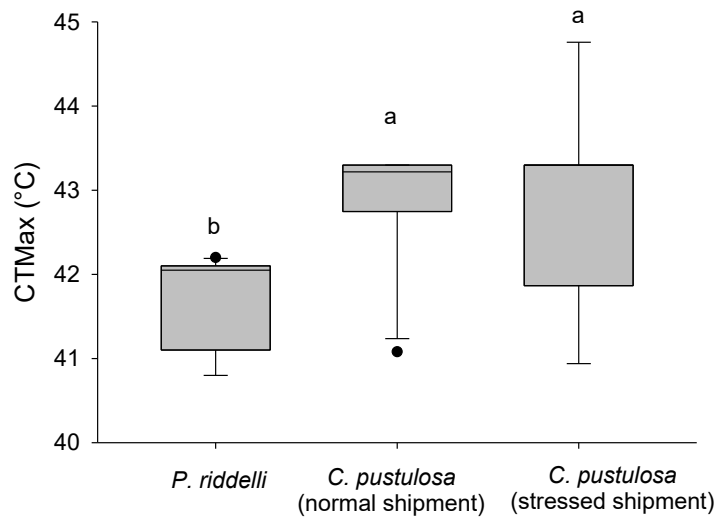


Figure 2. Critical thermal maximum as defined by gaping and no response to probing for *P. riddelli* and *C. pustulosa*. The “stressed shipment” data is for *C. pustulosa* that arrived several days late in a hot cooler and suffered heavy mortality within a few days of arrival. Lower case letters indicate a significant difference between groups.

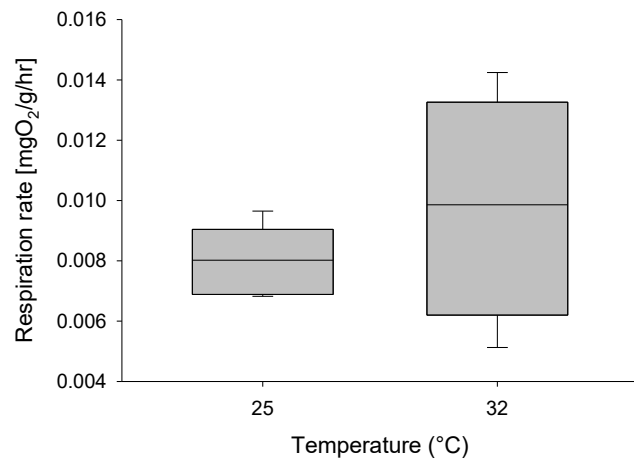


Figure 3. Respiration rate of *P. riddellii* under normoxic conditions at two temperatures.

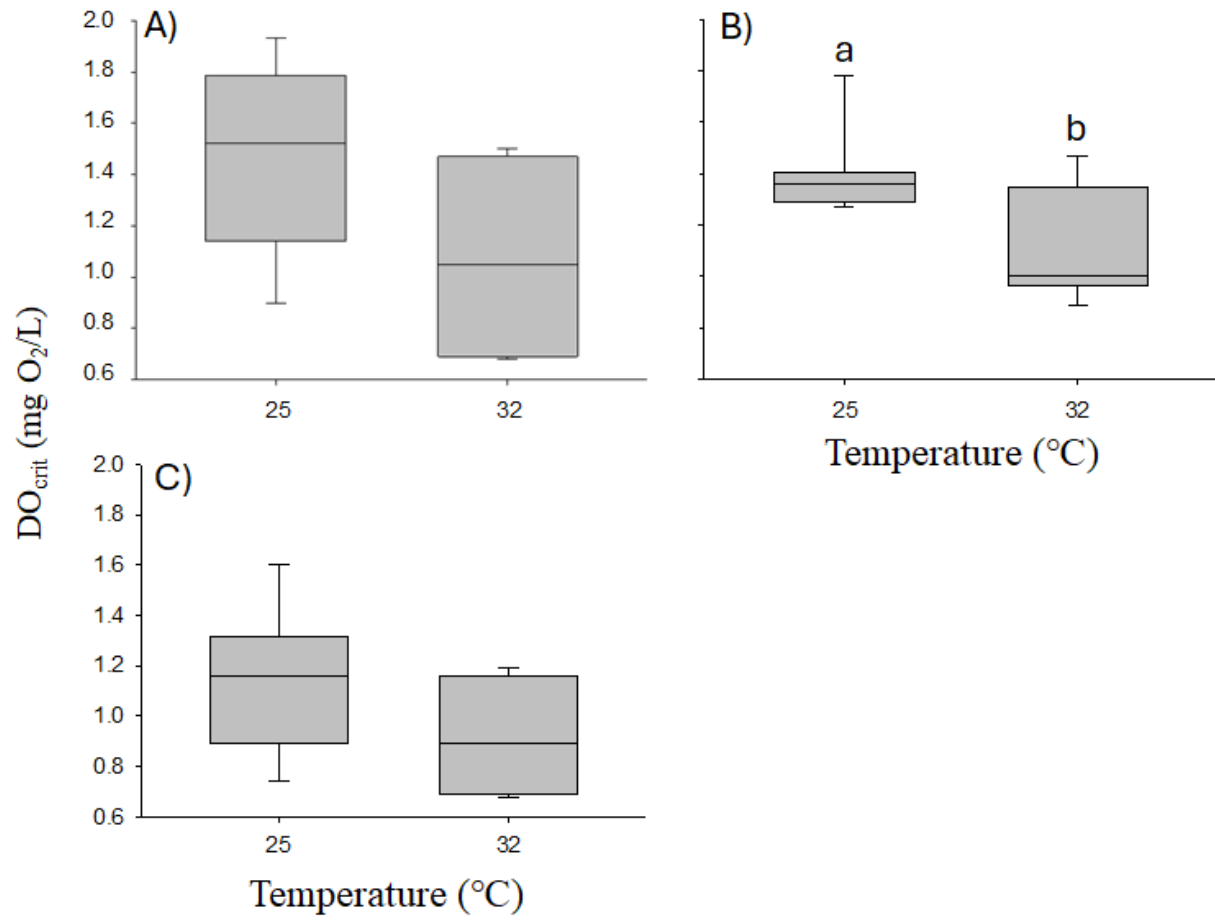


Figure 4. Critical dissolved oxygen concentration of A) *P. riddellii*, B) *L. straminea*, and C) *P. pustulosa* acclimated to 25 or 32°C. Lower case letters indicate significant differences between temperatures for a given species.

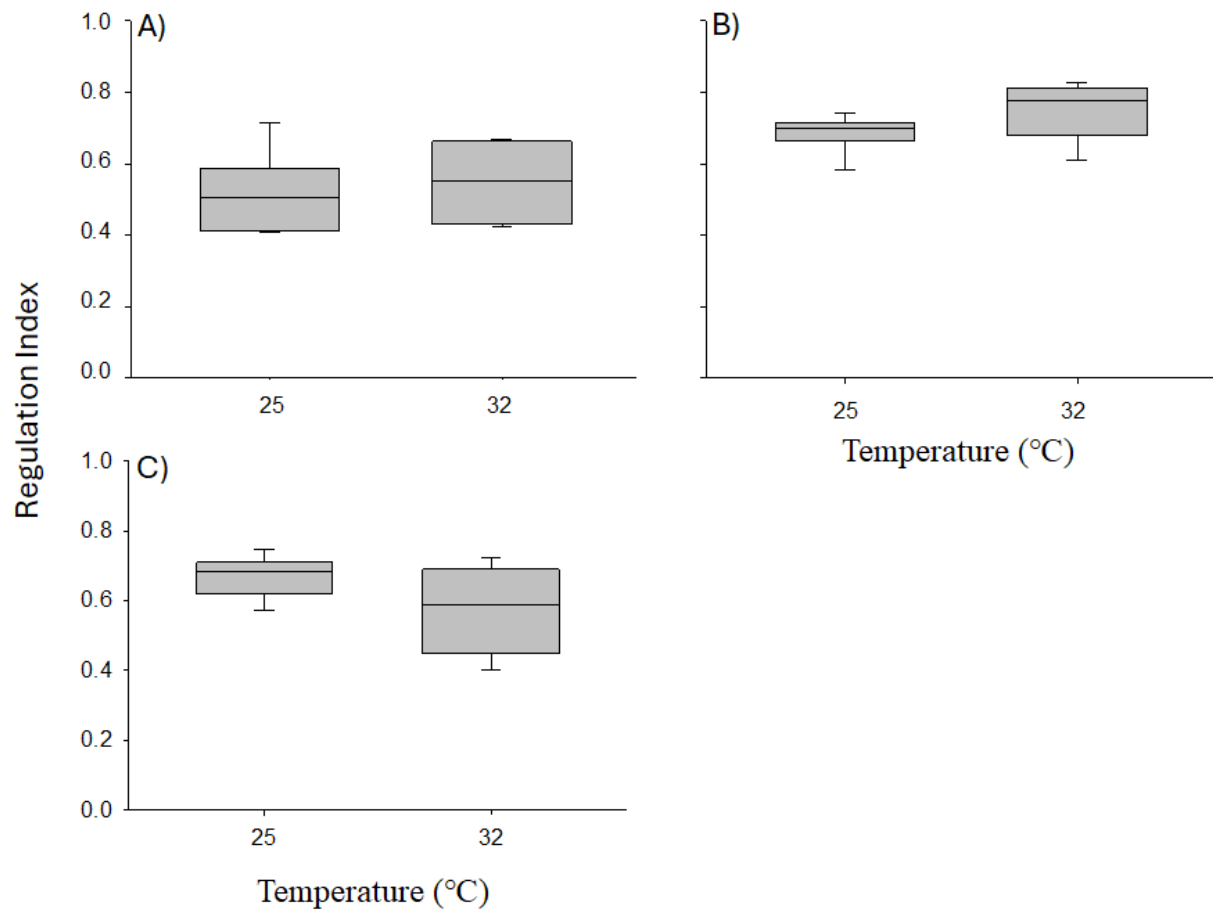


Figure 5. Regulation index of A) *P. riddellii* B) *L. straminea*, and C) *C. pustulosa* acclimated to 25 or 32°C.

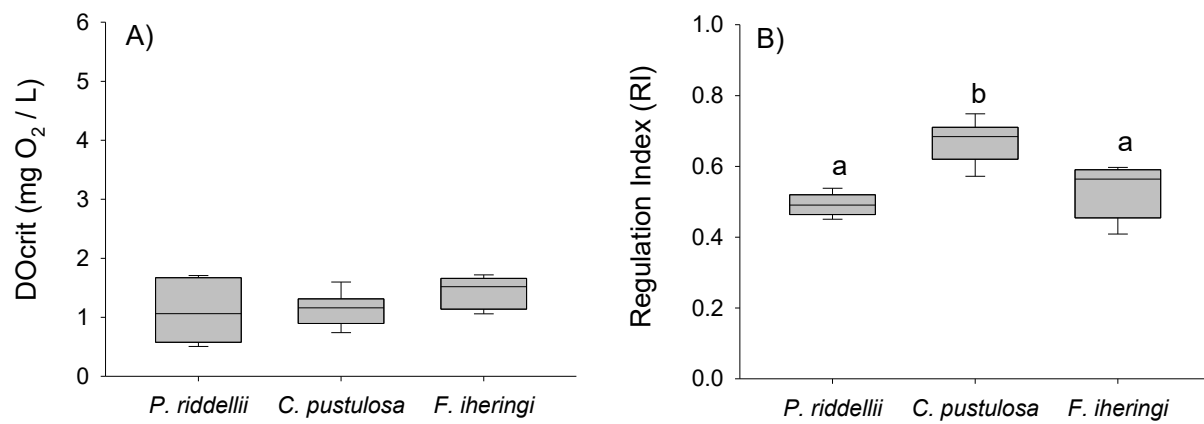


Figure 6. Comparison of A) DOcrit and B) Regulation Index among three species measured at 25 °C. Lower case letters indicate significant differences among species.

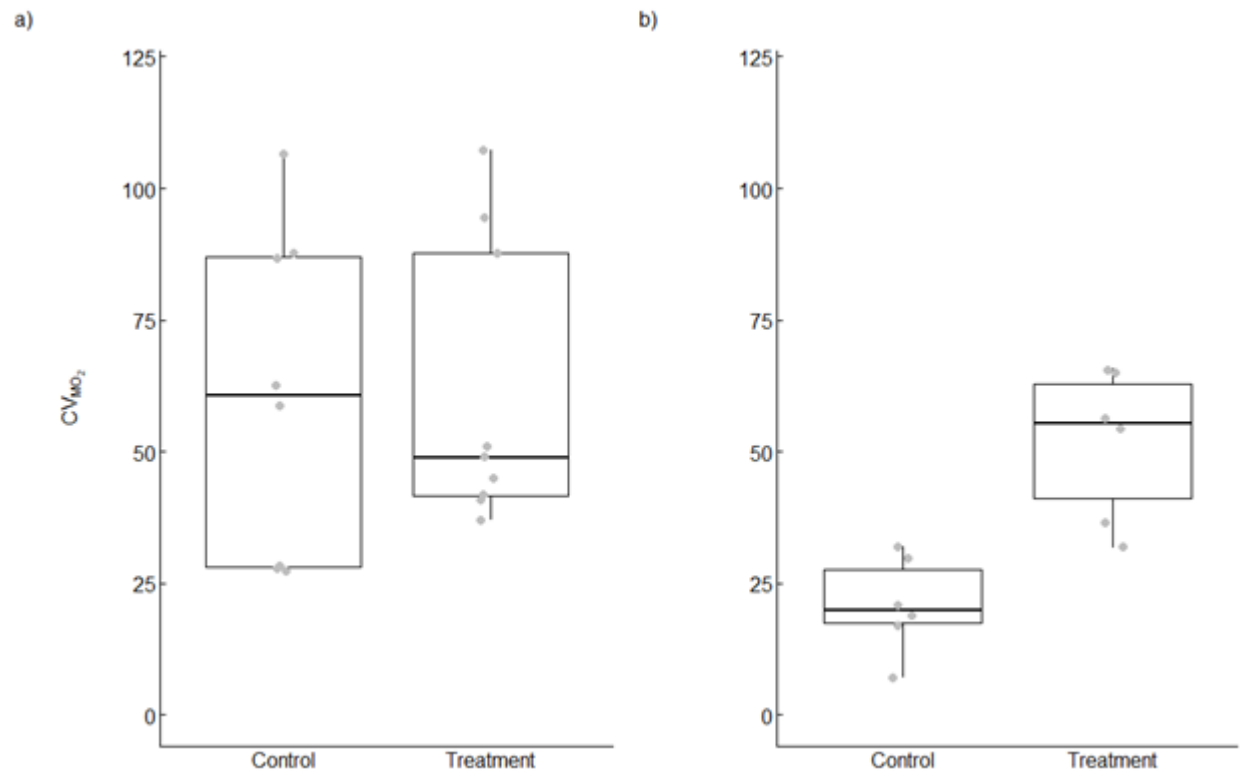


Figure 7. Coefficient of variation (CV) in mean respiration rates (mg O₂/kg/hr) of individual *P. riddelli* in experiments where the treatment group was exposed to a) 2.7 mg TAN/L and b) 3.9 mg TAN/L.

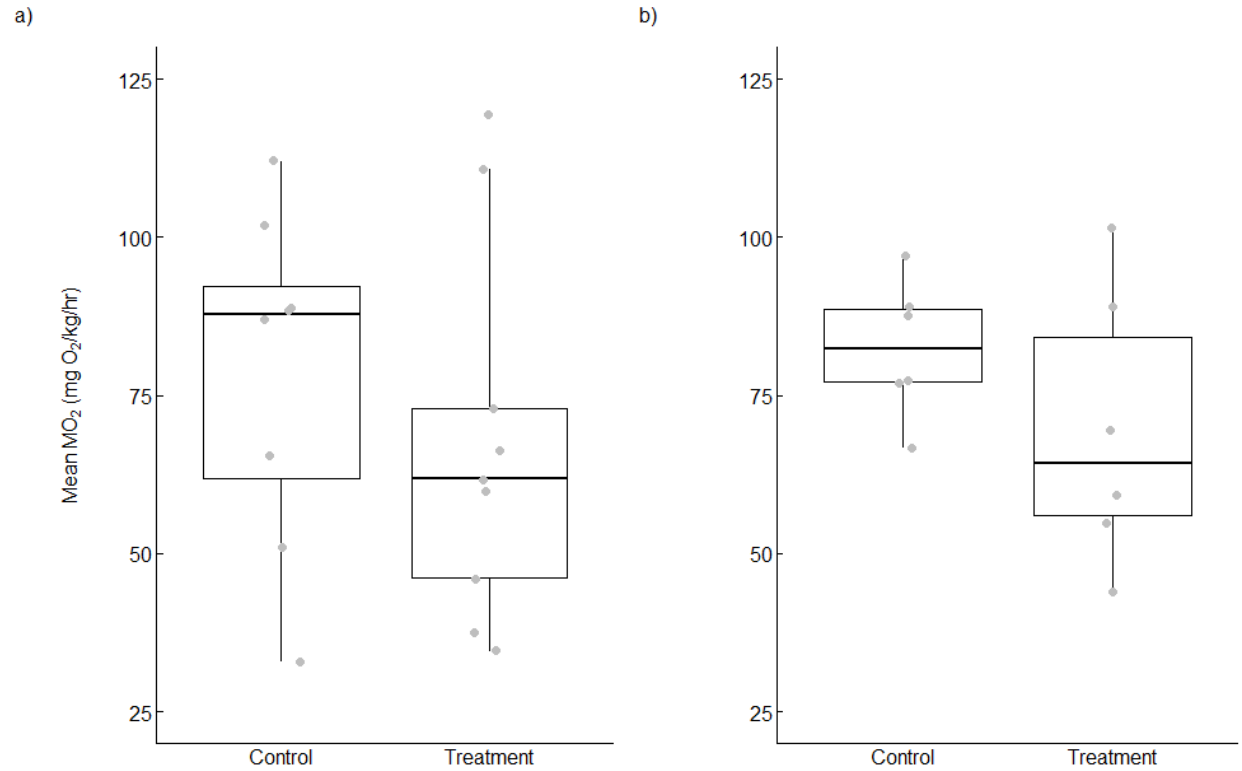


Figure 8. Mean MO_2 (mg O_2 /kg/hr) for individuals in experiments where the treatment group was exposed to a) 2.7 mg TAN/L and b) 3.9 mg TAN/L. No significant difference was observed between the control and treatment groups for either the lower ($t = -0.784$, $df = 16$, $p = 0.445$) or higher ammonia exposures ($t = -1.287$, $df = 11$, $p = 0.227$).

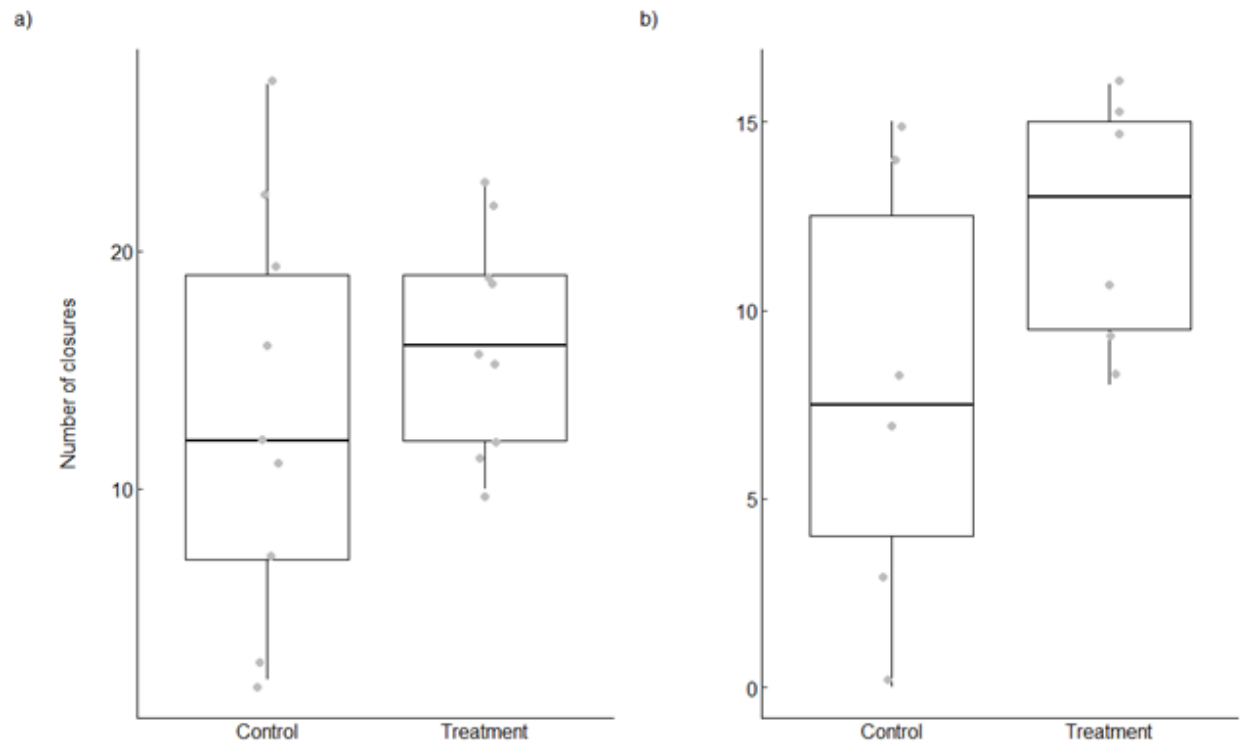


Figure 9. Number of closures for individuals in experiments where the treatment group was exposed to a) 2.7 mg TAN/L and b) 3.9 mg TAN/L.

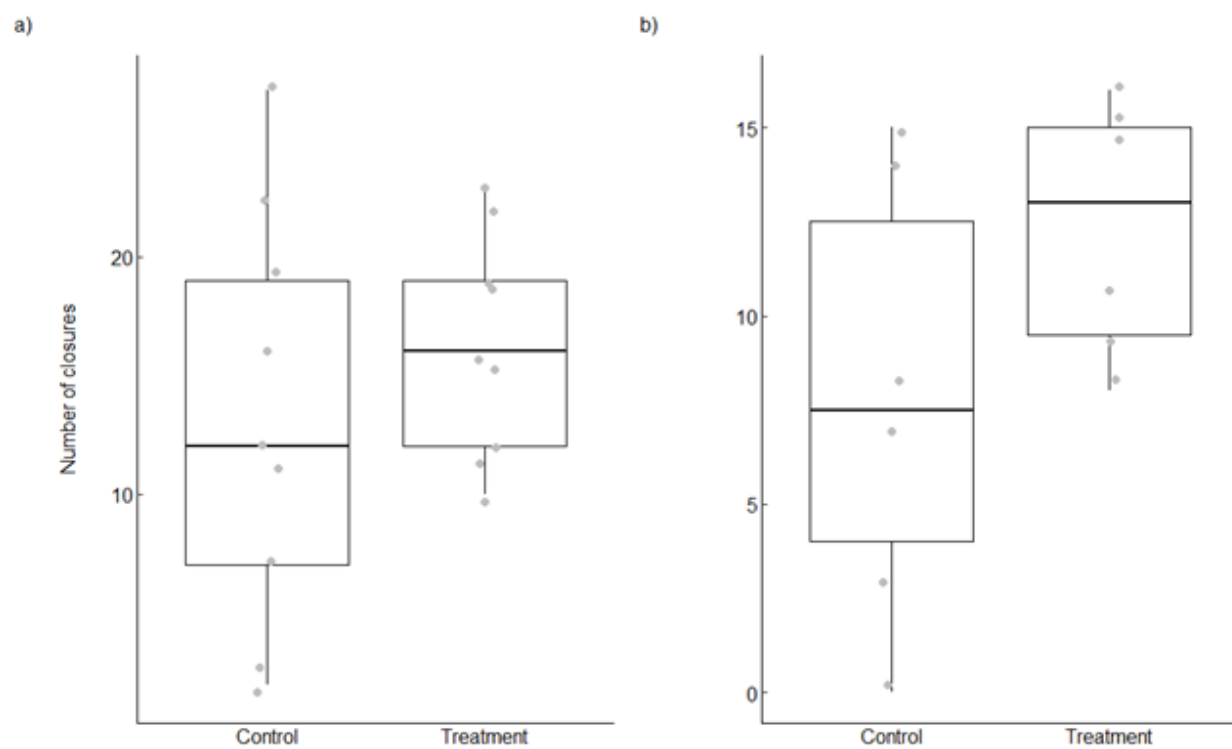


Figure 10. Number of closures for individuals in experiments where the treatment group was exposed to a) concentration A and b) concentration B.

Task 4: Species distribution models for Louisiana Pigtoe and Texas Heelsplitter.

Contributing authors: Alex Kiser and Charles Randklev

Study objectives

The goal of this task is to model the distribution of *Pleurobema riddellii*, Louisiana Pigtoe, and *Potamilus amphichaenus*, Texas Heelsplitter, using environmental data (e.g., climate, elevation, and land use) known to be important determinants of mussel occupancy. An ensemble modeling approach (ESDM), a type of SDM, was used to predict occupancy. Specifically, ESDMs works by taking individual SDMs (e.g., MAXENT, Random Forest, Boosted Regression Trees, etc.) and averaging their output into one final prediction, which greatly reduces the generalization error of single model approaches. The resulting models were then used to predict occupancy within a standardized cell (30 arc-second grid) with a unique identifier, which can then be used to identify stream segments for further sampling and/or restoration.

Methods

Species

Pleurobema riddellii (Louisiana Pigtoe) is a threatened freshwater mussel species found in the Trinity, Neches, Sabine, San Jacinto River basins of east Texas (Randklev et al., 2020). Occurrence records for this species (n = 448) were obtained from the Mussels of Texas (MoTX) database, an online repository of historical and contemporary mussel collections in Texas (Randklev et al., 2020). Duplicate records of the same species at the same coordinates over time were removed from the analysis to remove site sample bias in high access areas for an adjusted total of 471 observations.

Potamilus amphichaenus (Texas Heelsplitter) is a threatened freshwater mussel species found in the Trinity, Neches, and Sabine River basins of east Texas (Randklev et al., 2020). Occurrence records for this species (n = 242) were obtained from the Mussels of Texas (MoTX) database, an online repository of historical and contemporary mussel collections in Texas (Randklev et al., 2020). Duplicate records of the same species at the same coordinates over time were removed from the analysis to remove site sample bias in high access areas for an adjusted total of 229 observations.

Climate and environmental data

To model the distribution of *P. riddellii* and *P. amphichaenus*, we used climate, topographical characteristics, and land use. We chose these variables because previous studies have shown them to be important determinants of mussel occupancy (Hopkins, 2009; Santos et al., 2015; Gama et al., 2016; Kiser et al., 2022). Climate data were obtained from the WorldClim bioclimatic database (Fick & Hijmans, 2017) and included data on daily minimum and maximum levels, mean values and ranges, and quarterly summaries for temperature and precipitation on a global scale (Nix, 1986; Hijmans et al., 2005; Maria & Udo, 2017). Slope characteristics (% change, aspect, and water flow direction) were calculated from the elevation data set using the terrain function in the “raster” package of R (Hijmans et al., 2015) at the same resolution and extent as the WorldClim bioclimatic data. Land use data were obtained from the

Multi-Resolution Land Characteristic Consortium – National Land Cover Database (MRLC-NLCD, 2016) at the 30 m resolution. Percent coverage of each land use type was taken at the same resolution as climate and elevation data.

Two sets of variables were used for the SDM models: (v_i) climate and topography; (v_{ii}) climate, topography, and land use. Multicollinearity for both variable sets were evaluated using Pearson correlation and covariates with values greater than 0.8 were excluded from further analysis (Dormann et al., 2013). The variables (v_i) for the climate and topography models were: mean temperature of the wettest quarter, annual mean temperature, temperature seasonality, mean temperature of the driest quarter, mean temperature of the warmest quarter, precipitation of the wettest the month, precipitation of the driest the month, precipitation seasonality, precipitation of the warmest the quarter, elevation, and percent change the in the elevation. The variables (v_{ii}) for the climate, topography, and land use models were: mean diurnal range, temperature seasonality, max temperature of warmest month, mean temperature of wettest quarter, precipitation of the wettest month, precipitation seasonality, other, percent developed open land, percent developed low land, percent developed medium land, percent developed high land, percent barren, percent deciduous forest, percent evergreen forest, percent mixed forest, percent shrub, percent herbaceous, percent hay, percent row crop, percent woody wetland.

Variable of importance (VIP) was assessed using area under the curve (AUC) and Pearson Rank Correlation (PRC). The PRC measures the correlation between the predicted value and error of a model when a random variable is permuted, and all other variables are held equal to their mean. Declining model accuracy due to a variable permutation can be used to identify variables most affecting species presence and absence (Thuiller et al., 2009). Response curves for the four most important variables (based on AUC and PRC) were then created to show variable impact on the probability of occurrence of the species.

Modeling Protocol

To predict the geographical distribution, we used an ensemble modeling approach following the methods of Kiser et al. (2022) and overlaid the probability of occurrence estimates onto the Gridded River Identification System (GRIS; Kiser et al., 2023) to identify priority areas. Based on preliminary testing, the following models were used: General Linear Model (GLM), Support-Vector Model (SVM), Random Forest (RF), Boosted Regression Tree (BRT), Multivariate Adaptive Regression Splines (MARS), Maximum Entropy (MAXENT), Classification and Regression Trees (CART), Flexile Discriminate Analysis (FDA), and Mixture Discriminant Analysis (MDA). Other models available within the “SDM” package (Naimi & Araújo, 2016) were evaluated and removed due to poor overall performance compared to other model types (AUC < 0.8, true skill statistic (TSS) < 0.7). Pseudo-absences were generated because true absence data across Texas were not available. To do this, pseudo-absence points were randomly generated at two times the number of known presence observations of each species (Liu et al., 2013). To train the individual models, we used 80% of the observed and generated data for a given species to develop predictions. To improve parameter estimates, each training and testing group was randomly resampled using 100 bootstrap replicates for each model used. Ensemble models were then created by the combination of all species-specific individual model methods using a weighted mean based on maximum (sensitivity + specificity). All statistical analyses were performed using R version 4.1.1 (R Core Team, 2022).

Model assessment

To assess model performance, we used AUC of the receiver operating characteristic (ROC) and the TSS. Both AUC and TSS are arranged on a scale from 0 to 1, with higher values indicating better model performance. Models with AUC values less than 0.5 are considered worse than random, values from 0.5 to 0.7 are considered poor, 0.7 to 0.9 are considered fair, and values greater than 0.9 are considered excellent with regard to model fit (Swets, 1988). Model TSS values from 0.2 to 0.5 indicate poor model fit, values from 0.6 to 0.8 denote adequate model fit, and values greater than 0.8 are considered excellent model fit (Coetzee et al., 2009). In addition to AUC and TSS metrics, sensitivity (correctly predicted presences), specificity (correctly predicted absences) and Kappa (measure of homogeneity and test validity $[(\text{observed accuracy} - \text{expected accuracy}) / (1 - \text{expected accuracy})]$; range 0 – 1)), were used to assess final ensemble model performance.

To visualize predicted species distributions, we utilized two methods: binomial mapping and rank categorization. Binomial distribution maps were obtained by using the optimum threshold (OT) values from the weighted average (maximum (sensitivity + specificity)) of all species-specific models. Predicted values of a cell greater than the OT of a species were given a value of 1 to indicate predicted presence, and cells with predicted values less than OT were given a value of 0 to indicate predicted absence. To prioritize stream reaches, the final ensemble model outputs for each species were overlayed on the GRIS grid and the stream reaches were rank ordered from one to five based on the following probability of occurrence categories: 1 = 0.0-0.2, 2 = 0.2-0.4, 3 = 0.4-0.6, 4 = 0.6-0.8, and 5 = 0.8-1.0, respectively.

Results/Synthesis

Pleurobema riddellii

Model performance of both variable sets (v_i and v_{ii}) for all individual SDM methodologies were fair to excellent based on our criteria (AUC > 0.8, TSS > 0.6; Table 1). Sensitivity and specificity for all models were also high (> 0.87) indicating a high level of model fit. Random forest (v_i 0.987 AUC, 0.929 TSS; v_{ii} 0.992 AUC, 0.942 TSS) was the best fitting individual model for both variable sets. The least performing model, though still in our acceptable criteria was the GLM model (v_i 0.932 AUC, 0.751 TSS) and CART model (v_{ii} 0.944 AUC, 0.862 TSS). Ensemble model performance for both variable sets were excellent (v_i 0.936 AUC, 0.876 TSS; v_{ii} 0.949 AUC, 0.903 TSS). Model accuracy was consistently higher for the model group that included land use variables (v_{ii}) compared to the model group with climate and topometric only (v_i), although differences in model accuracy were not statistically significant ($p > 0.05$).

Variable of Importance

For v_i , the variable that contributed most to model accuracy was elevation followed by annual mean temperature, precipitation of the driest month, and mean temperature of the warmest quarter (Table 2, Figure 1). The least informative environmental variable was percent change in elevation between cells. Variable response curves for v_i show that *Pleurobema riddellii* prefers lower elevation rivers (<150m), annual mean temperature between 18.5°C and 20.0°C, less than 60 mm of rain during the driest month, and mean temperature during the warmest quarter less than 27.5 °C. For v_{ii} , the variable that contributed most to model accuracy was percent woody wetland followed by percent hay, precipitation seasonality, and precipitation of

the wettest month (Table 3, Figure 2). Variable response curves for v_{ii} show an increased POC with increasing woody wetlands, and a decreasing POC with the increase of agricultural influence (hay). Similarly, there is a decrease of POC with increasing precipitation seasonality and precipitation during the wettest month indicating *P. riddellii* may not cope well with high rainfall events. The least informative environmental variable was percent other land use types.

Species Distribution

Ensemble map predictions for both model groups show similar predictions in high probability of occurrence areas, with the v_{ii} group showing reduced predicted range near major river systems (Figures 3 & 4). Both model groups predict high rank priority reaches for the Neches River below Lake Palestine down to the coast. Similarly, both models show high priority for the Sabine River below Greg, Tx to the Toledo Bend Reservoir. The model groups show discrepancies below Lake Livingston on the Trinity River near the coast with the v_i model showing low probability in the main stem, and the v_{ii} model showing this as high probability. There are no known records of this species in this area, but this serves as a useful place for model validation.

Potamilus amphichaenus

Model performance of both variable sets (v_i and v_{ii}) for all individual SDM methodologies were fair to excellent based on our criteria (AUC > 0.8, TSS > 0.6; Table 4). Sensitivity and specificity for all models were also high (> 0.8) indicating a high level of model fit. Random forest (v_i 0.979 AUC, 0.887 TSS; v_{ii} 0.981 AUC, 0.886 TSS) was the best fitting individual model for both variable sets. The least performing model, though still in our acceptable criteria was the CART model (v_i 0.895 AUC, 0.733 TSS; v_{ii} 0.891 AUC, 0.728 TSS). Ensemble model performance for both variable sets were excellent (v_i 0.910 AUC, 0.825 TSS; v_{ii} 0.907 AUC, 0.818 TSS). Model accuracy was consistently higher for the model group that included land use variables (v_{ii}) compared to the model group with climate and topometric only (v_i), although differences in model accuracy were not statistically significant ($p > 0.05$).

Variable of Importance

For v_i , the variable that contributed most to model accuracy was elevation followed by annual mean temperature, precipitation of the driest month, and mean temperature of the warmest quarter (Table 5, Figure 5). The least informative environmental variable was percent change in elevation between cells. Variable response curves for v_i show that *Potamilus amphichaenus* prefers lower elevation rivers (<150m), annual mean temperature between 18.5 °C and 20.0°C, mean temperature during the warmest quarter less than 27.5°C, and moderate seasonality. For v_{ii} , the variable that contributed most to model accuracy was percent woody wetland followed by percent hay, percent herbaceous, and percent evergreen forest (Table 6, Figure 6). Variable response curves for v_{ii} show an increased POC with increasing woody wetlands, and a decreasing POC with the increase of agricultural influence (hay and herbaceous). Similarly, there is a decrease with evergreen forest presence. The least informative environmental variable was percent other land use types.

Species Distribution

Ensemble map predictions for both model groups show similar predictions in high probability of occurrence areas, with the v_{ii} group showing reduced predicted range near major river systems (Figures 7 & 8). Both model groups predict high rank priority reaches for the Neches River below Lake Palestine down to the coast. Similarly, both models show high priority for the Sabine River below Greg, Tx to the Toledo Bend Reservoir. The Angelina River also shows several areas of high probability from both models despite no known occurrence records in the area. The model groups show discrepancies near Beaumont, Tx near the coast with the v_i model showing high probability in the coastal tributaries, and the v_{ii} model showing this as low probability.

Table 1. Species distribution model and ensemble model performance for *Pleurobema riddellii*. Each individual species distribution methodology (General Linear Model (GLM), Support-Vector Model (SVM), Random Forest (RF), Boosted Regression Tree (BRT), Multivariate Adaptive Regression Splines (MARS), Maximum Entropy (MAXENT), Classification and Regression Trees (CART), Flexible Discriminate Analysis (FDA), and Mixture Discriminant Analysis (MDA)) was bootstrapped 100 times. Ensemble models were created from the weighted average of all individual methodologies based on the maximum (sensitivity + specificity). Performance metrics were based on area under the curve (AUC), true skill statistics (TSS), Sensitivity (correctly predicted presences) and Specificity (correctly predicted absences), and Kappa ([observed accuracy – expected accuracy] / [1 - expected accuracy]).

Model	Climate and Topometric					Climate, Topometric, and Land use				
	AUC	TSS	Sensitivity	Specificity	Kappa	AUC	TSS	Sensitivity	Specificity	Kappa
GLM	0.932	0.751	0.891	0.860	0.722	0.969	0.871	0.953	0.917	0.816
SVM	0.959	0.827	0.903	0.924	0.817	0.987	0.916	0.968	0.948	0.880
RF	0.987	0.929	0.959	0.970	0.924	0.992	0.942	0.970	0.972	0.925
BRT	0.965	0.837	0.919	0.918	0.820	0.975	0.872	0.940	0.932	0.833
MARS	0.965	0.863	0.941	0.922	0.842	0.969	0.896	0.942	0.955	0.873
MAXENT	0.969	0.880	0.950	0.931	0.861	0.985	0.920	0.968	0.953	0.888
CART	0.940	0.837	0.904	0.933	0.830	0.944	0.862	0.919	0.943	0.837
FDA	0.910	0.715	0.826	0.889	0.706	0.965	0.870	0.963	0.907	0.804
MDA	0.918	0.740	0.896	0.844	0.704	0.970	0.877	0.951	0.925	0.828
Ensemble	0.936	0.876	0.950	0.926	0.854	0.949	0.903	0.959	0.944	0.887

Table 2. Variable of importance from climate and topometrics ensemble model of nine species distribution models combined by weighted average of max (sensitivity + specificity) for *Pleurobema riddellii*. Pearson Rank Correlation (COR) and area under the curve (AUC) were used to evaluate importance, with higher values for each statistic indicating increasing level of significance to model accuracy.

Variable	AUC	COR
Elevation	0.463	0.761
Annual mean temperature	0.235	0.220
Precipitation of the driest month	0.194	0.122
Mean temperature of the warmest quarter	0.189	0.232
Temperature seasonality	0.171	0.203
Precipitation of the wettest month	0.136	0.180
Precipitation seasonality	0.106	0.192
Precipitation of the warmest quarter	0.078	0.097
Mean temperature of the wettest quarter	0.054	0.071
Mean temperature of the driest quarter	0.049	0.079
Percent change the in elevation	0.007	0.018

Table 3. Variable of importance from climate, topometrics, and land use ensemble model of nine species distribution models combined by weighted average of max (sensitivity + specificity) for *Pleurobema riddellii*. Pearson Rank Correlation (COR) and area under the curve (AUC) were used to evaluate importance, with higher values for each statistic indicating increasing level of significance to model accuracy.

Variable	AUC	COR
Percent woody wetland	0.331	0.443
Percent hay	0.079	0.095
Precipitation seasonality	0.074	0.128
Precipitation of the wettest month	0.056	0.090
Percent mixed forest	0.043	0.072
Temperature seasonality	0.032	0.043
Mean temperature of wettest quarter	0.021	0.036
Percent row crop	0.018	0.010
Max temperature of warmest month	0.017	0.035
Mean diurnal range	0.016	0.028
Percent evergreen forest	0.013	0.029
Percent herbaceous	0.007	0.013
Percent developed medium land	0.006	0.011
Percent developed low land	0.005	0.011
Other	0.005	0.006
Percent developed high land	0.004	0.006
Percent developed open land	0.003	0.007
Percent shrub	0.003	0.006
Percent barren	0.003	0.005
Percent deciduous forest	0.002	0.006

Table 4. Species distribution model and ensemble model performance for *Potamilus amphichaenus*. Each individual species distribution methodology (General Linear Model (GLM), Support-Vector Model (SVM), Random Forest (RF), Boosted Regression Tree (BRT), Multivariate Adaptive Regression Splines (MARS), Maximum Entropy (MAXENT), Classification and Regression Trees (CART), Flexile Discriminate Analysis (FDA), and Mixture Discriminant Analysis (MDA)) was bootstrapped 100 times. Ensemble models were created from the weighted average of all individual methodologies based on the maximum (sensitivity + specificity). Performance metrics were based on area under the curve (AUC), true skill statistics (TSS), Sensitivity (correctly predicted presences) and Specificity (correctly predicted absences), and Kappa ([observed accuracy – expected accuracy] / [1 - expected accuracy]).

Model	Climate and Topometric					Climate, Topometric, and Land use				
	AUC	TSS	Sensitivity	Specificity	Kappa	AUC	TSS	Sensitivity	Specificity	Kappa
GLM	0.924	0.773	0.946	0.827	0.721	0.937	0.804	0.918	0.886	0.775
SVM	0.926	0.723	0.901	0.821	0.680	0.966	0.849	0.941	0.908	0.823
RF	0.979	0.887	0.937	0.950	0.880	0.981	0.886	0.945	0.942	0.873
BRT	0.915	0.703	0.837	0.866	0.687	0.936	0.757	0.894	0.863	0.726
MARS	0.952	0.824	0.934	0.890	0.794	0.949	0.813	0.913	0.900	0.790
MAXENT	0.954	0.832	0.941	0.891	0.800	0.966	0.862	0.942	0.920	0.840
CART	0.895	0.733	0.838	0.895	0.725	0.891	0.728	0.837	0.891	0.718
FDA	0.915	0.749	0.926	0.823	0.701	0.942	0.809	0.932	0.877	0.774
MDA	0.886	0.681	0.856	0.826	0.649	0.948	0.813	0.921	0.891	0.785
Ensemble	0.910	0.825	0.947	0.878	0.786	0.907	0.818	0.930	0.889	0.788

Table 5. Variable of importance from climate and topometrics ensemble model of nine species distribution models combined by weighted average of max (sensitivity + specificity) for *Potamilus amphichaenus*. Pearson Rank Correlation (COR) and area under the curve (AUC) were used to evaluate importance, with higher values for each statistic indicating increasing level of significance to model accuracy.

Variable	AUC	COR
Mean temperature of the wettest quarter	0.071	0.093
Annual mean temperature	0.282	0.284
Temperature seasonality	0.221	0.265
Mean temperature of the driest quarter	0.078	0.121
Mean temperature of the warmest quarter	0.225	0.302
Precipitation of the wettest month	0.188	0.241
Precipitation of the driest month	0.263	0.171
Precipitation seasonality	0.132	0.231
Precipitation of the warmest quarter	0.107	0.149
Elevation	0.528	0.866
Percent change the in elevation	0.011	0.028

Table 6. Variable of importance from climate, topometrics, and land use ensemble model of nine species distribution models combined by weighted average of max (sensitivity + specificity) for *Potamilus amphichaenus*. Pearson Rank Correlation (COR) and area under the curve (AUC) were used to evaluate importance, with higher values for each statistic indicating increasing level of significance to model accuracy.

Variable	AUC	COR
Mean diurnal range	0.024	0.032
Temperature seasonality	0.024	0.037
Max temperature of warmest month	0.011	0.016
Mean temperature of wettest quarter	0.025	0.029
Precipitation of the wettest month	0.022	0.032
Precipitation seasonality	0.031	0.045
Other	0.003	0.005
Percent developed open land	0.006	0.010
Percent developed low land	0.011	0.018
Percent developed medium land	0.017	0.023
Percent developed high land	0.007	0.011
Percent barren	0.008	0.012
Percent deciduous forest	0.009	0.017
Percent evergreen forest	0.089	0.127
Percent mixed forest	0.048	0.073
Percent shrub	0.019	0.025
Percent herbaceous	0.103	0.136
Percent hay	0.151	0.211
Percent row crop	0.036	0.040
Percent woody wetland	0.154	0.222

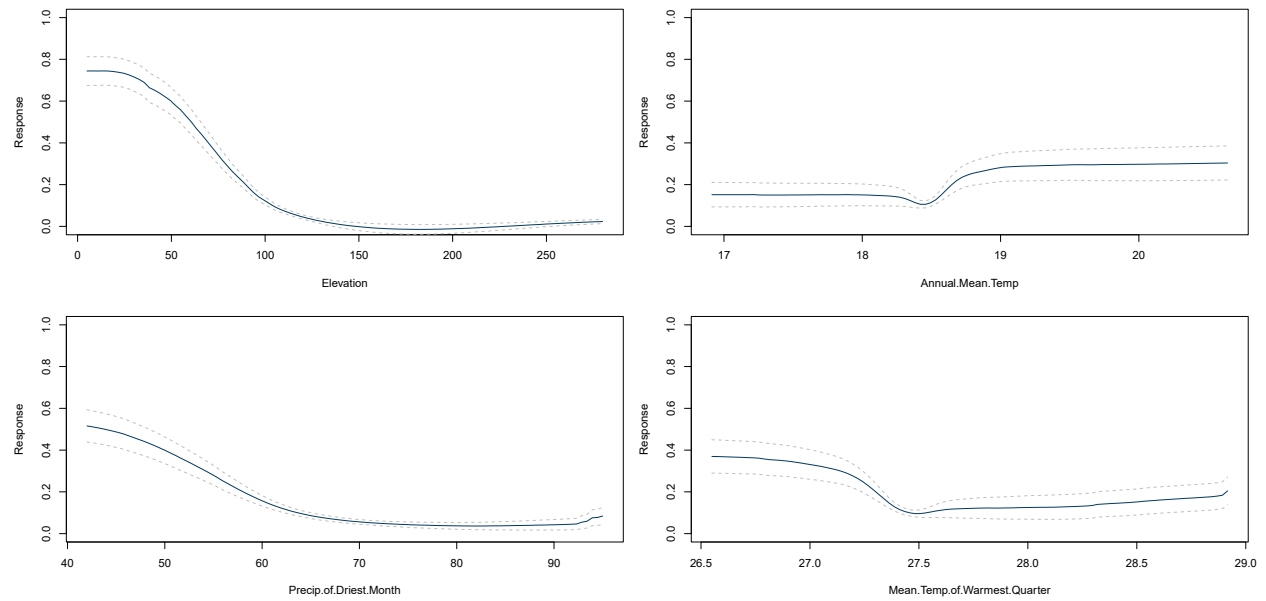


Figure 1. Variable response curves of the four most important variables (based on AUC and Pearson Rank Correlation) to model accuracy of the climate and topometric model (v_i) for *Pleurobema riddellii*.

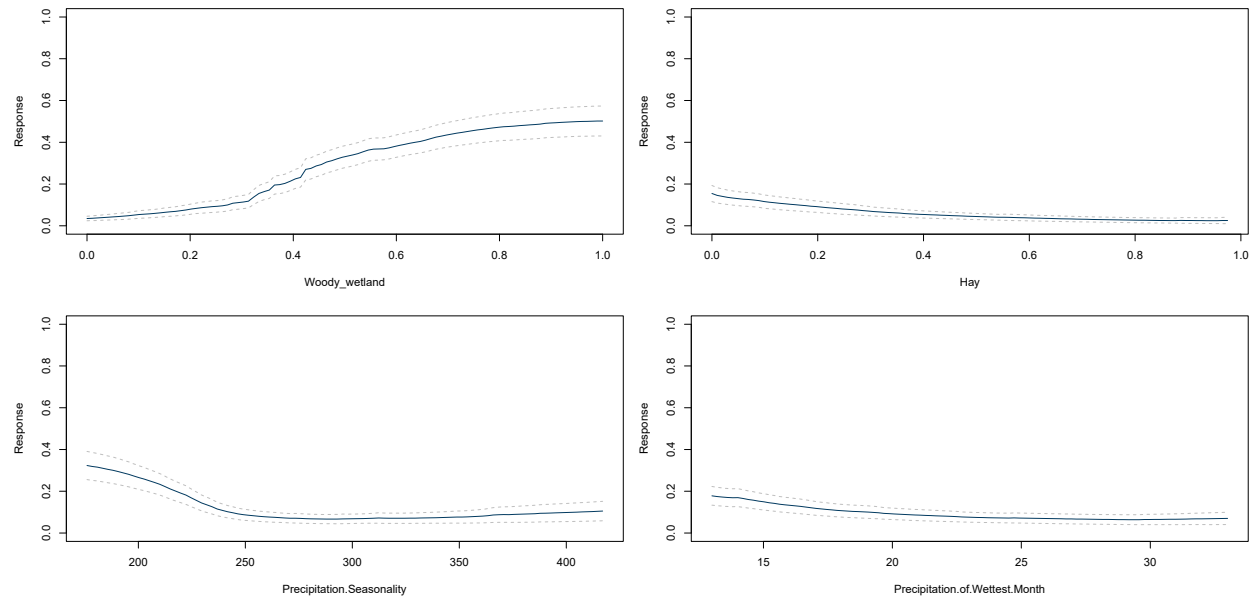


Figure 2. Variable response curves of the four most important variables (based on AUC and Pearson Rank Correlation) to model accuracy of the climate and topometric model (v_{ii}) for *Pleurobema riddellii*.

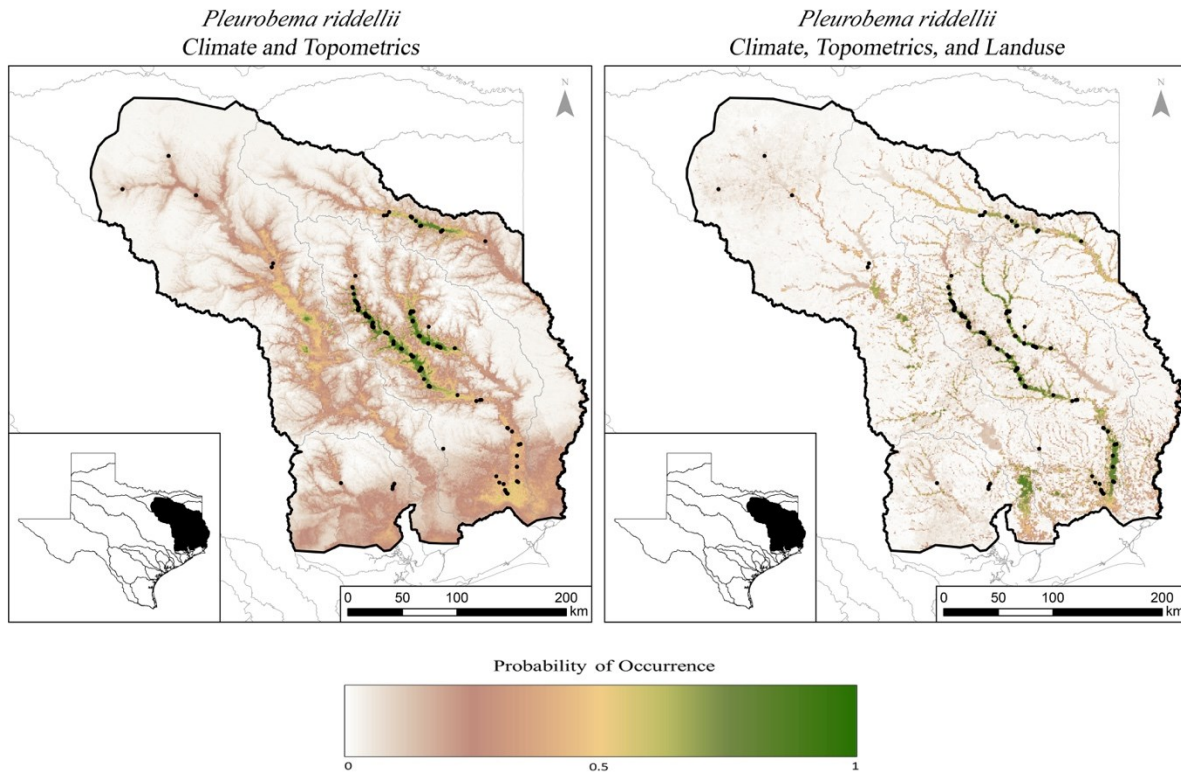


Figure 3. *Pleurobema riddellii* ensemble model outputs of two models: climate and topometric (v_i) and climate, topometric, and land use (v_{ii}). Weighted averages of nine individual species distribution model methodologies (General Linear Model, Support-Vector Model, Random Forest, Boosted Regression Tree, Multivariate Adaptive Regression Splines, Maximum Entropy, Classification and Regression Trees, Flexile Discriminate Analysis, and Mixture Discriminant Analysis) based on maximum (sensitivity + specificity). Red indicates higher probability of occurrence for a given cell (30 arc second grid, ~0.9 km).

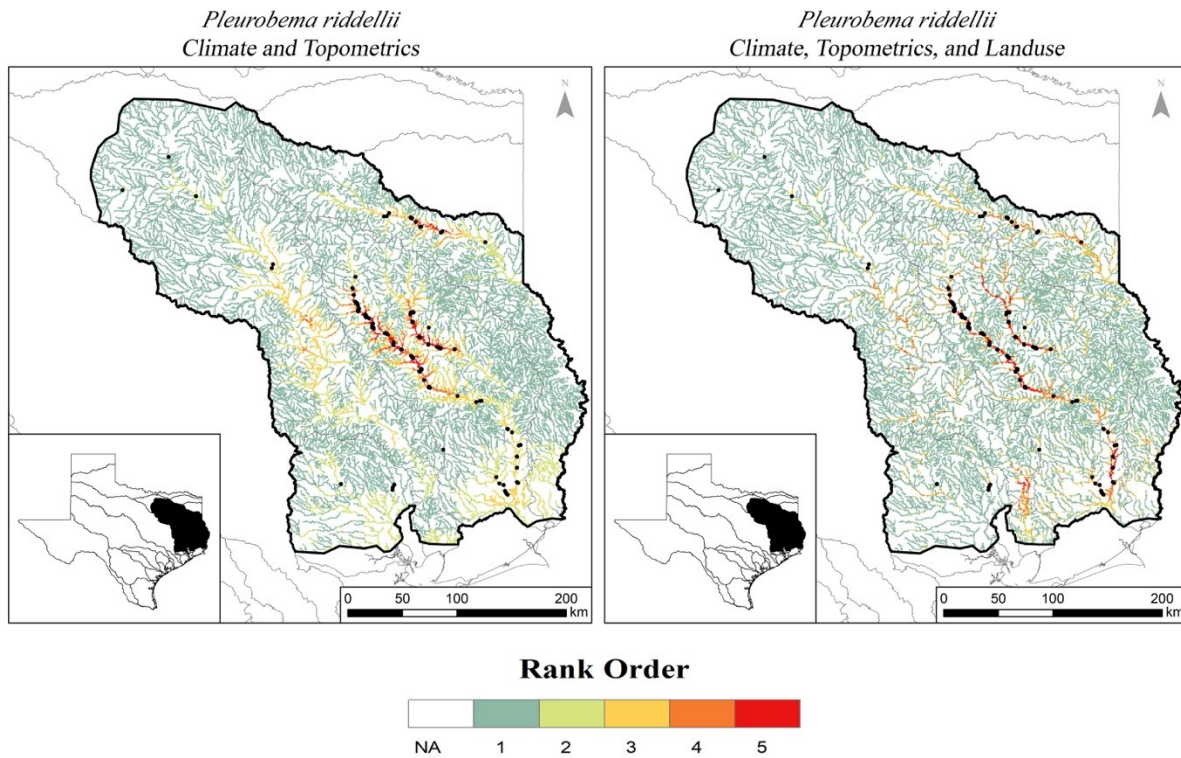


Figure 4. River map showing rank importance based on predicted probability of occurrence from *Pleurobema riddellii* ensemble models. Ranks 1 to 5 are determined by probability of occurrence 0.0-0.2, 0.2-0.4, 0.4-0.6, 0.6-0.8, and 0.8-1.0, respectively. Each cell is 30 arc-seconds (~0.9km) and is assigned a Gridded River Identification System (GRIS) number.

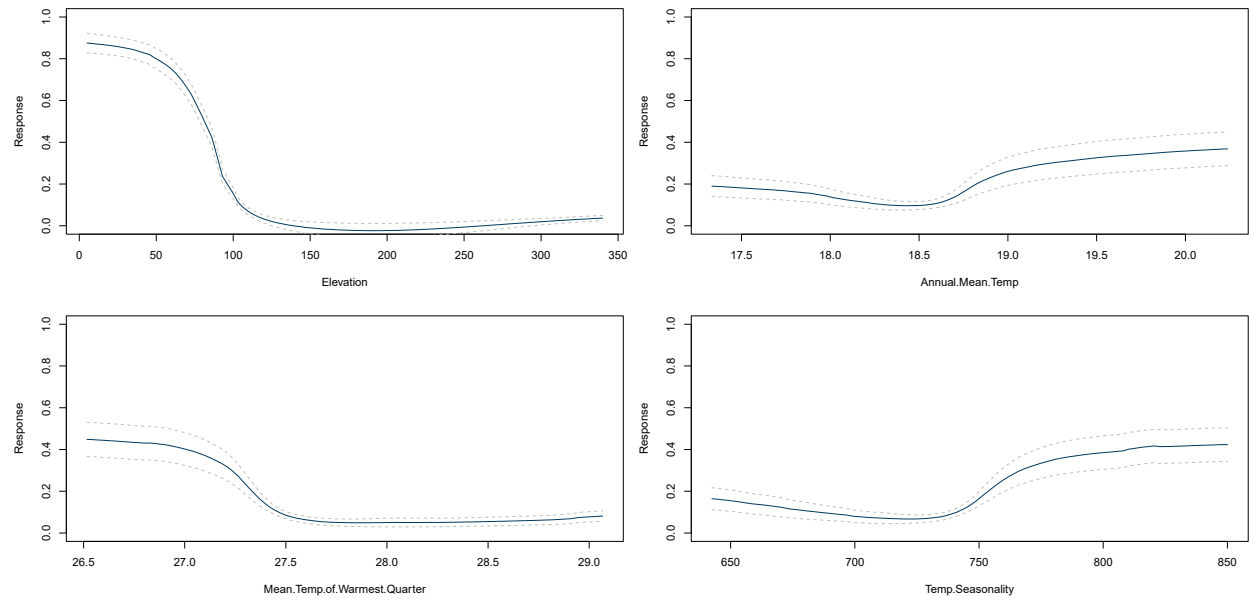


Figure 5. Variable response curves of the four most important variables (based on AUC and Pearson Rank Correlation) to model accuracy of the climate and topometric model (v_i) for *Potamilus amphichaenus*.

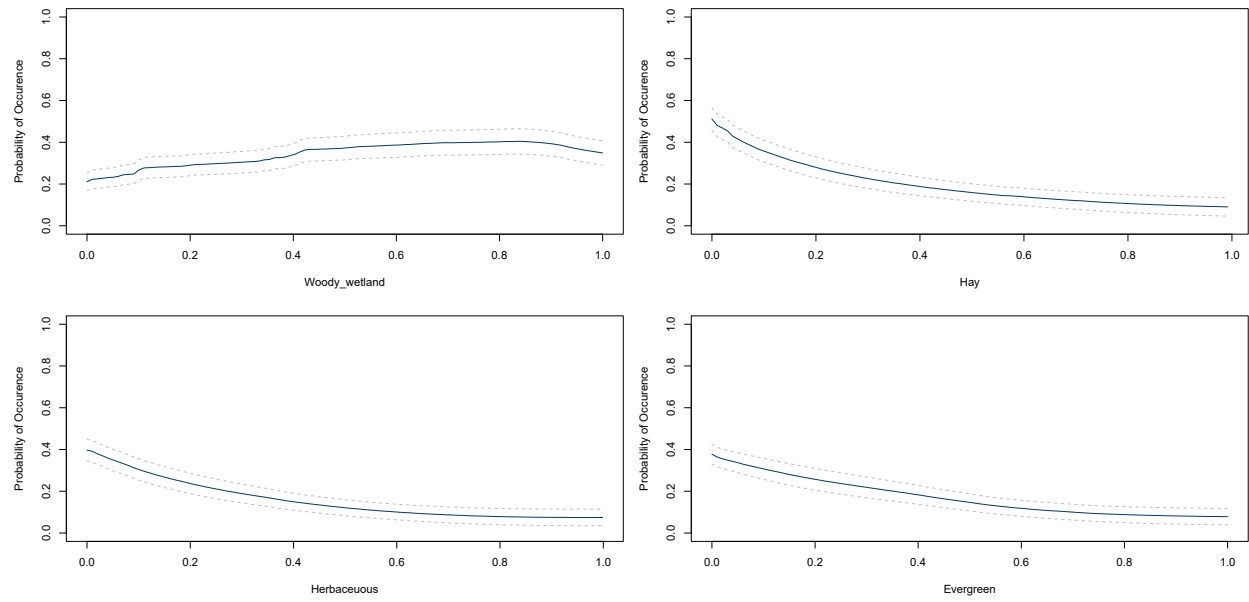


Figure 6. Variable response curves of the four most important variables (based on AUC and Pearson Rank Correlation) to model accuracy of the climate and topometric model (v_{ii}) for *Potamilus amphichaenus*.

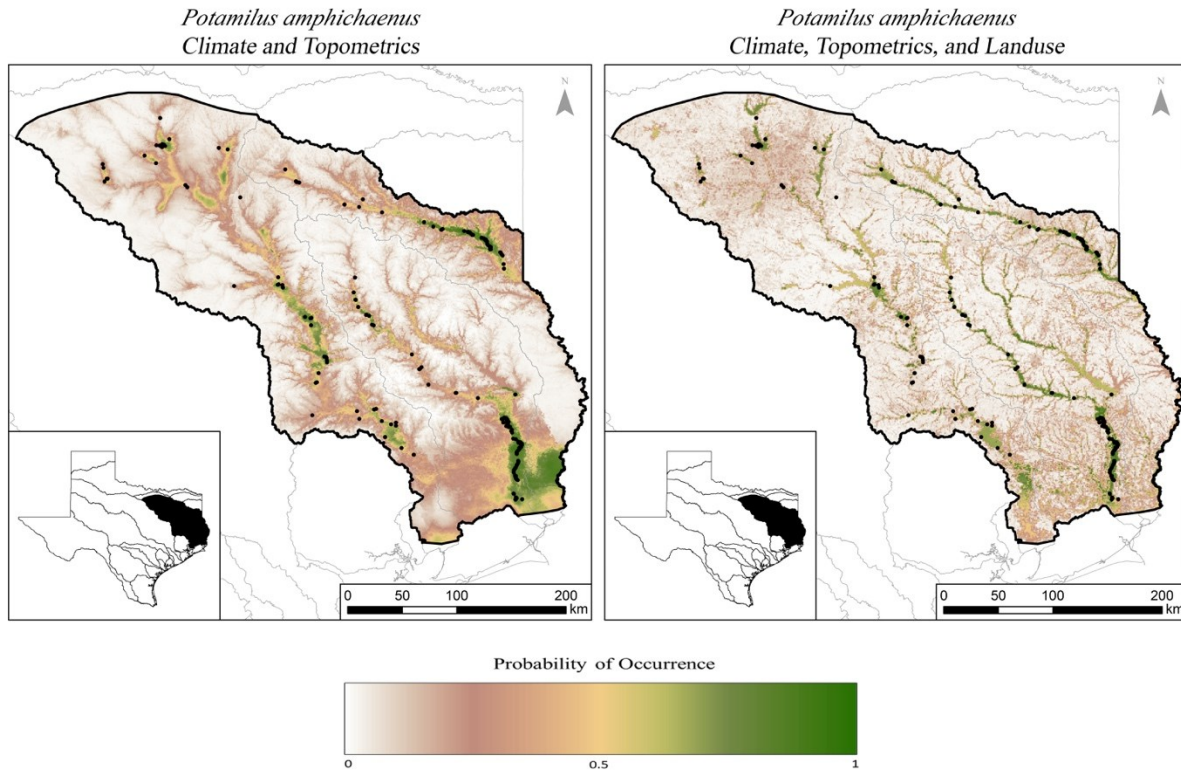


Figure 7. *Potamilus amphichaenus* ensemble model outputs of two models: climate and topometric (v_i) and climate, topometric, and land use (v_{ii}). Weighted averages of nine individual species distribution model methodologies (General Linear Model, Support-Vector Model, Random Forest, Boosted Regression Tree, Multivariate Adaptive Regression Splines, Maximum Entropy, Classification and Regression Trees, Flexible Discriminate Analysis, and Mixture Discriminant Analysis) based on maximum (sensitivity + specificity). Red indicates higher probability of occurrence for a given cell (30 arc second grid, ~0.9 km).

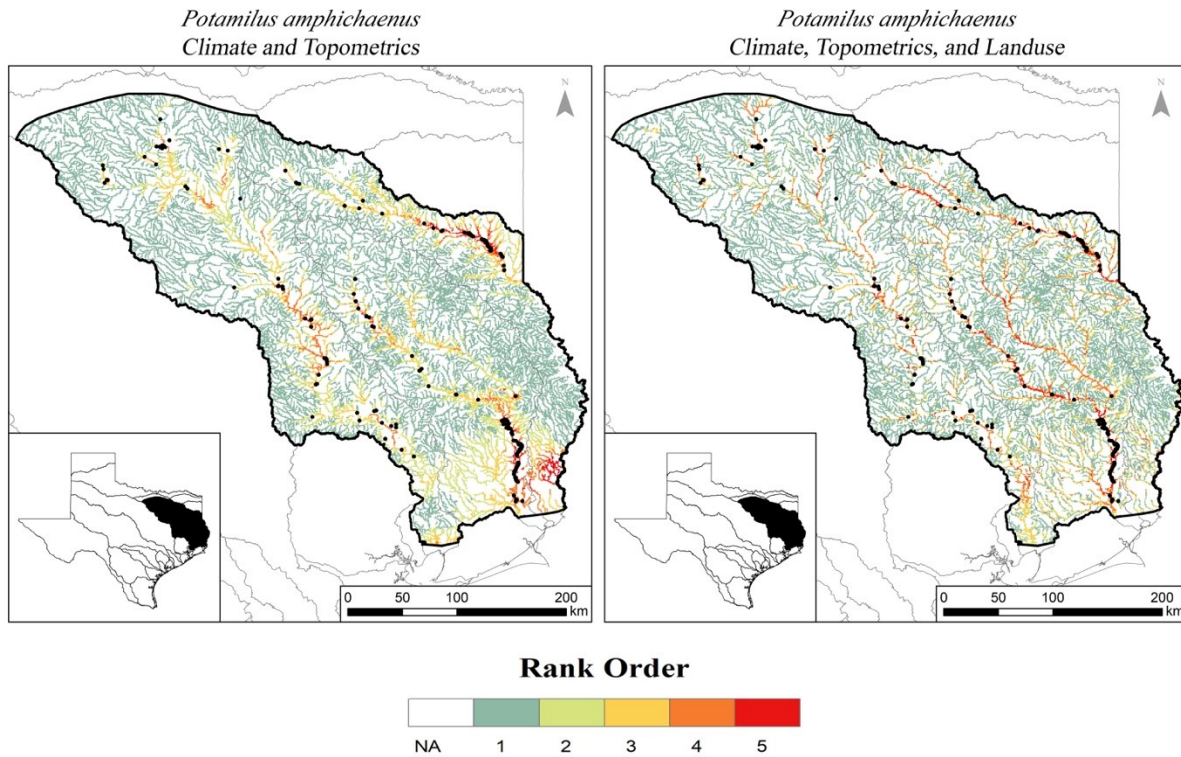


Figure 8. River map showing rank importance based on predicted probability of occurrence from *Potamilus amphichaenus* ensemble models. Ranks 1 to 5 are determined by probability of occurrence 0.0-0.2, 0.2-0.4, 0.4-0.6, 0.6-0.8, and 0.8-1.0, respectively. Each cell is 30 arc-seconds (~0.9km) and is assigned a Gridded River Identification System (GRIS) number.

Literature Cited

- Dormann, C. F., Elith, J., Bacher, S., Buchmann, C., Carl, G., Carré, G., Garcia-Marquez, J. R., Gruber, B., Lafourcade, B., Leitaó, P. J., Munkemüller, T., McClean, C., Osborne, P. E., Reineking, B., Schroder, B., Skidmore, A. K., Zurell, D., & Lautenbach, S. (2013). Collinearity: A review of methods to deal with it and a simulation study evaluating their performance. *Ecography*, 36, 27–46.
- Fick, S. E., & Hijmans, R. J. (2017). WorldClim 2: New 1–km spatial resolution climate surfaces for global land areas. *International Journal of Climatology*, 37, 4302–4315.
- Gama, M., Crespo, D., Dolbeth, M., & Anastácio, P. (2016). Predicting global habitat suitability for *Corbicula fluminea* using species distribution models: The importance of different environmental datasets. *Ecological Modelling*, 319, 163–169.
- Hijmans, R. J., Cameron, S. E., Parra, J. L., Jones, P. G., & Jarvis, A. (2005). Very high–resolution interpolated climate surfaces for global land areas. *International Journal of Climatology: A Journal of the Royal Meteorological Society*, 25(15), 1965–1978.
- Hijmans, R. J., Van Etten, J., Cheng, J., Mattiuzzi, M., Sumner, M., Greenberg, J. A., & Hijmans, M. R. J. (2015). Package ‘raster’. *R package*, 734.
- Hopkins, R. L. (2009). Use of landscape pattern metrics and multiscale data in aquatic species distribution models: a case study of a freshwater mussel. *Landscape Ecology*, 24(7), 943–955.
- Kiser, A. H., Cummings, K. S., Tiemann, J. S., Smith, C. H., Johnson, N. A., Lopez, R. R., & Randklev, C. R. (2022). Using a multi-model ensemble approach to determine biodiversity hotspots with limited occurrence data in understudied areas: An example using freshwater mussels in México. *Ecology and Evolution*, 12(5), e8909.F
- Liu, C., White, M., Newell, G., & Griffioen, P. (2013). Species distribution modelling for conservation planning in Victoria, Australia. *Ecological Modelling*, 249, 68–74.
- Maria, B., & Udo, S. (2017). Why input matters: selection of climate data sets for modelling the potential distribution of a treeline species in the Himalayan region. *Ecological Modeling*, 359(10), 92–102.
- Nix, H. A. (1986). A biogeographic analysis of Australian Elapid snakes. Atlas of Australian Elapid Snakes, Australian Flora and Fauna, Series 8, Australian Government Publishing Service, Canberra, Australia.
- R Core Team (2022). R: A language and environment for statistical computing. R Foundation for Statistical Computing, Vienna. www.R-project.org/
- Randklev, C. R., Ford, N. B., Fisher, M., Anderson, R., Robertson, C. R., Hart, M., et al. (2020). Mussels of Texas Project Database, Version 1.0.

- Santos, R. M. B., Fernandes, L. S., Varandas, S. G. P., Pereira, M. G., Sousa, R., Teixeira, A., Lopes-Lima, M., Cortes, R. M. V., & Pacheco, F. A. L. (2015). Impacts of climate change and land-use scenarios on *Margaritifera margaritifera*, an environmental indicator and endangered species. *Science of the Total Environment*, 511, 477–488.
- Swets, J. (1988). Measuring the accuracy of diagnostic systems. *Science*, 240, 1285–1293.
- Thuiller, W., Lafourcade, B., Engler, R., & Araújo, M. B. (2009). BIOMOD—a platform for ensemble forecasting of species distributions. *Ecography*, 32(3), 369–373.
- Wickham, J., Homer, C., Vogelmann, J., McKerrow, A., Mueller, R., Herold, N., & Coulston, J. (2014). The multi-resolution land characteristics (MRLC) consortium—20 years of development and integration of USA national land cover data. *Remote Sensing*, 6(8), 7424–7441.

Task 5: Establishing long-term monitoring protocols for Louisiana Pigtoe and Texas Heelsplitter via a series of standardized survey methods at varying spatial scales

Contributing authors: Kyle Sullivan and Brad Littrell

Study objectives:

Goals of this study were to establish long-term monitoring protocols to monitor population demographics of Louisiana Pigtoe (*Pleurobema riddellii*) and Texas Heelsplitter (*Potamilus amphichaenus*) at both site-specific and reach-level scales. At a site-specific scale, mark-recapture studies have previously been utilized to examine population demographics of Louisiana Pigtoe and Texas Heelsplitter at select sites within the Sabine and Neches Rivers of east Texas (BIO-WEST 2023; Ford et al. 2022). Although Louisiana Pigtoe are known to inhabit the San Jacinto River basin of east Texas, no data on vital rates of this population were available. Therefore, the study team established two mark-recapture sites within the East Fork of the San Jacinto River to examine population dynamics of Louisiana Pigtoe in this area. Robust-design mark-recapture models were fit to satisfy the following specific study objectives: 1) assess how detectability and temporary emigration effect sampling for Louisiana Pigtoe; 2) estimate trends in Louisiana Pigtoe abundance and apparent survival; 3) examine effects of shell length on apparent survival; and 4) fit models for Pimpleback (*Cyclonaias pustulosa*) and *Fusconaia* sp. (Texas/Wabash Pigtoe) to compare model estimates with Louisiana Pigtoe. Details of this study are presented in Section 5A below. Additional monitoring of these sites will assist in evaluating long-term population trajectory of the species in this area.

Although mark-recapture studies can provide detailed information on population dynamics, inferences are generally limited to the study area being monitored. Since mussel population demographics can vary among mesohabitats within a stream, results from select mark-recapture sites may not reflect overall population patterns at a larger scale. Therefore, recent survey data collected by the project team was compiled with other sources and utilized to guide development of reach-level long-term monitoring protocols for Louisiana Pigtoe and Texas Heelsplitter within key occupied portions of east Texas river drainages. Recommended long-term monitoring protocols are presented in Section 5B. Implementation of these monitoring protocols, combined with continued monitoring of mark-recapture sites, would provide stakeholders and managers with data on spatiotemporal trends in distribution, occurrence, and abundance of these species within currently occupied portions of east Texas river drainages.

5A. Mark-recapture Study

Methods--Sampling design

Mark-recapture sampling was initiated at two sites in the East Fork San Jacinto River (Plum Grove, Texas) to evaluate detectability and population dynamics of Louisiana Pigtoe. Site 1 and Site 2 were riffle habitats located ~650 ft upstream and downstream of FM 2090, respectively (Figure 1). Both sites were first sampled during an initial tagging event on August 1, 2022. At each site, 100-m² sampling areas were established and georeferenced so that the same area could be delineated during subsequent sampling events. Sites were then sampled for mussels

for four person-hours using visual/tactile survey methods. All mussels collected were identified to species, measured (mm), and tagged on each valve with matching unique numbered vinyl shellfish tags (Hallprint FPN 8x4mm). Louisiana Pigtoe were also tagged with Passive Integrated Transponder (PIT) tags (Biomark HPT 9) to improve detectability (Kurth et al. 2007). Cyanoacrylate glue was used to affix tags to the exterior portions of the mussel shell. PIT tags were also encapsulated with cyanoacrylate glue to decrease tag loss and handling time (Young & Isely 2008; Ashton et al. 2017).

Population monitoring was conducted using robust-design mark-recapture methods, consisting of primary and secondary sampling periods. Populations were assumed open between primary periods, meaning that migration and mortality can occur, and assumed closed between secondary periods within each primary period (Pollock 1982). Following initial tagging, additional sampling events occurred during two primary periods in 2023 (September 18 – 19) and 2024 (September 16 – 17). During each primary period, three secondary period surveys were conducted at each site and were separated by approximately 4 – 16 hours. Sites were first scanned with an electronic PIT tag reader (Biomark HPR Plus) at the start of each secondary period to detect PIT tagged mussels. Sites were then sampled for four person-hours, collecting all mussels encountered using visual and tactile search methods. Recaptured mussels were documented by tag number and measured. New captures were identified to species, measured, and tagged.

During primary period sampling, most habitat parameters measured were similar between sites. Substrates composition was visually estimated during each sampling event and both sites consisted of silt (0 – 5%), clay (5 – 10%), sand (40 – 60%), and gravel (30 – 50%). Standard water quality parameters were measured with a multiprobe meter (YSI-85). At each site, water temperature ranged from 24.4 – 27.9 °C, dissolved oxygen ranged from 4.4 – 7.4 mg/L, pH ranged from 7.7 – 7.9, and specific conductance ranged from 116 – 181 $\mu\text{S}/\text{cm}$. Hydraulics were the only variables that were relatively different compared to other habitat parameters. Water depth was 0.7 – 2.0 ft (median = 1.4 ft) at Site 1 and 0.6 – 1.0 ft (median = 1.0 ft) at Site 2. Mean current velocity ranged from 0.68 – 1.66 ft/s (median = 1.08 ft/s) at Site 1 and 1.05 – 2.11 ft/s (median = 1.95 ft/s) at Site 2.

Data analysis

Flow regime

U.S. Geological Survey (USGS) stream gage data were used to characterize flows conditions for the study duration and make assessments of potential flow-demography associations. Mean daily discharge (cubic feet per second [cfs]) data from the nearest USGS gage (East Fork San Jacinto River near Cleveland, Texas; gage #08070000) were obtained from 1990 – 2024 using the R package ‘dataRetrieval’ (DeCicco 2022) to quantify flow conditions. A discharge time-series over the study duration was visualized using the R package ‘ggplot2’ (Lin Pedersen 2024). Flow conditions were also summarized between sampling intervals using three discharge magnitude indices (i.e., minimum, median, maximum) and two frequency indices (i.e., # of days \leq Q10 flows, # of days \geq Q90 flows). Standardized discharge was calculated for each magnitude index to provide relative comparisons to the long-term median (cfs / Q50) and frequency indices were standardized as the proportion of days for a given interval (# of days / total # of days between events).

Model formulation

Cormack-Jolly-Seber robust design models were used to estimate abundance, apparent survival, site propensity, and detectability for Louisiana Pigtoe at each site. Models were also fit for Pimpleback and *Fusconaia* sp. to compare population demographics of the two most abundant species present with Louisiana Pigtoe. Data structure formatting and model parameterization were performed based on methods and code provided by Riecke et al. (2018) and Sotola et al. (2021). Complete mathematical descriptions of data structure and model parameterization can be found in Appendix A and are summarized as follows.

Observational data matrices required to fit each model included primary period detection histories (i.e., classifies whether an individual was detected or not detected in a given primary period) and secondary period detection histories within each primary period. Secondary period detection probability ($p_{t,j}$) was estimated as the probability of detecting an individual during secondary sample j in primary period t , conditional on being available for capture, and under the assumptions that the population was closed within each primary period (Huggins 1991). Moreover, $p_{t,j}$ was modeled as random variation around an overall mean. Primary period detection probability (p_t^*) was estimated as the probability of detecting an individual at least once during primary period t and calculated using estimates of $p_{t,j}$ (Kendall et al. 1995).

$$1) \quad p_t^* = 1 - \left[\prod_{j=1}^J (1 - p_{t,j}) \right]$$

Site propensity (γ) was estimated as a fixed parameter and defined as the probability an individual was available for encounter during each sampling event, which can be considered analogous to burrowing behavior. In other words, a mussel that temporarily emigrated ($1 - \gamma$) from the site was assumed to have vertically migrated to a depth where it was unavailable for encounter. The observation model of primary period encounter histories ($y_{i,t}$) was governed by the product of the true state of individual i at t ($z_{i,t}$) and $p_t^* \times \gamma$, which represents apparent encounter rate, defined as the probability of capturing an individual that was available for sampling (i.e., mussel is at or near the surface of the streambed) (Meador et al. 2011; Sandercock 2020). Encounter histories of the initial tagging event were included for analysis of each site to provide a third primary period. To do this, p_t^* for the initial tagging event was set equal to the overall mean estimated within the observation model of secondary period detection histories.

True state of individual i at the primary period that it was first captured (f_i) to primary period t was defined by latent variable $z_{i,t}$, modeled as a realization of a Bernoulli random variable governed by the product of the true state ($z_{i,t-1}$) and apparent survival ($\phi_{i,t-1}$) of individual i at primary period $t-1$. Survival was considered apparent because it is confounded with site fidelity; therefore, defined as the probability that an individual within the population

survives and remains in the sampling area from primary period $t-1$ to t (Lebreton et al. 1992; Marshall et al. 2004). In addition, apparent survival for each individual was modeled as a function of median shell length ($X.shell.length_i$) with a fixed slope ($\beta.\varphi$) and time-fixed intercepts for each sampling event ($\alpha.\varphi_t$). Median shell lengths were centered by their means for analysis.

$$2) \quad \text{logit}(\varphi_{i,t}) = \alpha.\varphi_t + \beta.\varphi \times (X.shell.length_i - \text{Mean.shell.length})$$

Population abundance cannot be estimated directly from the process model due to conditioning on the initial capture of each mussel (King 2012). Therefore, species abundance (N_t) was estimated for the initial tagging event and each primary period as a derived quantity based on the total number of individuals collected at event t (C_t), p_t^* , and γ (Nichols 1992). Therefore, N_t represents the total number of surface and subsurface individuals that are alive at event t .

$$3) \quad N_t = \frac{C_t}{p_t^* \gamma}$$

Model analysis and inference

All models were analyzed under a Bayesian framework with Markov Chain Monte Carlo (MCMC) methods using JAGS called from the R package ‘jagsUI’ (Kellner 2021). All priors were parameterized to express our current lack of knowledge about each parameter (Hobbs and Hooten 2015). Vague uniform prior distributions were used for all mean, variance, and slope parameters. A vague beta prior distribution was used for γ . Posterior distributions for each parameter were estimated based on the 5th sample from 150,000 iterations of three chains with burn-in period of 25,000 iterations per chain. Model convergence was assessed based on visual inspection of trace plots, the Gelman-Rubin statistic (\hat{R}), and density plots for each parameter. Convergence was considered successful if trace plots showed good mixtures of MCMC chains, \hat{R} was less than 1.1 (Gelman and Rubin 1992), and density plots showed similar shapes for each chain.

Parameter estimates were based on medians of their posterior distribution and were qualified by uncertainty using 90% Bayesian credible intervals (BCIs). Estimates of all parameters associated with the observation process (i.e., p , p^* , γ) were presented in a table. Estimates of abundance and apparent survival time-fixed intercepts ($\alpha.\varphi_t$) were visualized graphically to make site- and species-level comparisons. For each species, effect sizes of median shell length ($\beta.\varphi$) on apparent survival were summarized in a table and their functional relationships were visualized based on model predictions of apparent survival. All graphical results were built using the R package ‘ggplot2’ (Lin Pedersen 2024).

For Louisiana Pigtoe at Site 2, $\beta.\varphi$ was omitted from analysis because its BCI overlapped with zero. Further, γ could not be estimated at Site 2 since no Louisiana Pigtoe were

collected during the initial tagging event. Therefore, the model for this species at Site 2 was refit to only include α . φ_t to estimate apparent survival and did not include γ in the observation model of primary period encounter histories.

Results

Flow regime

Patterns in mean daily river discharge displayed a dynamic flow regime over the duration of this study. Flow conditions were below the long-term median (51 cfs) within each sampling event and increased from initial tagging event (13 cfs) to primary period 2 (39 – 42 cfs) (Figure 2). All magnitude indices measuring flow conditions between sampling events increased from initial event – primary period 1 (hereafter ‘first interval’) to primary period 1 – primary period 2 (hereafter ‘second interval’). Increases in minimum discharge were negligible (8 cfs to 12 cfs). Median discharge increased from 32 cfs to 73 cfs, which were 0.62 and 1.42 times the long-term median, respectively. Maximum discharge during both intervals were > Q99 discharge (3,820 cfs), though the maximum was substantially higher at the second interval (45,400 cfs) compared to the first (5,670 cfs). Accordingly, Q90 (432 cfs) frequency was also higher during the second interval (125 days) than the first interval (77 days). In contrast, flows never reached Q10 (15 cfs) at the second interval and occurred for 51 days during the first interval (Table 1).

Observation process

A total of 2,866 unique individuals represented by 15 species were observed during all mark-recapture efforts from 2022 to 2024. *Fusconaia* sp. and Pimpleback were the most dominant species, representing 53% and 36% of the overall mussel assemblage, respectively. Louisiana Pigtoe was the fourth most abundant species and characterized 3% of mussels observed. The remaining species accounted for 3% to less than 1% of the overall assemblage. For analysis, 2,109 mussels were used to fit models at Site 1 (Pimpleback – 859; *Fusconaia* sp – 1,185; Louisiana Pigtoe – 65) and 525 mussels were used for Site 2 (Pimpleback – 183; *Fusconaia* sp – 335; Louisiana Pigtoe – 7) (Table 2). All models converged with trace plots showing adequate mixtures of MCMC chains and \hat{R} less than 1.1 for all parameters. Density plots of marginal posterior distributions also aligned among MCMC chains.

Secondary period detection probability estimates ranged from 0.11 to 0.61 across species and sites. Mean secondary period detection probability was highest for *Fusconaia* sp. at Site 1 (0.89) and estimates for all other site-species combinations were similar and ranged from 0.39 to 0.40. Primary period detection probability estimates at Site 1 were similar between species during primary period 1 (0.88 – 0.89) and was marginally higher for Louisiana Pigtoe at primary period 2 (0.76) compared to other species (0.64 – 0.66). In contrast, primary period detection probabilities at Site 2 were similar between species for primary period 1 (0.88 – 0.93) and period 2 (0.75 – 0.78). Louisiana Pigtoe at Site 1 had the highest estimate of site propensity (0.86). Site propensity estimates for Pimpleback and *Fusconaia* sp. were higher at Site 2 (0.69 – 0.71) compared to Site 1 (0.42 – 0.49) (Table 3).

Abundance and apparent survival

Estimates of population abundance varied across sites and species. Abundance estimates were higher at Site 1 compared to Site 2 for all species. *Fusconaia* sp. (Site 1: 1,401.9 – 1,868.6 mussels; Site 2: 283.0 – 383.9 mussels) had the largest estimates of abundance, followed by

Pimpleback (Site 1: 993.1 – 1,234.1 mussels; Site 2: 151.2 – 189.4 mussels) and Louisiana Pigtoe (Site 1: 25.9 – 48.2 mussels; Site 2: 4.0 – 4.3 mussels). Abundance increased from initial tagging event to primary period 2 at each site for all three species, though overlapping BCIs indicated uncertainty in whether this represented true population growth (Figure 3 and 4). That said, BCIs for Louisiana Pigtoe abundance at Site 1 didn't overlap between the initial tagging event (16.9 – 46.0 mussels) and primary period 1 (53.6 – 86.4 mussels), suggesting a true increase in abundance during this time period (Figure 3).

Mean apparent survival probability (BCI range) at Site 1 decreased from the initial tagging event to primary period 1 for all species. Decreased mean apparent survival at Site 1 was marginal for Pimpleback, which declined from 0.94 (0.84 – 0.99) to 0.80 (0.65 – 0.94). Changes in apparent survival were more substantial for other species. Mean apparent survival of *Fusconaia* sp. decreased from 0.89 (0.75 – 0.98) to 0.60 (0.46 – 0.76) and 0.92 (0.69 – 0.99) to 0.46 (0.17 – 0.73) for Louisiana Pigtoe (Figure 3). Contrary to Site 1, mean apparent survival increased from initial tagging to primary period 1 at Site 2. Mean apparent survival of Pimpleback increased from 0.64 (0.44 – 0.90) to 0.78 (0.58 – 0.96) and from 0.83 (0.66 – 0.97) to 0.90 (0.76 – 0.98) for *Fusconaia* sp. (Figure 4). Louisiana Pigtoe mean apparent survival was much lower at Site 2 compared to other species and was estimated at 0.18 (0.01 – 0.65) for primary period 1, which was the lowest for all site-species combinations (Figure 3 and 4). Greater increases in abundance from one sampling period to the next were generally associated with higher mean apparent survival probability. For example, all species at Site 1 illustrated their largest increases in abundance from the initial tagging event to primary period 1 when mean apparent survival probability was about 0.9 (Figure 3). Decreased abundance, in contrast, was not associated with lower apparent survival probabilities, which typically had greater uncertainty in their estimates (Figure 3 and 4).

Median shell length was included as a covariate for apparent survival probability in all models except for Louisiana Pigtoe at Site 2. All slopes were positive and BCIs did not overlap with zero, supporting that median shell length influenced apparent survival. At Site 1, shell length effect size was higher for Louisiana Pigtoe (0.21) and Pimpleback (0.18) compared to *Fusconaia* sp. (0.12). Effect sizes for Pimpleback and *Fusconaia* sp. at Site 2 were both 0.16 (Table 4). Functional relationships illustrated smaller mussels less than or equal to about 30 mm generally had lower apparent survival probabilities ($\leq \sim 0.25$) and that apparent survival approached 1.0 as shell length increased toward their maximum values (Figure 5 and 6). Several exceptions included *Fusconaia* sp. and Louisiana Pigtoe at Site 1, which displayed apparent survival probabilities of about 0.25 at 40 mm during primary period 1 (Figure 5). Apparent survival also demonstrated a larger rate of increase with increasing shell length when mean apparent survival was highest at Site 1 and Site 2 during initial tagging event and primary period 1, respectively (Figure 5 and 6).

Synthesis

High variation in detection probability and site propensity emphasized the importance of accounting for sampling error to make unbiased estimates of population abundance and apparent survival (Royle and Dorazio 2008; Kéry and Royle 2020). Differences in abundance between the three species modeled aligned with expectations. During previous longitudinal surveys in the East Fork San Jacinto River, *Fusconaia* sp. and Pimpleback were also the dominant species overall and were consistently more abundant than Louisiana Pigtoe (Bonner et al. 2023). No

detectable trends in abundance were apparent at either site for *Fusconaia* sp. and Pimpleback, as shown by their overlapping BCIs among sampling events. Louisiana Pigtoe was the only species whose estimates indicated a true change in abundance. At Site 1, model estimates suggested Louisiana Pigtoe abundance approximately doubled in size from the initial tagging event to primary period 1. It is possible that new immigrants were displaced from upstream sources between these sampling events during a high flow pulse event (Watters 1994; Stanley et al. 2010), though the exact mechanism is unclear at this time.

Models that included a median shell length covariate indicated apparent survival was size dependent. Slope estimates supported shell length positively affected apparent survival. This aligned with previous mark-recapture studies that also found apparent survival was more probable for larger adult mussels compared to smaller individuals (Meador et al. 2011; Wisniewski et al. 2013). This result is not surprising, given that adult mussels are more resistant to displacement during high flow events and more tolerant of adverse environmental conditions during periods of reduced flows (Strayer 2008; Haag 2012).

Trends in mean apparent survival were not consistent between sites. At Site 1, decreased mean apparent survival seems plausible given an extreme high flow event occurred between primary periods (45,400 cfs). Decreases in apparent survival of mussels following extreme high flow events have been previously documented in the lower Colorado River, Texas (Sotola et al. 2021). That said, mean apparent survival increased at Site 2 for *Fusconaia* sp. and Pimpleback. Inverse trends in apparent survival between sites may be at least partially explained by characteristics of channel morphology near each site (Gangloff and Feminella 2007; Strayer 2008; Zigler et al. 2008). Site 1 was located on the downstream end of a straightaway and had greater water depths, whereas Site 2 was shallower and positioned just downstream of a riverbend. Based on this, it's possible that when compared to Site 2, mussels at Site 1 were less susceptible to environmental degradation during periods of reduced flow (initial tagging event to primary period 1), but more vulnerable to displacement during high flow events (flows from primary period 1 to primary period 2).

In summary, mark-recapture models developed for this study increased our understanding of patterns in encounter efficiency, abundance, and apparent survival for freshwater mussel populations in the East Fork San Jacinto River. Results also indicated that apparent survival was size dependent, meaning that mortality or permanent emigration was more probable for smaller mussels. Additional sampling would be needed to analyze potential effects on apparent survival by other factors like flow disturbance events. Characterizing reach-level channel morphology (e.g., geomorphic complexity, sinuosity) or local complex hydraulic conditions (e.g., Froude number, shear stress) could help to identify potential mechanisms that explain differences in apparent survival trends between habitat patches within the same river segment.

Literature Cited:

Ashton, M.J., J.S. Tiemann, and D. Hua. Evaluation of costs associated with externally affixing PIT tags to freshwater mussels using three commonly employed adhesives. *Freshwater Mollusk Biology and Conservation* 20:114–122.

- Bonner, T., B. Littrell, N. Martin, and D. Stitch. 2023. Range-wide Survey for Louisiana Pigtoe (*Pleurobema riddellii*) and Texas Heelsplitter (*Potamilus amphichaenus*). Final Report to Texas Comptroller of Public Accounts. Texas State University, San Marcos, TX, 78 pages.
- DeCicco, L. 2022. dataRetrieval: Retrieval functions for USGS and EPA Hydrologic and Water Quality Data. R package version 2.7.1.1.
- Gangloff, M.M., and J.W. Feminella. 2007. Stream channel geomorphology influences mussel abundance in southern Appalachian stream, U.S.A. *Freshwater Biology* 52:64–74.
- Gelman, A., and D.B. Rubin. 1992. Inference from iterative simulation using multiple sequences. *Statistical Science* 7:457–511.
- Haag, W.R. 2012. North American Freshwater Mussels: Natural History, Ecology, and Conservation. Cambridge University Press, New York, NY, 505 pages.
- Hobbs, N.T., and M.B. Hooten. 2015. Bayesian Models: A Statistical Primer for Ecologist. Princeton University Press, Princeton, NJ, 299 pages.
- Huggins, R.M. 1991. Some practical aspects of a conditional likelihood approach to capture experiments. *Biometrics* 47:725–732.
- Kellner, K. 2021. jagsUI: A wrapper around ‘rjags’ to streamline ‘JAGS’ analyses. R package version 1.5.2.
- Kendall, W.L., K.H. Pollock, and C. Brownie. 1995. A likelihood-based approach to capture-recapture estimation of demographic parameters under the robust design. *Biometrics* 51:293–308.
- Kéry, M., and J.A. Royle. 2020. Applied Hierarchical Modeling in Ecology: Analysis of distribution, abundance, and species richness in R and BUGS. Volume 2, Academic Press, Cambridge, MA, 787 pages.
- King, R. 2012. A review of Bayesian state-space modeling of capture-recapture-recovery data. *Interface Focus* 2:190–204.
- Kurth, J., C. Loftin, J. Zydlewski, and J. Rhymer. 2007. PIT tags increase effectiveness of freshwater mussel recaptures. *Freshwater Science* 26:253–260.
- Lebreton, J.D., K.P. Burnham, J. Clobert, and D.R. Anderson. 1992. Modeling survival and testing biological hypothesis using marked animals: A unified approach with case studies. *Ecological Monographs* 62:67–118.
- Lin Peterson, T. 2024. ggplot2: Create elegant data visualizations using the grammar of graphics. R package version 3.5.0.
- Marshall, M.R., D.R., Diefenbach, L.A. Wood, and R.J. Cooper. 2004. Annual survival estimation of migratory songbirds confounded by incomplete breeding site-fidelity: Study designs that may help. *Animal Biodiversity and Conservation* 27:59–72.

- Meador, J.R., J.T. Peterson, and J.M. Wisniewski. 2011. An evaluation of the factors influencing freshwater mussel capture probability, survival, and temporary emigration in a large lowland river. *Journal of the North American Benthological Society* 30:507–521.
- Nichols, J.D. 1992. Capture-Recapture Models. *BioScience* 42:94–102.
- Pollock, K.H. 1982. A capture-recapture design robust to unequal probabilities of capture. *Journal of Wildlife Management* 46:757–760.
- Riecke, T.V., A.G. Leach, D. Gibson, and J.S. Sedinger. 2018. Parameterizing the robust design in the BUGS language: Lifetime carry-over effects of environmental conditions during growth on a long-lived bird. *Methods in Ecology and Evolution* 9:2294–2305.
- Royle, J.A., and R.M. Dorazio. 2008. *Hierarchical Modeling and Inference in Ecology: The Analysis of Data from Populations, Metapopulations and Communities*. Academic Press, Burlington, MA, 444 pages.
- Sandercock, B.K. 2020. Mark-recapture models for estimation of demographic parameters. Pages 157–190 *in* *Population Ecology in Practice* (editors: D.L. Murray and B.K. Sandercock). Wiley-Blackwell Publishing, Oxford, UK, 448 pages.
- Sotola, V.A, K.T. Sullivan, B.M. Littrell, N.H. Martin, D.S. Stich, and T.H. Bonner. 2021. Short-term responses of freshwater mussels to floods in a southwestern U.S.A. river estimated using mark-recapture sampling. *Freshwater Biology* 66:346–361.
- Stanley, E.H., S.M. Powers, and N.R. Lottig. The evolving legacy of disturbance in stream ecology: concepts, contributions, and coming challenges. *Journal of the North American Benthological Society* 29:67–83.
- Strayer, D.L. 2008. *Freshwater Mussel Ecology: A multifactor approach to distribution and abundance*. University of California Press, Berkeley, CA, 216 pages.
- Watters, G.T. 1994. Form and function of Unionoidean shell sculpture and shape (Bivalvia). *American Malacological Bulletin* 11:1–20.
- Wisnkiewski, J.M., C.P. Shea, S. Abbott, and R.C. Stringfellow. 2013. Imperfect Recapture: a potential source of bias in freshwater mussel studies. *American Midland Naturalist* 170:229–247.
- Young, S.P. and J.J. Isely. 2008. Evaluation of methods for attaching PIT tags and biotelemetry devices to freshwater mussels. *Molluscan Research* 28:175–178.
- Zigler, S.J., T.J. Newton, J.J. Steuer, M.R. Bartsch, and J.S. Sauer. 2008. Importance of physical and hydraulic characteristics to unionid mussels: a retrospective analysis in a reach of large river. *Hydrobiologia* 598:343–360.

Table 1. Flow indices summarizing mean daily discharge (cfs) between sampling events during freshwater mussel mark-recapture surveys conducted from 2022 – 2024 in the East Fork San Jacinto River near Cleveland, Texas (USGS gage #08070000).

Flow Index	Initial Event - Primary 1 (413 days)		Primary 1 - Primary 2 (363 days)	
	Value	Standardized	Value	Standardized
Magnitude (cfs)				
Minimum	8	0.16	12	0.23
Median	32	0.62	73	1.42
Maximum	5670	111.00	45400	890
Frequency (# of days)				
Q10	51	0.12	0	0.00
Q90	77	0.19	125	0.34

Table 2. Total number of mussels tagged for all species observed during mark-recapture sampling at two sites in the East Fork San Jacinto River, Texas.

Scientific Name	Common Name	Site 1	Site 2	Total
<i>Amblema plicata</i>	Threeridge	1	0	1
<i>Cyclonaias pustulosa</i>	Pimpleback	859	183	1042
<i>Fusconaia</i> sp.	Texas/Wabash Pigtoe	1185	335	1520
<i>Lampsilis hydiana</i>	Louisiana Fatmucket	12	4	16
<i>Lampsilis teres</i>	Yellow Sandshell	15	6	21
<i>Leaunio lienosa</i>	Little Spectaclecase	2	0	2
<i>Megaloniaias nervosa</i>	Washboard	83	2	85
<i>Plectomerus dombeyanus</i>	Bankclimber	51	8	59
<i>Pleurobema riddellii</i>	Louisiana Pigtoe	65	7	72
<i>Potamilus fragilis</i>	Fragile Papershell	2	0	2
<i>Potamilus purpuratus</i>	Bleufer	13	1	14
<i>Quadrula quadrula</i>	Mapleleaf	2	0	2
<i>Toxolasma parvum</i>	Lilliput	1	0	1
<i>Toxolasma texasiense</i>	Texas Lilliput	3	0	3
<i>Truncilla truncata</i>	Deertoe	19	7	26
Species Richness		15	9	15
Total		2313	553	2866

Table 3. Estimates (Est) and associated 90% Bayesian credible intervals lower bound (LB) and upper bound (UB) for parameters of the observation process.

Parameter	Primary Period	Secondary Period	Site 1			Site 2		
			Est	LB	UB	Est	LB	UB
Pimpleback	-	-						
p	1	1	0.52	0.48	0.56	0.61	0.52	0.70
		2	0.46	0.42	0.50	0.35	0.28	0.43
		3	0.56	0.53	0.60	0.50	0.41	0.59
	2	1	0.31	0.27	0.34	0.51	0.43	0.59
		2	0.14	0.11	0.17	0.20	0.13	0.28
		3	0.39	0.36	0.43	0.44	0.36	0.52
p_μ	-	-	0.39	0.25	0.56	0.43	0.29	0.59
p_σ	-	-	0.93	0.55	1.96	0.80	0.44	1.76
p^*	1	-	0.89	0.87	0.90	0.88	0.83	0.91
	2	-	0.64	0.61	0.67	0.78	0.73	0.83
γ	-	-	0.49	0.42	0.57	0.71	0.55	0.90
Fusconaia sp.	-	-						
p	1	1	0.47	0.43	0.51	0.53	0.46	0.59
		2	0.41	0.38	0.44	0.40	0.35	0.45
		3	0.61	0.57	0.64	0.57	0.50	0.63
	2	1	0.29	0.26	0.32	0.50	0.44	0.55
		2	0.11	0.09	0.13	0.30	0.24	0.36
		3	0.47	0.43	0.50	0.37	0.32	0.43
p_μ	-	-	0.89	0.75	0.98	0.44	0.34	0.56
p_σ	-	-	0.60	0.46	0.76	0.55	0.30	1.22
p^*	1	-	0.88	0.86	0.89	0.88	0.85	0.90
	2	-	0.66	0.64	0.69	0.78	0.74	0.81
γ	-	-	0.42	0.35	0.52	0.69	0.61	0.79
Louisiana Pigtoe	-	-						
p	1	1	0.44	0.32	0.56	0.61	0.30	0.92

		2	0.46	0.34	0.59	0.41	0.15	0.70
		3	0.60	0.47	0.72	0.60	0.30	0.92
	2	1	0.21	0.12	0.33	0.28	0.05	0.57
		2	0.23	0.13	0.35	0.18	0.01	0.52
		3	0.59	0.46	0.71	0.50	0.23	0.81
p_μ	-	-	0.42	0.25	0.61	0.43	0.19	0.70
p_σ	-	-	0.97	0.50	2.14	1.34	0.18	3.62
p^*	1	-	0.88	0.82	0.93	0.93	0.73	0.99
	2	-	0.76	0.66	0.84	0.75	0.43	0.92
γ	-	-	0.86	0.62	0.99	-	-	-

Table 4. Estimates (Est) and associated 90% Bayesian credible intervals lower bound (LB) and upper bound (UB) for effect sizes of median shell length on apparent survival probability.

Species	Site 1			Site 2		
	Est	LB	UB	Est	LB	UB
Pimpleback	0.18	0.08	0.31	0.16	0.07	0.35
Fusconaia sp.	0.12	0.06	0.20	0.16	0.08	0.27
Louisiana Pigtoe	0.21	0.06	0.40	-	-	-

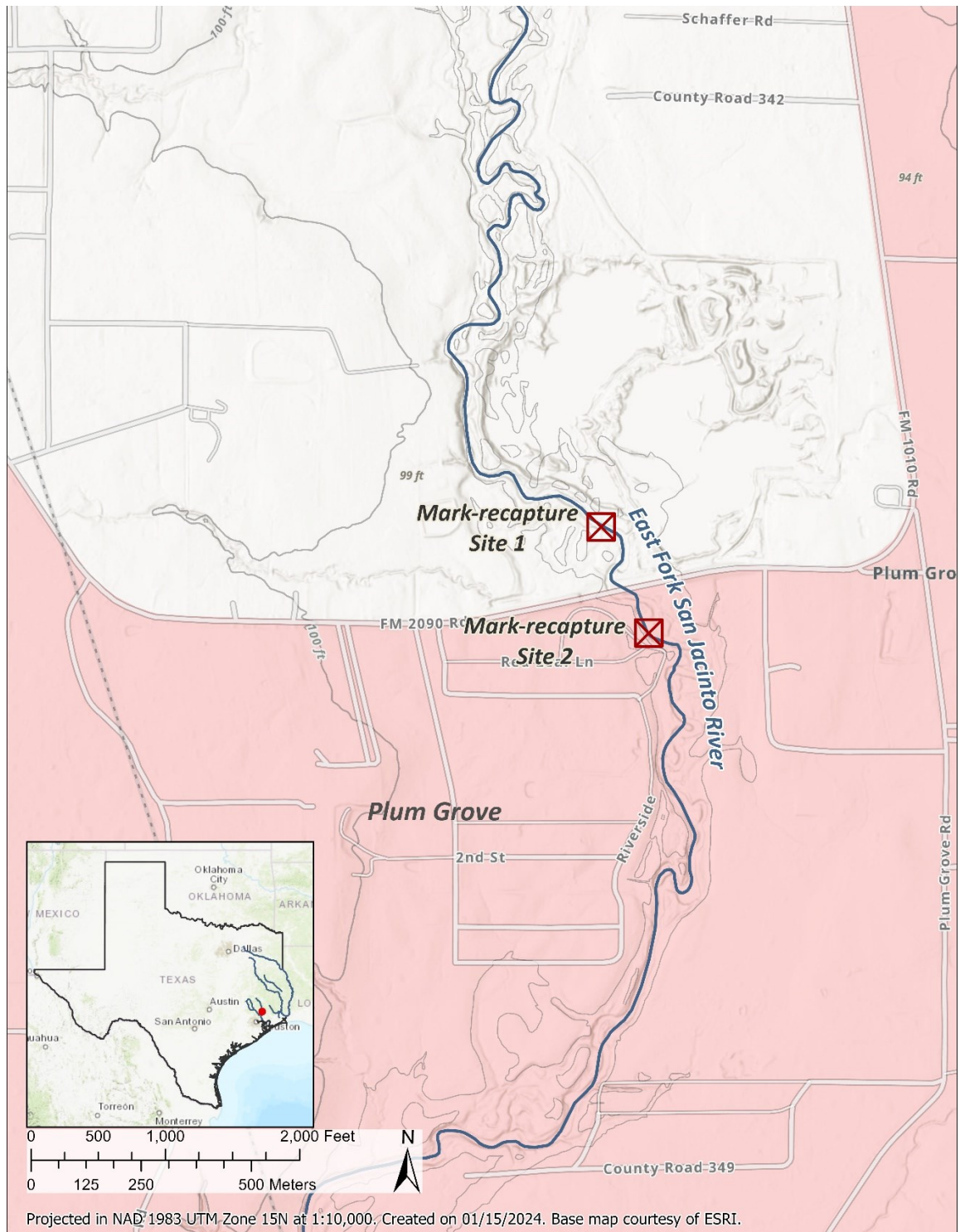


Figure 1. Map of the study area displaying the mark-recapture sample sites used for assessing population dynamics of freshwater mussels in the East Fork San Jacinto River, Texas.

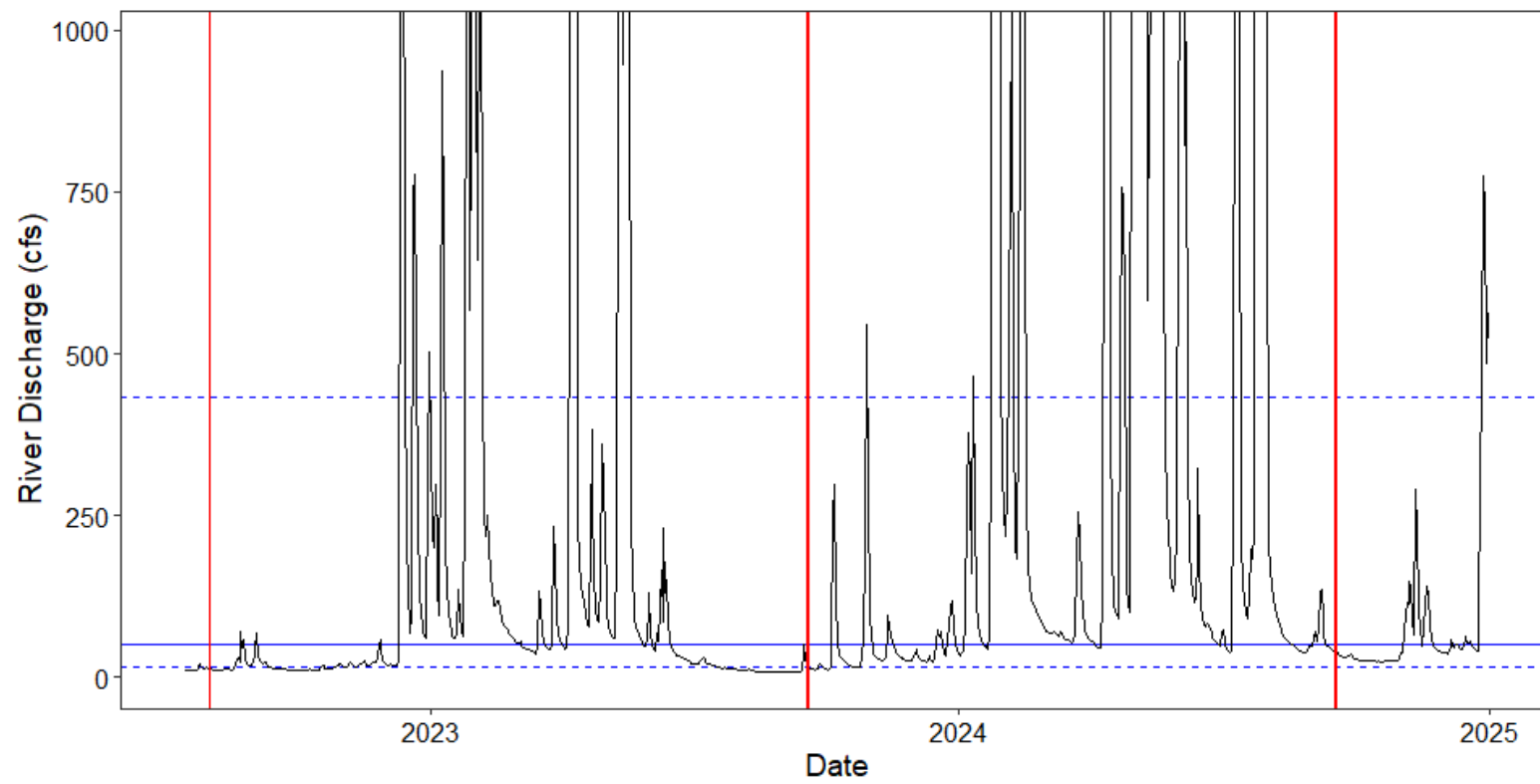


Figure 2. Time-series displaying mean daily discharge (cfs) during mark-recapture sampling in East Fork San Jacinto River near Cleveland, Texas (USGS gage #08070000) from 2022 – 2024. Red vertical lines denote sampling events, the solid blue line represents the long-term median (51 cfs), and dashed blue lines are Q10 (15 cfs) and Q90 (432 cfs) flow magnitudes. Multiple high flow pulses > 1,000 cfs that occurred over the study duration were above the y-axis scale and not shown to here to make the time-series easier to interpret.

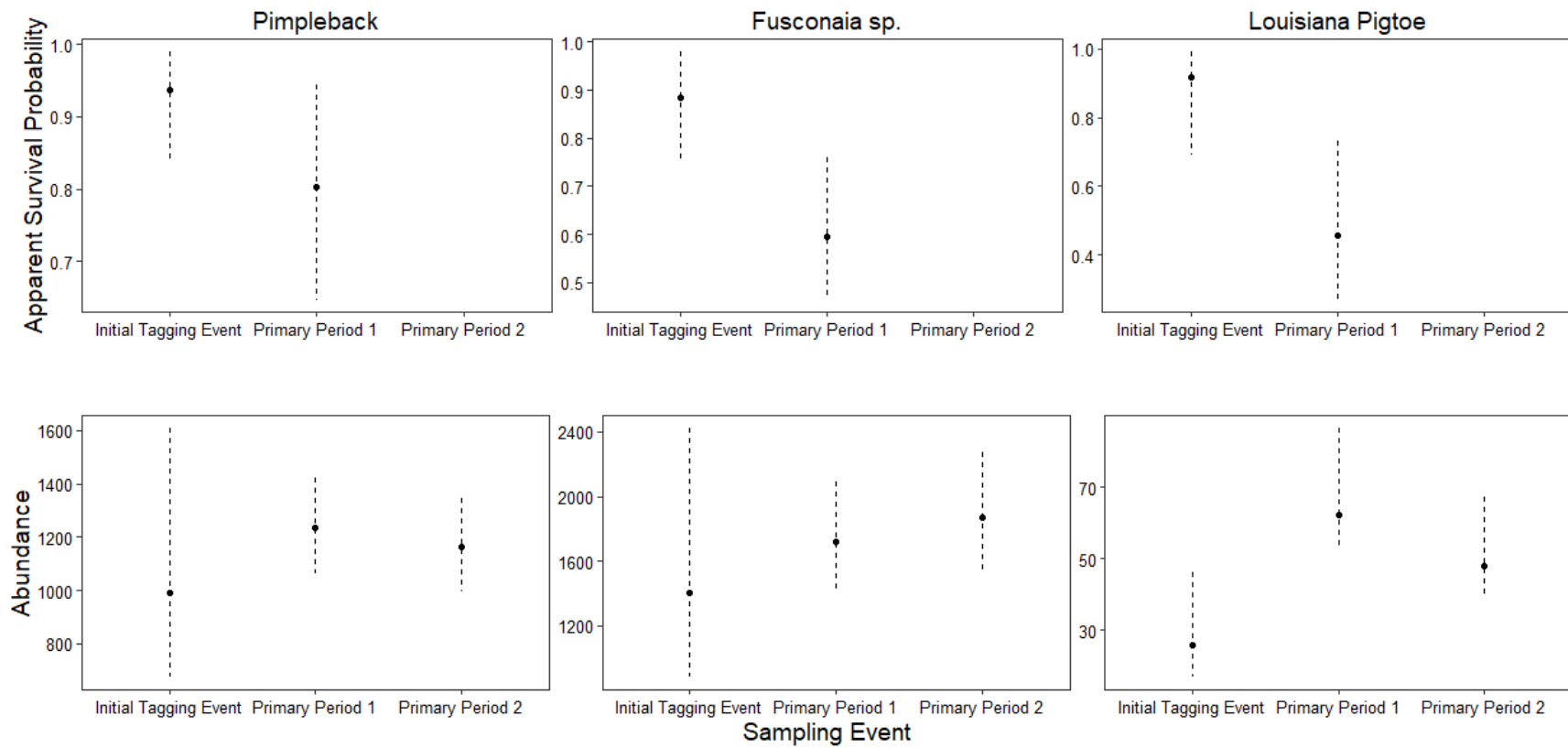


Figure 3. Estimates and 90% Bayesian credible intervals of apparent survival (top row) and abundance (bottom row) during each mark-recapture sampling event at Site 1.

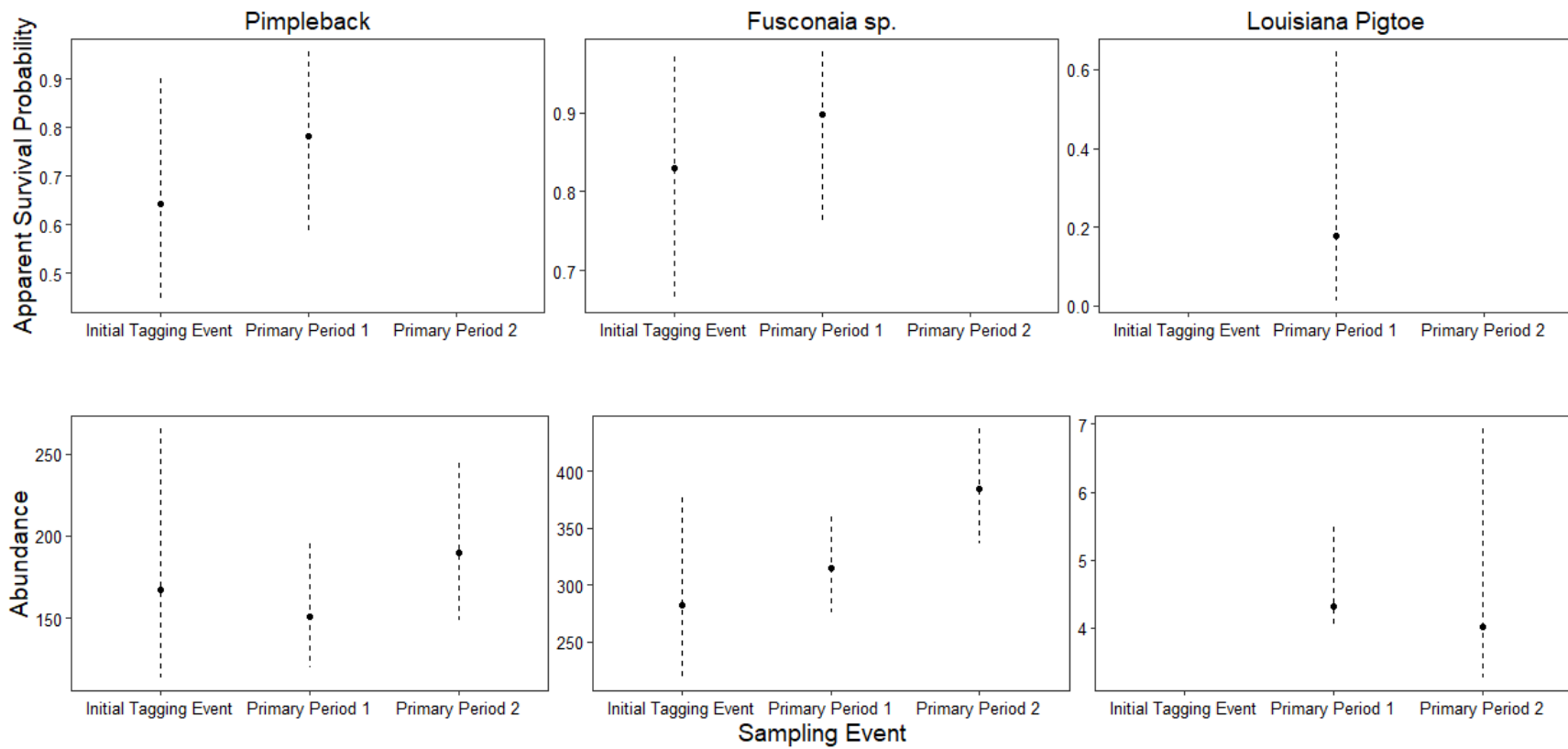


Figure 4. Estimates and 90% Bayesian credible intervals of apparent survival (top row) and abundance (bottom row) during each mark-recapture sampling event at Site 2.

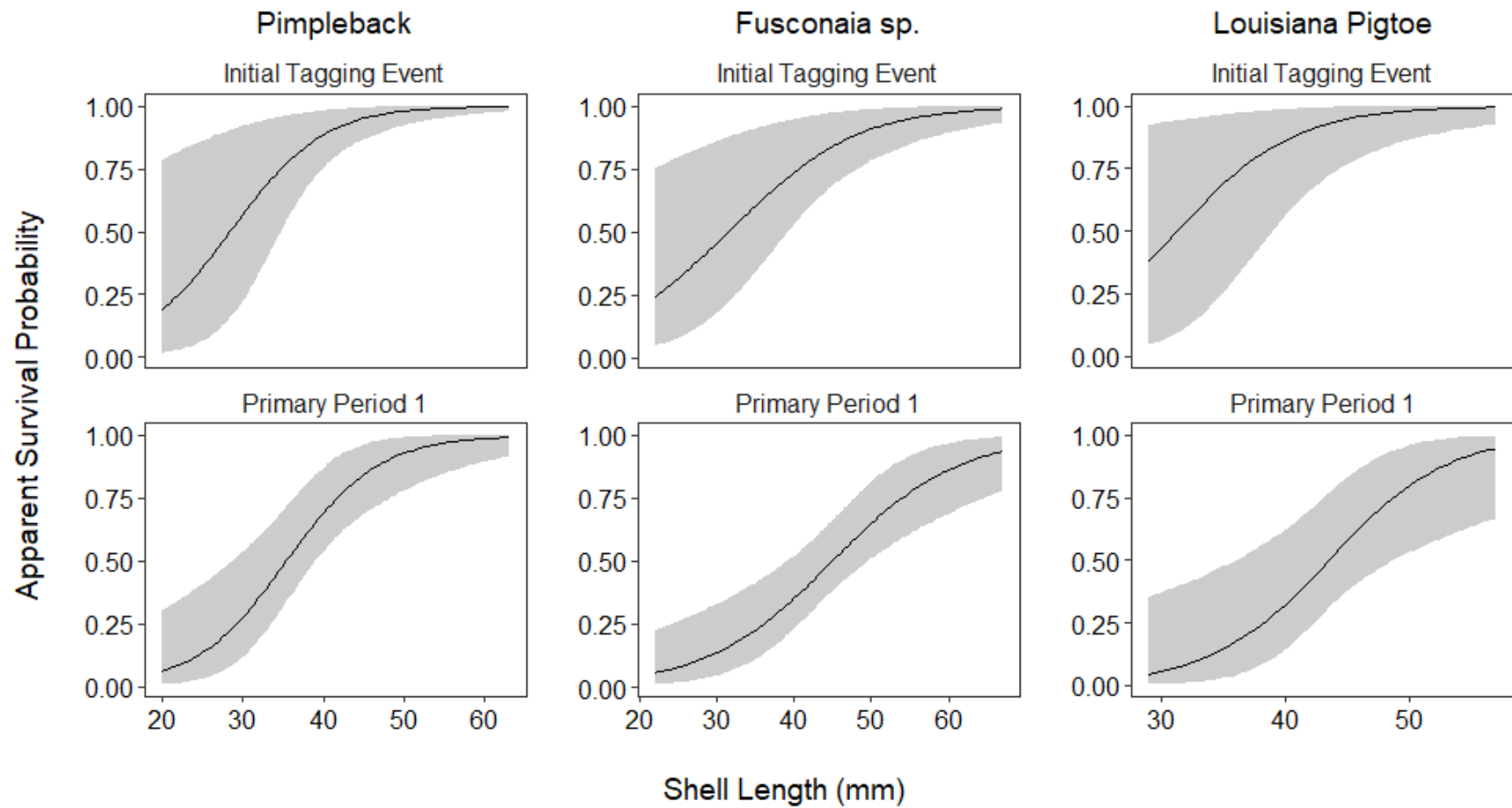


Figure 5. Fitted functions displaying apparent survival probability's relationship with median shell length at Site 1. Solid lines represent median apparent survival probability predictions and solid polygons denote 90 % Bayesian credible intervals.

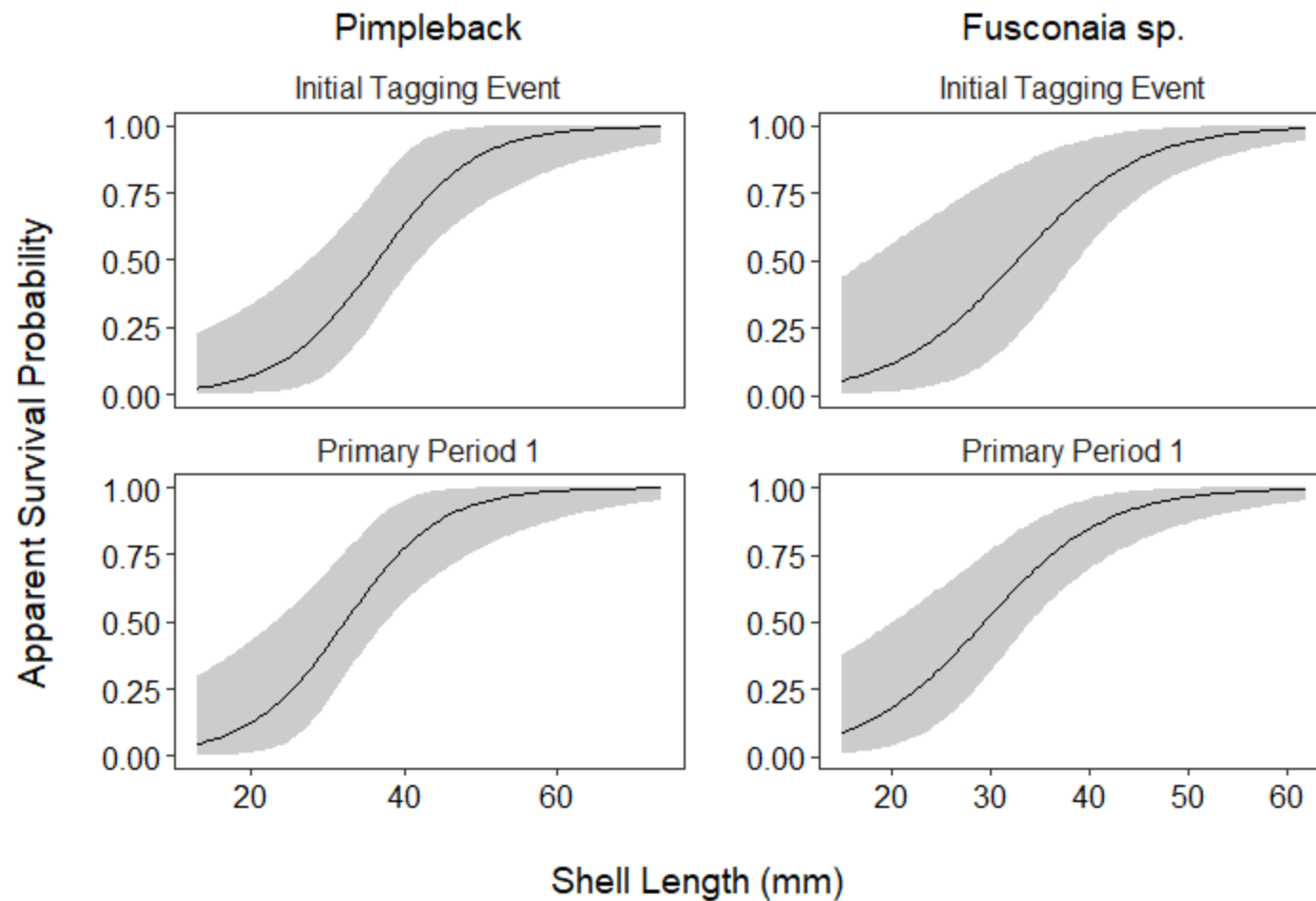


Figure 6. Fitted functions displaying apparent survival probability's relationship with median shell length at Site 2. Solid lines represent median apparent survival probability predictions and solid polygons denote 90 % Bayesian credible intervals.

Appendix A: Model Formulation – Full description of data structure and model parameterization

Cormack-Jolly-Seber robust design models were used to estimate abundance, apparent survival, site propensity, and detectability for each species. Data structure and model parameterization were performed based on code provided by Riecke et al. (2018) and Sotola et al. (2021). Three observational data matrices were required to fit each model: 1) primary period encounter history ($y_{i,t}$) – $i \times t$ matrix that classifies whether an individual (i) was detected or not detected in a given primary period (t); 2) secondary period detection history ($DH_{t,j}$) – $t \times j$ matrix denoting the number of mussels detected in secondary period j within primary period t ; and 3) secondary period nondetection history ($NDH_{t,j}$) – $t \times j$ matrix denoting the number of mussels not detected in secondary period j within primary period t but was detected during another j sample in the same primary period.

Each model parameter is defined in Table A1 and model parameterization is defined as follows. Secondary period detection probability ($p_{t,j}$) was the probability of detecting an individual during sample j in primary period t ($DH_{t,j}$), conditional on being available for capture ($Total_{t,j} = DH_{t,j} + NDH_{t,j}$). $DH_{t,j}$ was modeled under the assumptions that the population was closed within each primary period and that the observed detections histories are a realization of binomial random variables with probability of success equal to $p_{t,j}$ and the number of individuals available for sampling equal to $Total_{t,j}$ (Huggins 1991).

$$1) \quad DH_{t,j} \sim \text{Binomial}(p_{t,j}, Total_{t,j})$$

Secondary period detection probability per primary period was modeled as random variation ($\varepsilon.p_{t,j}$) around a mean ($\alpha.p$).

$$2) \quad \begin{aligned} \text{logit}(p_{t,j}) &= \alpha.p + \varepsilon.p_{t,j} \\ \varepsilon.p_{t,j} &\sim \text{Normal}(0, \tau.p^2) \end{aligned}$$

Secondary period detection probability was used to estimate primary period probability (p_t^*), which was the probability of detecting an individual at least once during primary period t , given it was present (Kendall et al. 1995). During the October 2021 event with one secondary period, p_t^* was set equal to mean secondary detection probability ($\alpha.p$).

$$3) \quad p_t^* = 1 - \left[\prod_{j=1}^J (1 - p_{t,j}) \right]$$

True state of individual i at the primary period that it was first captured (f_i) to primary period t was defined by latent variable $z_{i,t}$ modeled as a realization of a Bernoulli random variable governed by the product of the true state ($z_{i,t-1}$) and apparent survival ($\varphi_{i,t-1}$) of individual i at primary period $t-1$.

$$4) \quad \begin{aligned} z_{i,f_i} &= 1 \\ z_{i,t} &\sim \text{Bernoulli}(z_{i,t-1}\varphi_{i,t-1}) \end{aligned}$$

Survival was considered apparent because it is confounded with site fidelity; therefore, defined as the probability that an individual within the population survives and remains in the sampling area from primary period $t-1$ to t (Lebreton et al. 1992; Marshall et al. 2004). In addition, apparent survival for each individual was modeled as a function of median shell length ($X.\text{shell.length}_i$) with a fixed slope ($\beta.\varphi$) and time-fixed intercepts for each sampling event ($\alpha.\varphi_t$).

$$5) \quad \text{logit}(\varphi_{i,t}) = \alpha.\varphi_t + \beta.\varphi \times X.\text{shell.length}_i$$

The observation process of encounter histories ($y_{i,t}$) was also modeled as a realization of a Bernoulli trial where success probability was governed by the product of $z_{i,t}$, p_t^* , and site propensity (γ), which is the probability that an individual remains available for encounter during each sampling event.

$$6) \quad y_{i,t} \sim \text{Bernoulli}(z_{i,t}p_t^*\gamma)$$

The product of p_t^* and γ represents apparent encounter rate, defined as the probability of capturing an individual that is available for sampling (i.e., mussel is at or near the surface of the streambed) (Meador et al. 2011; Sandercock 2020). Site propensity was modeled as a fixed parameter.

Population abundance cannot be estimated directly from the process model due to conditioning on the initial capture of each mussel (King 2012). Therefore, species abundance (N_t) was estimated for the initial tagging event and each primary period as a derived parameter based on the total number of individuals collected at event t (C_t), p_t^* , and γ (Nichols 1992). Parameter N_t represents the total number of surface and subsurface individuals that are alive at event t .

7)

$$N_t = \frac{C_t}{p_t^* \gamma}$$

Table A1. Definitions of demographic parameters specified in the Bayesian open robust design mark recapture models.

Parameter	Notation	Definition
Abundance	N_t	Total abundance at sampling event t .
Apparent survival	$\varphi_{i,t}$	Probability individual i at sampling event t survives and remains in the sampling area at $t+1$.
Site propensity	γ	Probability that an individual is available for encounter during each sampling event, conditional upon φ_t .
Primary period detection	p_t^*	Probability that an individual was detected at least once during primary period t .
Apparent encounter rate	$p_t^* \gamma$	Probability that an individual was detected at least once during primary period t , given it was available for sampling.
Secondary period detection	$p_{t,j}$	Probability that an individual was detected during secondary period j within primary period t .

5B. Reach-level Monitoring Protocols

Methods: Protocol Development

Data from recent and ongoing east Texas mussel surveys by the study team were compiled and analyzed in conjunction with other available data sources to examine current distribution of Louisiana Pigtoe and Texas Heelsplitter within the San Jacinto, Neches, and Sabine river drainages of east Texas. This information was utilized to identify key monitoring areas within each basin. Recommended monitoring methodologies were developed based on existing literature and were based on similar methodologies currently being implemented to monitor listed mussels in other Texas river basins.

Results: Protocol

Experimental Design

A variety of sampling designs, population metrics, and modeling frameworks have been utilized to monitor spatiotemporal trends of mussel populations (Strayer and Smith 2003; Pandolfo et al. 2016; Carey et al. 2019). Selection of an appropriate experimental design and metrics to assess population performance should be based on goals of the study and best available information on the species to develop sampling methodologies that can provide reliable inferences and easily interpreted results (Yoccoz et al. 2001; Kéry and Royle 2015). Due to the cryptic nature of freshwater mussels, and low catch rates shown of the target species, it may be difficult to reliably estimate abundance. Thus, abundance data may have limited utility for evaluating population performance. In contrast, occurrence (i.e., presence/absence) is often a more practical metric for evaluating population trends of rare species. Occurrence is typically positively related to abundance; therefore, changes in occurrence can reliably reflect population changes. Lastly, the increased popularity of using occurrence data for ecological research has led to the development of a multitude of modeling frameworks to help make unbiased estimates for population parameters of interest (i.e., site-occupancy models) (Kéry and Royle 2015; MacKenzie et al. 2018).

A multiscale hierarchical study design was recently developed in coordination with United States Fish and Wildlife Service (USFWS) and implemented to monitor changes in occupancy for federally listed mussel populations within the Brazos River basin (BIO-WEST/BRA 2023). A similar methodology was also utilized to collect data on listed mussel species within the Guadalupe River basin in 2024. This sampling methodology was designed to increase search area and improve detection rates at a given sampling site compared to previously used methodologies. It also provides replication at multiple spatial scales and complements a variety of analytical approaches (Hastie et al. 2009; Kéry and Royle 2015; MacKenzie et al. 2018).

Spatial subsampling within the methodology provides the ability to make inferences into population condition at multiple levels and account for imperfect detection (Figure 1). Level 1 represents the population of the target species at the basin level. Level 2 corresponds to the sub-basins occupied by the target species. Level 3 represents distinct survey reaches established based on access points within the occupied portion of each sub-basin. Typically, three reaches have been surveyed per sub-basin. Level 4 represents individual sampling sites within each survey reach which correspond to riffle/run complexes or gravel bars to ensure that a variety of

mesohabitat types are available for sampling. Three to four sites are generally surveyed per reach; however, the number of sites and survey replicates may be tailored to the species being targeted. Level 5 represents the mesohabitat spatial scale, with sampling conducted within three mesohabitat types (swift [e.g., riffles]; moderate velocity [e.g., runs]; and slackwater [e.g., pools and backwaters]) at each site. Lastly, Level 6 represents replication within each mesohabitat in the form of 10-m long sampling transects. Four transects are generally conducted within each mesohabitat, with each being delineated as bank (associated with the stream edge) or non-bank (not associated with the edge).

Sampling Methodology

Prior to field surveys, potential sampling sites within accessible areas of survey reaches can be identified using desktop analysis of aerial/satellite imagery. For each sampling event, a minimum of three sampling sites are then selected randomly and loaded onto a handheld GPS device. In the field, each sampling site is sub-divided into swift (riffles), moderate velocity (runs), and slackwater (pools and backwaters) habitats. Four 10-m long transects (lead core rope with anchors on each end) are placed within each mesohabitat. Surveyors search a 1-meter-wide path along each transect using visual and/or tactile survey methods. After visual/tactile searches, five substrate sieve samples ($\approx 4,500 \text{ cm}^3$ each collected over an approximately 0.25 m^2 area) are collected along each transect using a small garden shovel and sieve to locate small or sub-surface individuals, which may be overlooked using standard survey methods. Using this method, surveys cover a 10 m^2 search area per transect and 120 m^2 search area per sampling site. Search time is recorded per transect to allow quantification of effort in person-hours. All mussels are placed in mesh bags sorted by transect and kept in the water until survey completion. Following completion, all native unionids are enumerated by species, shell lengths are measured to the nearest millimeter for at least 20 individuals of each species, and target species are visually examined for gravidity. Following data collection, all mussels are returned to the area of collection.

To characterize habitat conditions at each transect, water depth (ft), benthic velocity (ft/s), and mean column velocity (ft/s) are measured with an incremental wading rod and flowmeter. Percent substrate composition is visually estimated at each transect, along with percent cover of various habitat attributes such as large woody debris and undercut bank. Lastly, standard water quality parameters are measured at each mesohabitat using a handheld water quality sonde.

Monitoring Areas

Based on the most current information regarding the distribution and abundance of the target species, the following monitoring areas are recommended to implement the above protocol within Texas portions of the San Jacinto, Neches, and Sabine River basins. Based on current uncertainty regarding the taxonomic status of Louisiana Pigtoe within the Red/Cypress River drainage of Texas, it is not included here.

San Jacinto River Basin

Texas Heelsplitter does not occur within the San Jacinto River drainage, so monitoring locations are focused on Louisiana Pigtoe. Historical records (pre-1995) of Louisiana Pigtoe exist in the West Fork San Jacinto River below Lake Conroe and in the East Fork of the San Jacinto River near and downstream of Cleveland, Texas (Randklev et al. 2023). However, information from contemporary survey data suggests that the current distribution of Louisiana Pigtoe is limited to two areas within the San Jacinto River basin (Figure 2; USFWS 2020, Randklev et al. 2023). First, the species has been documented from six localities in a segment of the East Fork San Jacinto River near Plum Grove, Texas and downstream towards Lake Houston. Second, the species has been observed at two locations within a 0.5-mile segment of Lake Creek, a tributary to the West Fork San Jacinto River. Based on this rather limited distribution in the basin, monitoring for Louisiana Pigtoe is recommended at two reaches, one within each currently occupied portion of the basin (Table 1).

Trinity River Basin

Although historically documented within the basin, Louisiana Pigtoe has not been documented from the Trinity River during contemporary surveys (Randklev et al. 2023). Therefore, monitoring areas focused on Texas Heelsplitter. Texas Heelsplitter is currently known to occupy three areas within the basin: the mainstem Trinity River upstream from Lake Livingston, a short segment of Bédias Creek near Madisonville, and Grapevine Lake within the Dallas metro complex (Figure 3; USFWS 2023). However, the Grapevine Lake population is considered functionally extirpated by USFWS and is not considered here (USFWS 2023). Although recent survey efforts did not locate Texas Heelsplitter within Bédias Creek, it has been documented as recently as 2017, and therefore monitoring of this reach was included here (Figure 3, Randklev et al. 2023). Given the length of the occupied segments, one reach is recommended in Bédias Creek and a minimum of three are recommended within the mainstem Trinity River upstream of Lake Livingston (Table 1).

Neches River Basin

Louisiana Pigtoe is currently distributed in five major areas of the Neches River basin: 1) the upper Neches River from Lake Palestine Dam to BA Steinhagen Reservoir; 2) the lower Neches River from BA Steinhagen Reservoir to near the confluence of Pine Island Bayou; 3) Village Creek; 4) the Angelina River from approximately FM 343 to Sam Rayburn Reservoir; and 5) perennial portions of the LNVA Canal System near Beaumont, Texas (Figure 4; USFWS 2023, Randklev et al. 2023). Within these areas, Texas Heelsplitter is also found in the upper and lower Neches River sub-basins. A minimum of three survey reaches are recommended in each of these occupied sub-basins (Table 1).

Sabine River Basin

Within the Sabine River basin, the current distribution of Texas Heelsplitter is limited to the upper Sabine River mainstem from Lake Tawakoni to Toledo Bend Reservoir and lower segments of Lake Fork Creek. Within this, the current distribution of Louisiana Pigtoe within the mainstem Sabine River extends from approximately FM 14 near Hawkins, Texas to State Highway 43 near Tatum, Texas. Neither species has been documented within the mainstem lower Sabine River (Figure 4, Figure 5; USFWS 2023, Randklev et al. 2023). However, Louisiana Pigtoe is known from portions of Anacoco Bayou, a Louisiana tributary to the lower Sabine. Recommended monitoring areas focus on Texas portions of the upper Sabine River, with

prioritization of the segment from FM 14 to Hwy. 43, where both species occur. A minimum of three survey reaches are recommended within the upper Sabine River sub-basin (Table 1).

Synthesis

The protocol outlined above would result in monitoring of a minimum of 24 reaches covering all the stream reaches in Texas currently occupied by Louisiana Pigtoe and Texas Heelsplitter. The exact number of sites per reach and transect replicates per mesohabitat can be adjusted based on the species being targeted and known habitat conditions across reaches to maximize power to detect trends. Monitoring of each reach on an annual or biennial basis could generate data on spatiotemporal trends in occurrence to inform species management. For Louisiana Pigtoe, this would result in monitoring of a minimum of 20 occupied reaches in the San Jacinto, Neches, and Sabine River basins. For Texas Heelsplitter, monitoring would be focused on at least 13 reaches of the Trinity, Neches, and Sabine River basins. Reaches where the two species overlap, such as the mainstem upper Neches River, lower Neches River, and upper Sabine River, should be particularly prioritized for monitoring. Exact locations of survey reaches within each occupied sub-basin will be dependent upon available access points and can be chosen in coordination with stakeholders or funding agencies. As more survey data becomes available, boundaries to occupied areas, recommended number of survey reaches or sites, and other details may need to be modified through adaptive management.

A similar version of the protocol outlined above is currently being utilized to monitor listed freshwater mussel populations in other central Texas river basins. Additionally, the Sabine River Authority has plans to implement this multiscale protocol within the upper Sabine River sub-basin. Monitoring other occupied sub-basins in east Texas will be important to fully evaluate population condition across the range of Louisiana Pigtoe and Texas Heelsplitter and inform species management and conservation. Implementing a multiscale sampling design such as this also offers opportunities for investigating effects of broad-scale (e.g., flow regime, landcover) and local-scale (e.g., substrate, current velocity) environmental factors on occupancy. This would provide inferences about potential determinants on patterns of occurrence to ensure assessments and decisions for mussel populations of interest are conducted in a more ecologically rigorous manner.

Literature Cited

- BIO-WEST, Inc. (BIO-WEST) and Texas State University (TSU). 2023. Sabine River Basin Freshwater Mussel Monitoring 2023 Report. Final Report to Sabine River Authority of Texas. May 2024. 25 pp.
- BIO-WEST/BRA (Brazos River Authority). 2023. Candidate Conservation Agreement with Assurances for Balcones Spike and Texas Fawnsfoot in the Brazos River Basin: Methodology for Long-term Monitoring of Key Populations. 15 pp.
- Carey, C.S., J.W. Jones, R.S. Butler, M.J. Kelly, and E.M. Hallerman. 2019. A comparison of systematic quadrat and capture-mark-recapture sampling designs for assessing freshwater mussel populations. *Diversity* 11, doi:10.3390/d11080127.
- Ford, D.F., E.D. Plants-Paris, N.B. Ford. 2022. Density, apparent survival, and local population size of Louisiana Pigtoe (*Pleurobema riddellii*) in the Neches River, Texas. *Freshwater Mollusk Biology and Conservation* 25(2): 74-81 (2022).
- Hastie, H., R. Tibshirani, and J. Friedman. 2009. *The Elements of Statistical Learning: Data Mining, Inference, and Prediction*. 2nd edition. Springer, New York, NY.
- Kéry, M., and J.A. Royle. 2015. *Applied Hierarchical Modeling in Ecology: Analysis of distribution, abundance, and species richness in R and BUGS*. Volume 1, Academic Press, Cambridge, MA.
- MacKenzie, D.I., J.D. Nichols, J.A. Royle, K.H. Pollock, L.L. Bailey, and J.E. Hines. 2018. *Occupancy Estimation and Modeling: Inferring Patterns and Dynamics of Species Occurrence*. 2nd edition, Academic Press, Cambridge, MA.
- Pandolfo T.J., T.J. Kwak, W.G. Cope, R.J. Heise, R.B. Nichols, and K. Pacifici. 2016. Species traits and catchment-scale habitat factors influence the occurrence of freshwater mussel populations and assemblages. *Freshwater Biology* 61:1671-1684.
- Randklev, C.R., C. Robertson, C.H. Smith, A.H. Kiser, N.B. Ford, M. Hart, J. Khan, M. Fisher, and R. Lopez. (2023). *Mussels of Texas Project Database, Version 2.0*.
- Strayer, D.L., and D.R. Smith. 2003. *A Guide to Sampling Freshwater Mussel Populations*. American Fisheries Society, Bethesda, MD.
- United States Fish and Wildlife Service (USFWS). 2023. Proposed Rule. Endangered Species Status with Critical Habitat for Texas Heelsplitter, and Threatened Status with Section 4(d) Rule an Critical Habitat for Louisiana Pigtoe. *Federal Register* 88(53): 16776-16832. March 20, 2023.
- USFWS. 2020. Draft Species Status Assessment Report for Two Freshwater Mussels: Louisiana Pigtoe (*Pleurobema riddellii*) and Texas Heelsplitter (*Potamilus amphichaenus*). Version 1.1 May 2020. USFWS Region 2, Albuquerque, New Mexico.
- Yoccoz, N.G., J.D. Nichols, and T. Boulinier. 2001. Monitoring of biological diversity in space and time. *Trends in Ecology & Evolution* 16:446–453.

Table 1. Currently occupied sub-basins for monitoring Louisiana Pigtoe and Texas Heelsplitter along with recommended minimum number of survey reaches.

Basin	Occupied Sub-basin Recommended for Monitoring	Louisiana Pigtoe	Texas Heelsplitter	General Area / Boundaries	Recommended Minimum Number of Survey Reaches
San Jacinto	East Fork San Jacinto River	X		Near FM 2090 Crossing near Plum Grove	1
	Lake Creek	X		Near Honea-Egypt Road Crossing	1
Trinity	Trinity River		X	Ennis, Tx to Lake Livingston Hwy. 75 Crossing to Trinity River	3
	Bedias Creek		X	Confluence	1
Neches	Neches River	X	X	Lake Palestine Dam to BA Steinhagen	3
	Lower Neches River	X	X	Town Bluff Dam to Saltwater Barrier	3
	Village Creek	X		All of Village Creek	3
	Angelina River	X		FM 343 to US 59	3
	LNVA Canal System	X		Perennial portions of the canal system	3
Sabine	Upper Sabine River	X	X	Lake Tawakoni to Toledo Bend	3
Total Number of Survey Reaches					24

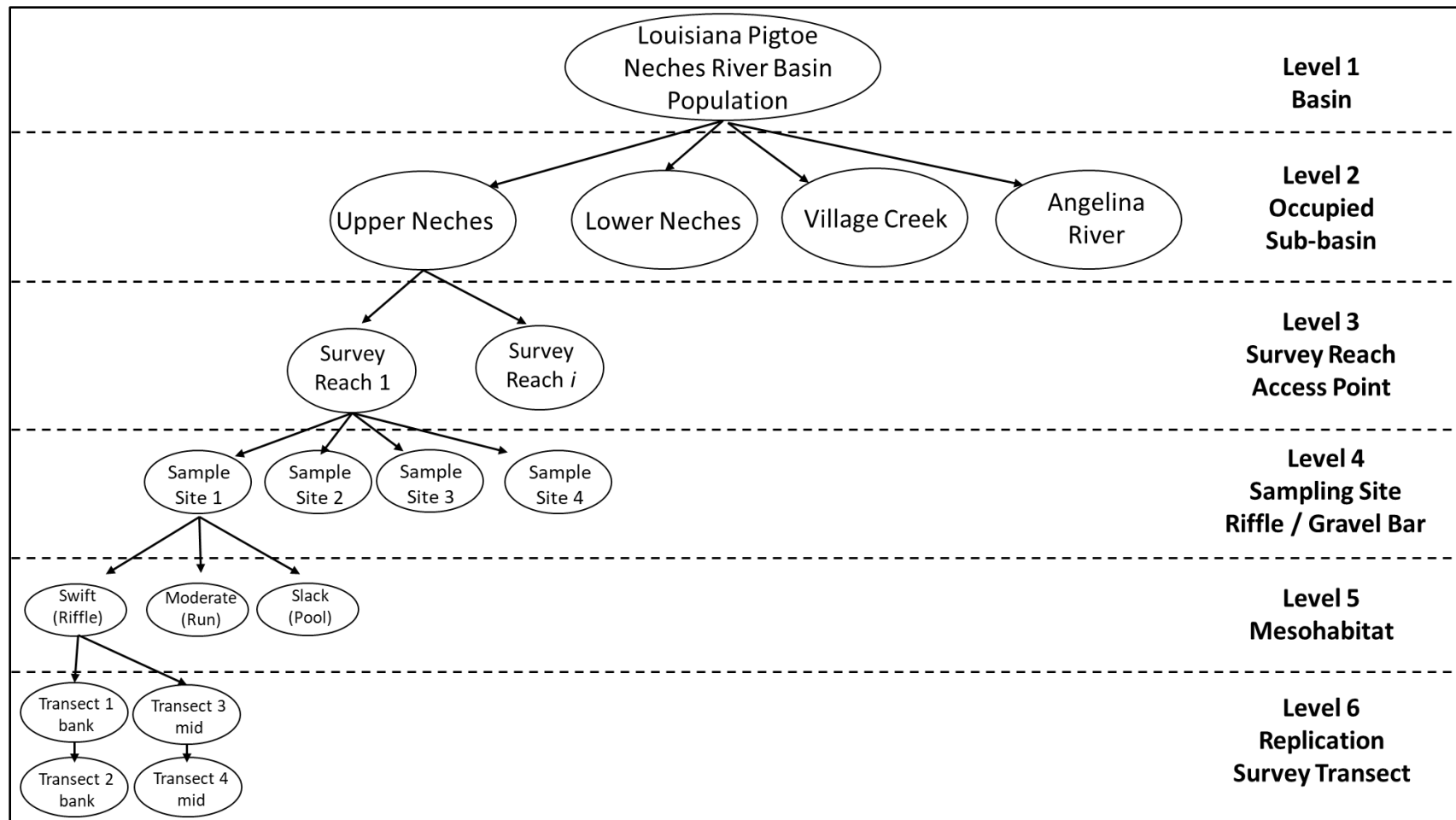


Figure 1. Example of multiscale hierarchal experimental design within the Neches River basin.

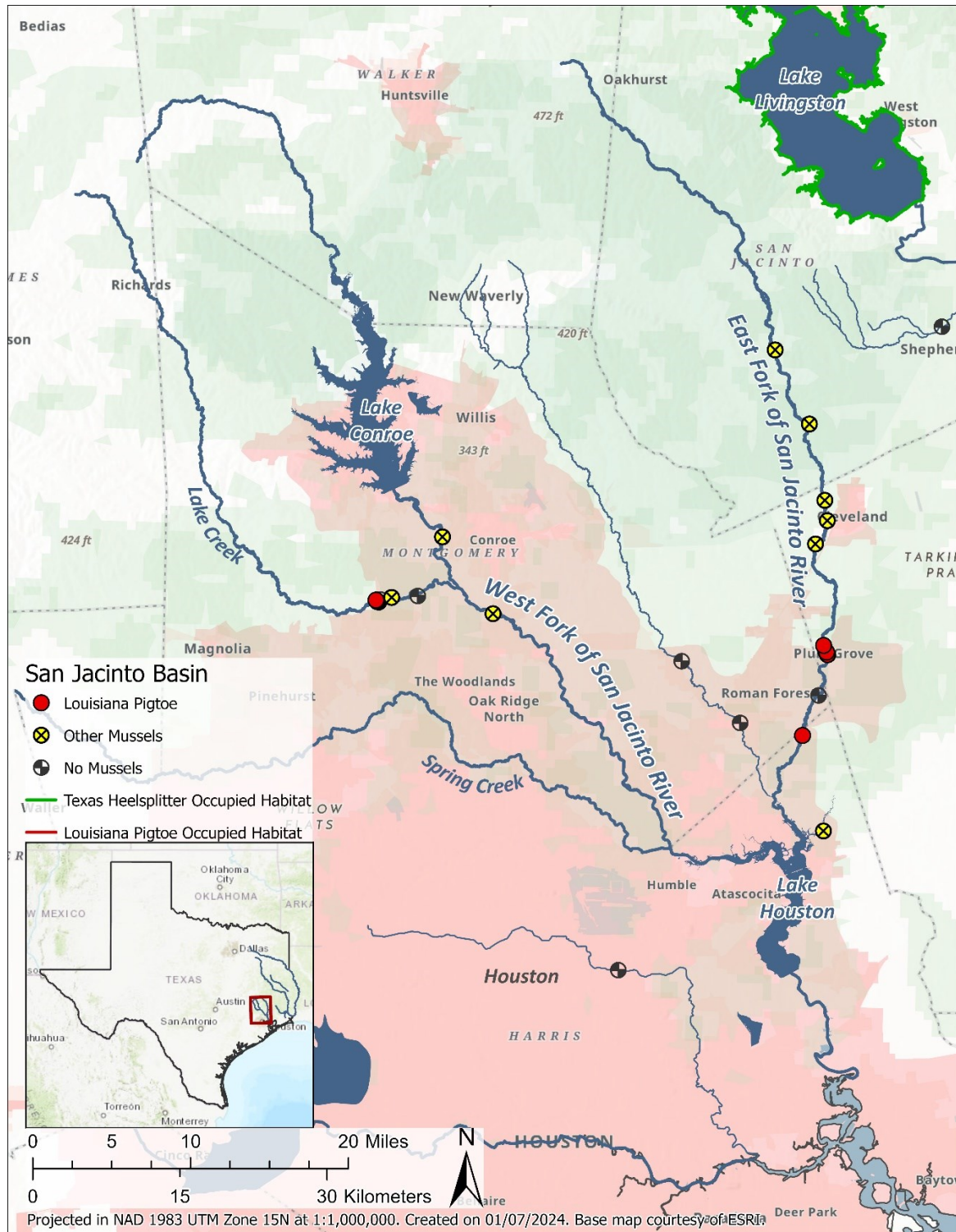


Figure 2. Map showing Louisiana Pigtoe occurrence within the San Jacinto River basin. Occupied habitat information from USFWS 2023 and USFWS 2020 is represented by colored lines, with point data reflecting recent survey data collected by the study team.

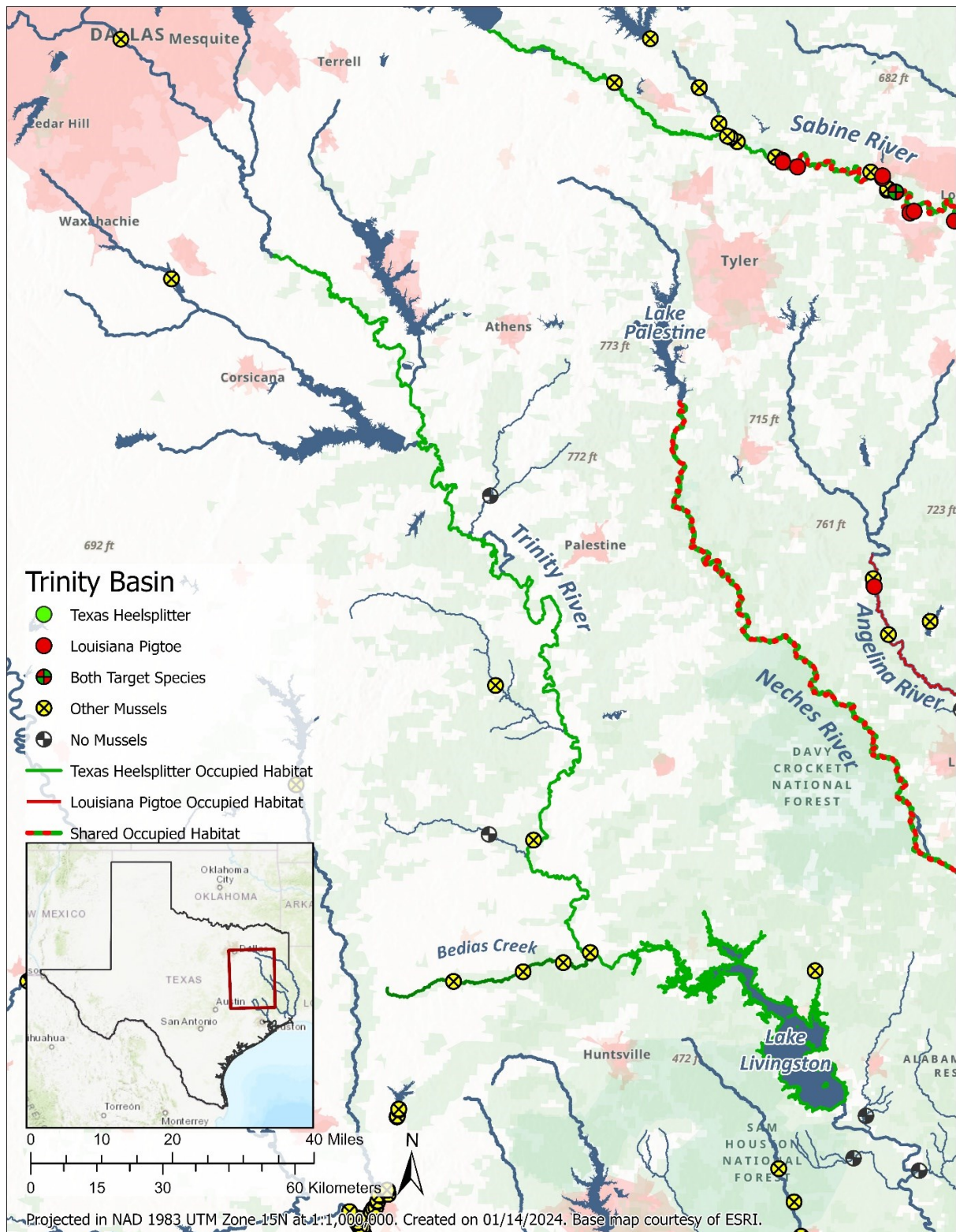


Figure 3. Map showing Texas Heelsplitter occurrence within the Trinity River basin. Occupied habitat information from USFWS 2023 and USFWS 2020 is represented by colored lines, with point data reflecting recent survey data collected by the study team.

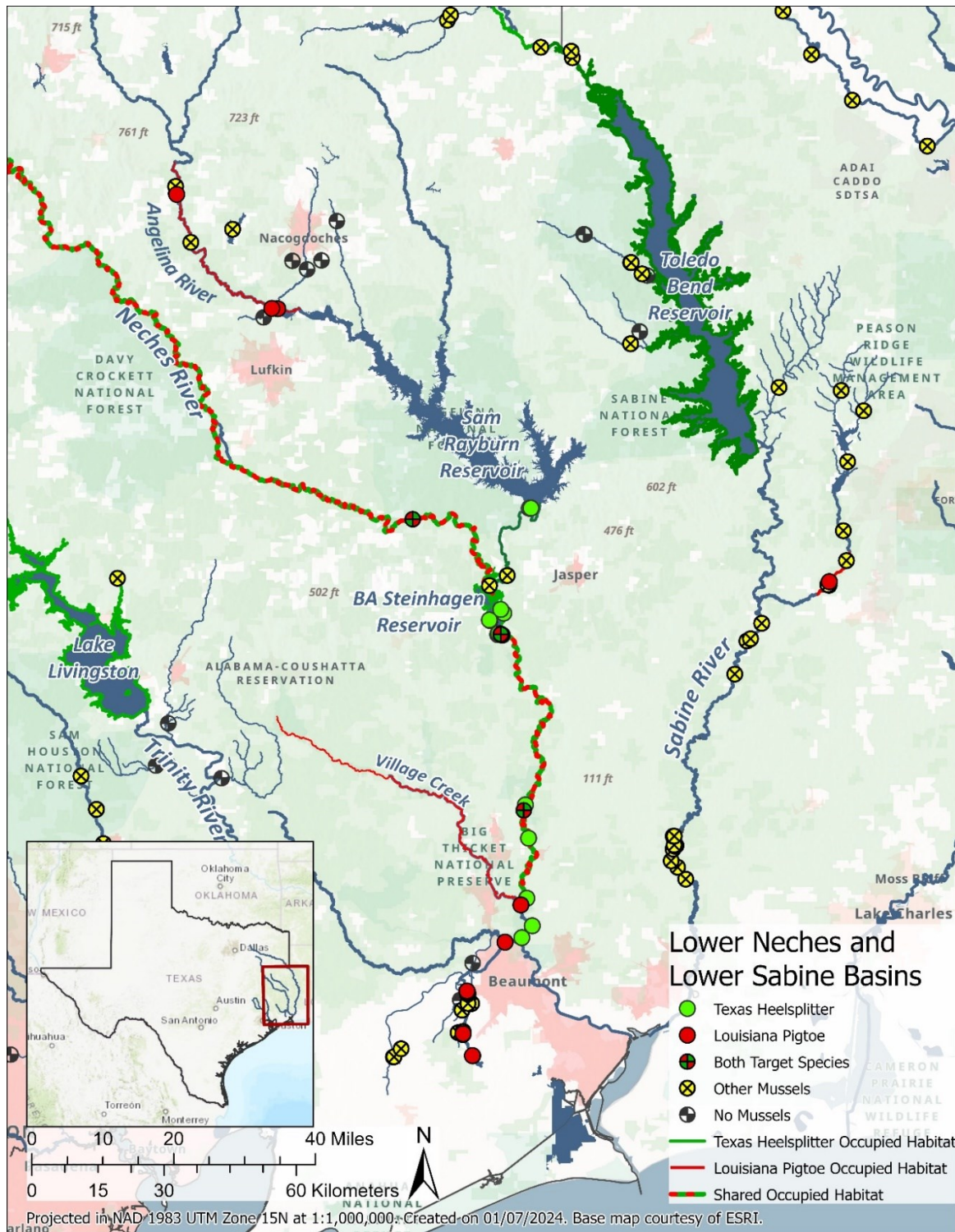


Figure 4. Map showing Louisiana Pigtoe and Texas Heelsplitter occurrence within the Neches, Angelina, and lower Sabine rivers. Occupied habitat information from USFWS 2023 and USFWS 2020 is represented by colored lines, with point data reflecting recent survey data collected by the study team.

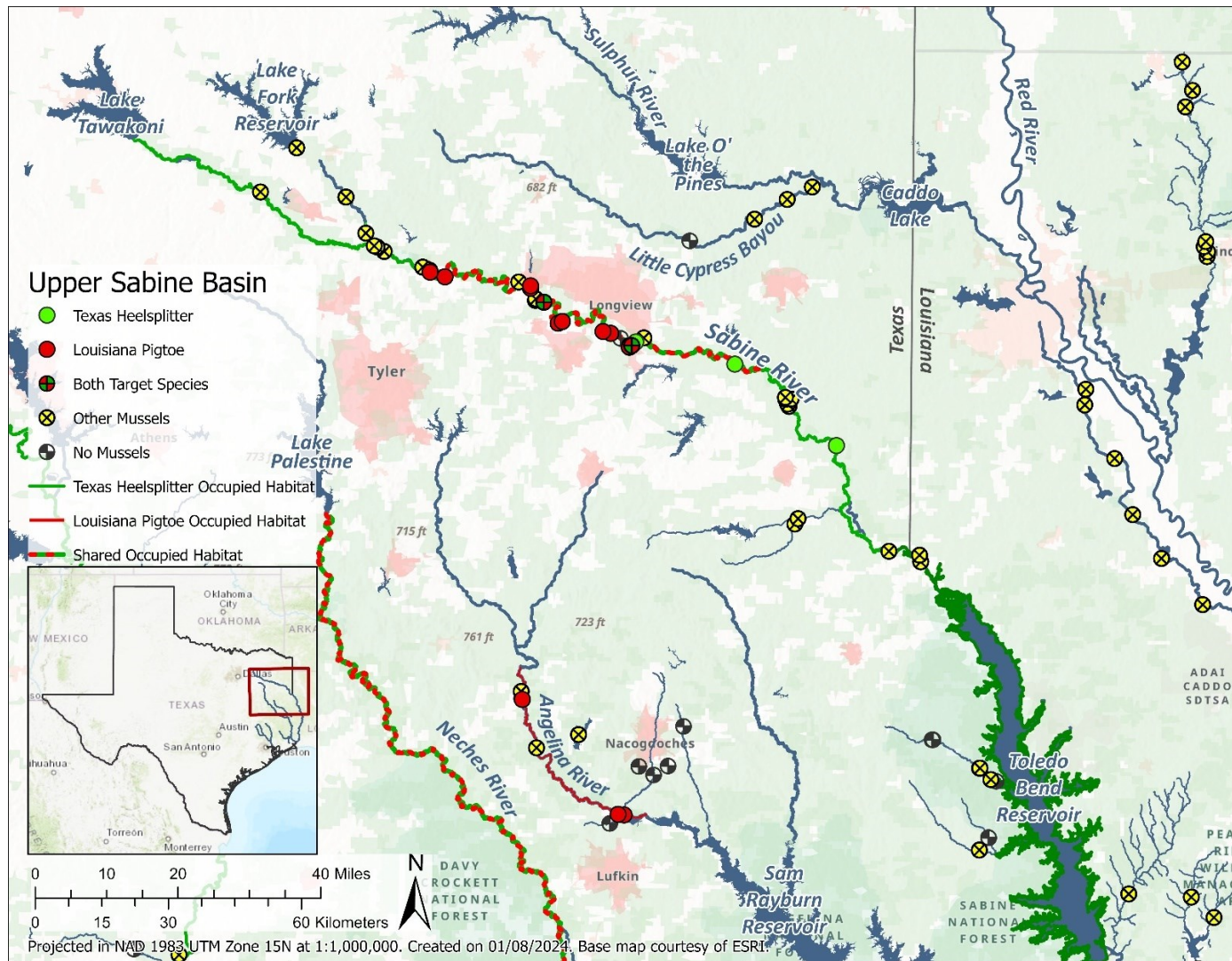


Figure 5. Map showing Louisiana Pigtoe and Texas Heelsplitter occurrence within the upper Sabine River. Occupied habitat information from USFWS 2023 and USFWS 2020 is represented by colored lines, with point data reflecting recent survey data collected by the study team.